ACTA UNIVERSITATIS OULUENSIS
C Technica 482

JANI KANGAS

SEPARATION PROCESS MODELLING

Highlighting the predictive capabilities of the models and the robustness of the solving strategies

Academic dissertation to be presented with the assent of the Doctoral Training Committee of Technology and Natural Sciences of the University of Oulu for public defence in Kuusamonsali (Auditorium YB210), Linnanmaa, on 14 March 2014, at 12 noon

UNIVERSITY OF OULU, OULU 2014

Acta Univ. Oul. C 482, 2014

Supervised by
Professor Juha Tanskanen

Reviewed by
Professor Ville Alopaeus
Professor Andrzej Górak

Opponent
Professor Rajamani Krishna

ISBN 978-952-62-0375-1 (Paperback)
ISBN 978-952-62-0376-8 (PDF)

ISSN 0355-3213 (Printed)
ISSN 1796-2226 (Online)

Cover Design
Raimo Ahonen

JUVENES PRINT
TAMPERE 2014

Kangas, Jani, Separation process modelling. Highlighting the predictive capabilities of the models and the robustness of the solving strategies

University of Oulu Graduate School; University of Oulu, Faculty of Technology, Chemical Process Engineering

Acta Univ. Oul. C 482, 2014

University of Oulu, P.O. Box 8000, FI-90014 University of Oulu, Finland

Abstract

The aim of this work was to formulate separation process models with both predictive capabilities and robust solution strategies. Although all separation process models should have predictive capabilities, the current literature still has multiple applications in which predictive models having the combination of a clear phenomenon base and robust solving strategy are not available. The separation process models investigated in this work were liquid-liquid phase separation and membrane separation models.

The robust solving of a liquid-liquid phase separation model typically demands the solution of a phase stability analysis problem. In addition, predicting the liquid-liquid phase compositions reliably depends on robust phase stability analysis. A phase stability analysis problem has multiple feasible solutions, all of which have to be sought to ensure both the robust solving of the model and predictive process model. Finding all the solutions with a local solving method is difficult and generally inexact. Therefore, the modified bounded homotopy methods, a global solving method, were further developed to solve the problem robustly. Robust solving demanded the application of both variables and homotopy parameter bounding features and the usage of the trivial solution in the solving strategy. This was shown in multiple liquid-liquid equilibrium cases.

In the context of membrane separation models, predictive capabilities are achieved with the application of a Maxwell-Stefan based model. With the Maxwell-Stefan approach, multicomponent separation can be predicted based on pure component permeation data alone. On the other hand, the solving of the model demands a robust solving strategy with application-dependent knowledge. These issues were illustrated in the separation of a H_2/CO_2 mixture with a high-silica MFI zeolite membrane at high pressure and low temperature. Similarly, the prediction of mixture adsorption based on pure component adsorption data alone was successfully demonstrated.

In the context of membrane separation models, predictive capabilities are achieved with the application of a Maxwell-Stefan based model. With the Maxwell-Stefan approach, multicomponent separation can be predicted based on pure component permeation data alone. On the other hand, the solving of the model demands a robust solving strategy with application-dependent knowledge. These issues were illustrated in the separation of a H_2/CO_2 mixture with a high-silica MFI zeolite membrane at high pressure and low temperature. Similarly, the prediction of mixture adsorption based on pure component adsorption data alone was successfully demonstrated.

Keywords: adsorption, homotopy methods, Maxwell-Stefan, membrane separation, phase stability analysis, process modelling, solving methods, surface diffusion, vapour pressure

Kangas, Jani, Erotusprosessien mallinnus. Mallien ennustuskyky ja ratkaisustrategian luotettavuus
Oulun yliopiston tutkijakoulu; Oulun yliopisto, Teknillinen tiedekunta, Kemiallinen prosessitekniikka
Acta Univ. Oul. C 482, 2014
Oulun yliopisto, PL 8000, 90014 Oulun yliopisto

Tiivistelmä

Työn tavoitteena oli muotoilla prosessin käyttäytymisen ennustamiseen kykeneviä erotusprosessimalleja ja niiden ratkaisuun käytettäviä luotettavia strategioita. Vaikka kaikkien erotusprosessimallien tulisi olla ennustavia, on tällä hetkellä useita kohteita, joissa prosessin käyttäytymistä ei voida ennustaa siten, että käytettävissä olisi sekä ilmiöpohjainen malli että ratkaisuun soveltuva luotettava strategia. Tässä työssä erotusprosessimalleista kohteina tarkasteltiin neste-neste-erotuksen ja membraanierotuksen kuvaukseen käytettäviä malleja.

Neste-neste-erotusmallien luotettava ratkaisu vaatii yleensä faasistabiilisuusongelman ratkaisua. Lisäksi faasien koostumusten luotettava ennustaminen pohjautuu faasistabiilisuusanalyysiin. Faasistabiilisuusongelmalla on useita mahdollisia ratkaisuja, jotka kaikki tulee löytää, jotta voitaisiin varmistaa luotettava mallin ratkaisu sekä prosessimallin ennustuskyvyn säilyminen. Kaikkien ratkaisujen löytäminen on sekä vaikeaa että epätarkkaa paikallisesti konvergoituvilla ratkaisumenetelmillä. Tämän vuoksi globaaleihin ratkaisumenetelmiin kuuluvia modifioituja rajoitettuja homotopiamenetelmiä kehitettiin edelleen, jotta faasistabiilisuusongelma saataisiin ratkaistua luotettavasti. Ratkaisun luotettavuus vaati sekä muuttujien että homotopiaparametrin rajoittamista ja ongelman triviaalin ratkaisun käyttöä ratkaisustrategiassa. Tämä käyttäytyminen todennettiin useissa neste-nestetasa-painoa kuvaavissa esimerkeissä.

Membraanierotusta tarkasteltaessa ennustava malli voidaan muotoilla käyttämällä Maxwell-Stefan pohjaista mallia. Maxwell-Stefan lähestymistavalla voidaan ennustaa monikomponenttiseosten erotusta perustuen puhtaiden komponenttien membraanin läpäisystä saatuun mittausaineistoon. Toisaalta mallin ratkaisu vaatii luotettavan ratkaisustrategian, jossa hyötykäytetään kohteesta riippuvaa tietoa. Näitä kysymyksiä havainnollistettiin H_2 /CO_2 seoksen erotuksessa MFI-zeoliitti-membraanilla korkeassa paineessa. Samoin seosten adsorboitumiskäyttäytymistä ennustettiin onnistuneesti pelkästään puhtaiden komponenttien adsorptiodatan pohjalta.

Kokonaisuutena voidaan todeta, että tarkasteltujen erotusprosessimallien ennustavuutta voidaan parantaa yhdistämällä malli, jolla on selkeä ilmiöpohja ja luotettava ratkaisustrategia. Lisäksi mallien käytettävyys erotusprosessien suunnittelussa on parantunut työn tulosten pohjalta.

Asiasanat: adsorptio, faasistabiilisuusanalyysi, homotopiamenetelmät, höyrynpaine, Maxwell-Stefan, membraanierotus, pintadiffuusio, prosessimallinnus, ratkaisumenetelmät

Dedicated to Pihla and Roosa

In memory of Toini and Vilho Kangas, my dear late grandparents

Preface

This study was carried out in the Chemical Process Engineering group of Faculty of Technology at the University of Oulu. The thesis work was performed mainly during the period 2008-2013, albeit that the ‘seeds’ of the present work were planted back at the start of 2003.

First, I would like to thank my supervisor Prof. Juha Tanskanen for the helpful comments and discussions during my thesis work.

I would also like to express my gratitude to Prof. Ville Alopaeus from Aalto University and Prof. Andrzej Górak from Technische Universität Dortmund who reviewed the manuscript of this thesis.

I want to express my sincere thanks to all the co-authors and co-workers who made this thesis possible.

My special thanks goes to my colleague Dr Ilkka Malinen for the illuminating and lively discussions regarding the thesis work and especially everything not related to this thesis. Ilkka, your contribution was vital in completing this thesis work.

Finally, my warm thanks to my family for their steady support during my thesis work.

This work has been partially funded by the Finnish Academy (project numbers 135339 and 253871) and the postgraduate program Graduate School in Chemical Engineering (GSCE).

Oulu, January 2014 Jani Kangas

List of symbols and abbreviations

a	Fitted constant relating degree of correlations for unary diffusion [-]
A	Specific area of adsorbent [m^2]
b	Domain boundary [-], Langmuir single-site adsorption isotherm constant [bar^{-1}] or constant relating degree of correlations for unary diffusion [-]
B	Maxwell-Stefan diffusivity matrix element [s^1 m^{-2}]
B	Maxwell-Stefan diffusivity matrix [s^1 m^{-2}]
c	Constant relating degree of correlations for unary diffusion [-]
c	Vector of component concentrations
d	Dimension of tangent plane distance surface
D	Tangent plane distance or diffusivity [m^2 s^{-1}]
e	Eigenvalue
e	$n \times 1$ vector where every element has the value one
E	Energy [J mol^{-1}]
f	Fugacity [bar]
f	Equation set
f'	Jacobian matrix of **f**
F	Total number of phases
g	Auxiliary function in the homotopy equation
G	Reduced molar Gibbs energy or the experimentally defined parameter in NRTL model [-]
h	Homotopy function
H	Enthalpy [J mol^{-1}]
H	Hessian matrix
k	Coefficient
l	Lower inner boundary [-], axial coordinate [m] or mean free path length [m]
m	Reduced Gibbs energy of mixing [-]
M	Parameter in modified bounded homotopies with the homotopy parameter bounding
N	Number of stationary points, total molar amount [mol] or diffusive flux [mol m^{-2} s^{-1}]
n	Number of components, dimension of a vector or number of adsorption sites
nz	Number of non-zero elements in Jacobian

p	Partial pressure [bar]
P	Pressure [bar]
$\mathbf{P}$	Penalty matrix
q_i	Loading of component i on an adsorbent [moles of i on a kg of adsorbent]
r	Radial coordinate
R	Ideal gas constant, 8.314 J mol^{-1} K^{-1}
s	Integration variable in the spreading pressure evaluation or a function including liquid phase non-idealities of TPDF problem
t	Time or exponent in Tóth's adsorption isotherm
tol	Tolerance
T	Temperature [K]
u	Upper inner boundary [-] or energy in Nitta adsorption isotherm [J mol^{-1}]
v	Exponent in the Dual-Langmuir-Sips adsorption isotherm or jump frequency
$\mathbf{v}$	Auxiliary function in the bounded homotopy equation
W	Weighting parameter
$\mathbf{W}$	Weighting matrix
x	Mole fraction [-]
$\mathbf{x}$	Variable vector
$\hat{\mathbf{x}}$	Mole fraction vector with $n - 1$ elements
y	Mole fraction in bulk gas phase [-]
z	Membrane cross length coordinate [m], coordination number of lattice or number of neighbour sites
$\mathbf{z}$	Composition of studied mixture [-] or trivial root [-]

Greek Letters

α	Adsorbent dependent fitted parameter, interaction parameter defined experimentally in NRTL model
β	Affinity coefficient of an adsorbent in Dubinin-Radushkevich and Dubinin-Astakhov isotherms, adsorbent dependent fitted parameter, molar amount or function in Reed-Ehrlich approach
δ	Thickness [nm], Kronecker delta or relative measure for bounding zone width
δe	Infinitesimal amount [mol]

δE	Reduction in energy barrier per nearest neighbour [J mol^{-1}]
ε	Adsorption potential or function
φ	Fugacity coefficient
γ	Activity coefficient
$\mathbf{\Gamma}$	Thermodynamic factor or matrix
η	Function
κ	Function
λ	Mean free path [m] or displacement of the adsorbed molecular species
Λ	Interaction parameter in Wilson activity coefficient model
μ	Chemical potential
$\mathbf{\Pi}$	Penalty matrix
π	Spreading pressure [Pa] or penalty function
θ	Occupancy fraction or homotopy parameter
ρ	Density [kg m^{-3}]
τ	Interaction parameter defined experimentally in NRTL model
ξ	Auxiliary variable

Subscripts

0	Reference or starting point
a	Activation
A	Adsorption site A
b	Bounded
B	Adsorption site B
BET	BET adsorption isotherm
DA	Dubinin-Astakhov
defect	Defect
film	Zeolite film
g	Gas
H	Henry's law
i	*i*th component or *i*th element
i,*j*	Interaction of component *i* and *j*
j	*j*th element or component
k	*k*th element or component
L	Single-site Langmuir
LF	Langmuir-Freundlich

max	Maximum
min	Minimum
n	*n*th element or component
Nit	Nitta
perm	Permeate
s	Solid
sad	Saddle
self	Self
T	Tóth
v	Vacancy
x	Variable
θ	Homotopy parameter

Superscripts

0	Reference state or pure component
∞	Infinite dilution
ads	Adsorption or adsorbed phase
b	Bounded
d	Number of components minus 1
even	Even
exit	Departure from the specified variable-homotopy domain
E	Excess
fluid	Fluid
inf	Infinity
L	Liquid
max	Maximum
min	Minimum
mod	Modified
M	Mixing
odd	Odd
s	Surface
sat	Saturated
tot	Total
V	Vapour
*	Solution point or relevant site
•	Temperature independent

'	Boundary
¯	Weighted average

Abbreviations

ASPENPlus	AspenPlus is a process modelling tool in AspenTech's aspenONE® Process Engineering applications
BET	Brunauer–Emmett–Teller adsorption isotherm
BVP	Boundary Value Problem
CSTR	Continuous Stirred Tank Reactor
DADM	Dynamic Bubble Column with Axial Dispersion in Romanainen (1994)
EtOH	Ethanol
FM	The Film Model in Romanainen (1994)
FPM	The Film-Penetration Model in Romanainen (1994)
IAST	Ideal Adsorbed Solution Theory
KMC	Kinetic Monte Carlo
LLE	Liquid-Liquid Equilibrium
MATLAB	MATLAB® is a commercial product package for computing launched by MathWorks™
MD	Molecular Dynamics
MFI	Mordenite Framework Inverted
MPTA	Multicomponent Potential Theory of Adsorption
NaA	Zeolite with composition $[Na_{12}(H_2O)_{27}]$ $[Al_{12}Si_{12}O_{48}]$
NLE	Non-Linear Equation
NRTL	Non-Random Two-Liquid
ODE	Ordinary Differential Equation
PDE	Partial Differential Equation
PRAST	Predictive Real Adsorbed Solution Theory
RAST	Real Adsorbed Solution Theory
SADM	Steady State Bubble Column with Axial Dispersion in Romanainen (1994)
STS	Steady State Tanks-in-Series Model in Romanainen (1994)
TPDF	Tangent Plane Distance Function
VLE	Vapour-Liquid Equilibrium
VST	Vacancy Solution Theory

List of original papers

This thesis is based on the following publications, which are referred to in the text by their Roman numerals:

I Kangas J, Sandström L, Malinen I, Hedlund J & Tanskanen J (2013) Maxwell-Stefan modeling of the separation of H_2 and CO_2 at high pressure in an MFI membrane. J Memb Sci 435: 186–206.

II Leppäjärvi T, Kangas J, Malinen I & Tanskanen J (2013) Mixture adsorption on zeolites applying the P_i^{sat} temperature-dependency approach. Chem Eng Sci 89: 89–101.

III Malinen I, Kangas J & Tanskanen J (2012) A new Newton homotopy based method for the robust determination of all the stationary points of tangent plane distance function. Chem Eng Sci 84: 266–275.

IV Leppäjärvi T, Malinen I, Kangas J & Tanskanen J (2012) Utilization of P_i^{sat} temperature-dependency in modelling adsorption on zeolites. Chem Eng Sci 69: 503–513.

V Kangas J, Malinen I & Tanskanen J (2011) Modified bounded homotopies in the solving of phase stability problems for liquid–liquid phase-splitting calculations. Ind Eng Chem Res 50: 7003–7018.

In Papers I and V, the models, solving approaches and manuscript writing were the author's contribution. In Papers II and III, the author created the models used and collaborated with the co-authors in the manuscript writing. In Paper IV, the author's contribution was the interpretation of the results and participating in the manuscript writing.

Contents

1 Introduction

1.1 Background

The efficient design of separation processes demands both accurate experimental data and models to predict the behaviour of the process at different operating conditions. Essentially, the design could be performed based on experimental work alone. However, the design is restricted both in terms of time and allocated resources i.e. money and work force. In addition, the process layout changes as the design project proceeds and multiple promising process alternatives have to be investigated. Thus, the demand for new experiments would be constant, and basically exhaustive, at each stage of the separation process design. Hence, the repetition of the experiments is not, in practice, a feasible approach. Thus, the current best practice in chemical process design is to include in the process synthesis, analysis and evaluation models with a *predictive* nature (see e.g. Seider *et al.* 1999). As a result, as stated by Biegler *et al.* (1997): "*the more or less ad hoc analysis of process flowsheets has been replaced by systematic numerical solution techniques that are now widely implemented in computer modelling systems and simulation packages for both preliminary and detailed design*".

1.2 Predictive separation process models

The title 'predictive separation process models' can be viewed as self-evident in the field of separation process modelling. Every separation process model created during process design should have, as a premise, predictive capabilities, at least to a certain extent. Especially the capability of predicting behaviour inside the domain explored with the experimental work, i.e. *interpolation*, is a fundamental property of the model. In contrast, predicting outside the domain of the experimental work, i.e. *extrapolation*, is not generally an obvious property of the formulated models. The capability of a process model to predict process phenomena outside the experimentally defined domain is emphasised in the present work.

The predictive capabilities of a separation process model can also be viewed as a more profound issue. Even though the model in itself can be stated to have predictive capabilities, without a robust solving strategy the predictive capabilities may be lost or maintained, depending on the selection of the solving strategy, as

will be shown in this thesis. The next issue to be tackled is to select how the predictive capabilities are enabled.

1.2.1 Experimental parameters

The first of the enabling factors is that the parameters acquired from experimental data present in the literature or obtained from one's own experiments are applicable to the system investigated. Applicability in this context denotes that the experimental data used is sufficiently accurate for the purpose intended and the experiments performed cover the investigated domain, embodying the main features of the system. These criteria can be fulfilled by appropriately designing both the experimental set-up and experiments. The proper design of experimental work should include the usage of a statistically qualified experimental design method, e.g. the Taguchi method. On the other hand, the physical relevance of the experimental data can be tested in certain applications for their consistency. A good example of this is the use of the Gibbs-Duhem equation in conjunction with phase equilibrium measurements data to test the thermodynamic consistency of the data.

The second factor enabling the predictive capabilities of the constructed model is the proper estimation of parameters based on the experimental data. The successful execution of the estimation requires a number of issues to be addressed (adapted from Englezos and Kalogerakis (2001)):

- decision on the structure of the models used
- selection of the objective function
- selection of the solution technique to minimize the objective function
- statistical properties/accuracy of estimated parameters
- statistical properties/uncertainty of model-based calculated values
- tests for model adequacy
- selection between different rival models
- factorial experimental design
- sequential experimental design

All these issues have an effect on the outcome of the parameter estimation, and naturally the predictive capabilities of the formulated model. In addition to these issues, the physical relevance of the estimated parameters in particular is important when building a predictive phenomenon-based process model. Therefore, the careful investigation of the parameter estimation results statistically,

validating the physical relevance of the parameters, and comparison with literature data are important to ascertain that the formulated model can be stated to be predictive. The third factor enabling the predictive capabilities is the model formulation. This factor is emphasized in the present work.

1.2.2 Model formulation

Predictive separation process models are generally built based on the phenomena prevailing in the investigated part of the process. The creation of a predictive process model is enabled by introducing relations founded on the firm basis of thermodynamics and relations describing the rate of the phenomena. For decades, the formulation of predictive process models has been an important task in the field of process systems engineering, and numerous books have been dedicated to the presentation of predictive property methods (see e.g. Poling *et al.* 2001) and predictive process models (see e.g. Taylor and Krishna 1993). On the other hand, satisfactory prediction of a multiphase equilibrium requires that adequate thermodynamic models for the phases are available (Michelsen and Mollerup 2007). Thus, it can be argued that the existence of methods and models with a predictive capability is one cornerstone of the current chemical engineering practice.

The main phenomena inducing the targeted separation behaviour in separation processes are dependent on the combination of the driving force creating the *potential* of components to separate and the forces slowing or accelerating the *flux* of the components. In some separation processes, like distillation columns and decanters, it is a good first guess that the thermodynamic potential is the factor determining the separation selectivity and efficiency achieved. Similarly, the membrane separation of gaseous components with microporous materials, like zeolites, is dependent on the thermodynamic potential. However, the forces exerted by the mass transfer resistances also have a major role in the attainment of separation within reasonable time scale in the separation of components with a microporous membrane.

In decanters, separation occurs through the liquid-liquid phase equilibrium (LLE). In contrast, in microporous membranes the equilibrium between the bulk gas phase and the adsorbed phase is observed. Nevertheless, the analogy of the phase equilibrium phenomena can be utilized to describe the phenomena. The main distinctive factor is that in membrane separation, the membrane material adds one component to the system, which complicates the generalization of the

created description from one application to another. Therefore, the description of pure component adsorption on a zeolite for example in itself is in fact a binary adsorption model. The pure component adsorption data can be used further to predict binary mixture adsorption based on a model, like the adsorption solution theory of Myers and Prausnitz (1965), which relies on thermodynamics. This is analogous to the description of liquid-liquid phase equilibrium, where generally pure component and binary liquid-liquid equilibrium data are used to predict multicomponent phase equilibrium. Hence, models with predictive capabilities are of high value in both membrane and liquid-liquid phase separation.

The main complicating issue associated with separation process models utilizing LLE is the potential existence of a "trivial" solution, i.e. a solution with both liquid phases of identical composition and with identical properties, leading to the automatic satisfaction of the model equations. Therefore, a separation process model utilizing LLE may have multiple feasible solutions. Similarly, phase stability analysis, an important sub-problem of the LLE separation process model investigated in the present work, may have multiple feasible solutions. Multiplicity means in practice that the correct solution has to be selected from among all the feasible solutions. The predictive capabilities of the model would be lost without the appropriate means to perform the selection. Luckily, the selection can be performed by evaluating the total Gibbs energy of the system at feasible solutions. The solution yielding the minimum Gibbs energy for the system can be used further for process design purposes.

However, a selection based on the evaluation of the Gibbs energy of the system is not generally sufficient in the classification of the solutions obtained. Instead, the (dynamic) stability of the steady-state solutions dictates the selection between multiple steady-state solutions. For example, distillation column models may have multiple feasible steady-state solutions (see e.g. Kienle *et al.* 1995, Kannan *et al.* 2005, Bekiaris *et al.* 1996). The process conditions corresponding to the stable solution(s) are generally preferred in the process design. In the later stages of process design, potential control issues such as difficulties in control, areas of attraction of potential steady states, suitable start-up strategy, and control-design interactions need to be addressed (Kannan *et al.* 2005). Hence, this will also have an effect on the selection of a suitable steady-state solution.

The stability analysis of the multiple feasible solutions (state distributions) of a distillation column can be performed by converting the steady-state process model to a time-dependent form and making small disturbances to the variable values at the steady-state solutions and evaluating the state distribution of the

distillation column after a long (infinite) time period. If the variables converge to the investigated feasible solution, the solution can be stated to be stable. (Hangzhou *et al.* 2011) Alternatively, the stability of the solutions can be checked by evaluating the poles of the characteristic equation of the described system (Luyben 1996).

On the other hand, both the membrane separation and liquid-liquid phase separation models are defined within the physical domain only, which adds complexity to the solving of the models. Hence, robust solution strategies are also required in the modelling.

1.3 Robust solution strategies

The solving of created separation process models is not straightforward. This is generally due to the non-linear characteristics of the models. The non-linearity of the models typically originates from the non-ideality of the phenomena described by the models. Examples of non-ideal behaviour are the appearance of azeotropes and the presence of multiple liquid phases in the studied system. In some instances, the mathematical formulation of the process also propagates difficulties in the solving. In addition, as stated above, chemical engineering oriented process models are generally only applicable within some pre-defined variable domain. Extrapolation outside the domain during solving may cause the solving to cease. The simplest example of this is entering the domain of negative mole fractions, which in turn cannot be typically substituted into thermodynamic property calculation routines.

Generally, finding a feasible state distribution of the process, i.e. one solution of the model, demands either application-dependent knowledge or having a solving method that is able to find *robustly* the solution(s) from a generally defined initial guess. In the present work, the following definition of the robustness of a solving strategy has been applied (Malinen 2010): *Robustness is a fundamental property that describes the ability to determine one or more solutions for a non-linear equation set, i.e. the model, representing the behaviour of a separation process. In addition to the robustness of the solving method, the robustness of the utilized solving strategy must be taken into account when considering the overall robustness of a solving approach*. Based on this definition, assuming that the equation-oriented solving approach has been selected, the robustness can be improved by using:

- problem-tailored solving strategies in conjunction with locally convergent solving methods,
- a commonly defined solving strategy in conjunction with globally convergent solving methods, or
- both problem-tailored solving strategies and globally convergent solving methods.

The selection of an appropriate way to improve robustness is case-sensitive. Well-established solution methods, like the Newton-Raphson based methods, can be used in many cases to solve a process model with a high success rate, provided an initial guess at the proximity of the solution has been supplied. Hence, in the case the problem-tailored solving strategies are used to improve robustness. However, the Newton-Raphson based methods cannot guarantee that multiple solutions, or even one solution, are found. Therefore, the solution methods are generally termed *local*, or *locally convergent*. In addition, some process models may have multiple feasible solutions. Finding all of them from an initial guess is not generally possible. Thus, the formulation of solving methods with the capability of finding all the feasible solutions of a process model *robustly* from an initial guess has been an important target for decades in the field of process systems engineering, especially since the development of computers. The current status is that this aim has not been reached, not even with the exponential increase of computation power of modern computers.

1.4 Aim of this study

At the start of this study it was evident based on the literature that there is a lack of a tool that can robustly solve a general chemical process model with multiple solutions. Previously, Malinen and Tanskanen (2007, 2008, 2010) had formulated usable solving methods for solving different NLE models. However, the methods had not been applied to phase stability analysis. In addition, the focus in the studies of Malinen and Tanskanen is on the solving of a general NLE problem, i.e. $\mathbf{f}(\mathbf{x}) = \mathbf{0}$. The application of the solving methods to new objects can be utilized, as will be shown, to further improve the *robustness* of the solving methods.

In addition, the literature regarding the description of zeolite membrane separation showed clear shortcomings. Even though Krishna and co-workers (Krishna 1990; Kapteijn *et al.* 2000; Skoulidas *et al.* 2003; Krishna and Baur 2003, 2004; Krishna and Paschek 2000, 2002; Krishna *et al.* 2004; Krishna and

van Baten 2005, 2009, 2010a, 2010b, 2010c, 2011) had formulated a number of useful methods to predict membrane separation behaviour, the application of the methods in the field has been limited. An important reason for this is that in the field of membrane separation research there is a clear division between 'experimentalists' and 'modellers'. Also, the emphasis in membrane separation research is on experimental work and membrane synthesis rather than predicting membrane behaviour. The formulation of a model with predictive capabilities has undoubted benefits in:

- the understanding of membrane behaviour,
- the realization of the best or/and optimal performance of the membrane,
- performing appropriate changes to the membrane synthesis, and
- the design of a process utilizing membrane separation.

Thus, the formulation of a description of membrane separation with *predictive* capabilities emerged as an important extension to the field of membrane research.

Similarly, a basic problem in the formulation of a model for membrane separation is that both adsorption and diffusion lack a vast experimentally obtained data bank with mixture data, i.e. not even binary data, unlike the situation in the field of vapour-liquid phase equilibrium. The shortage of experimental data originates, naturally, from the membrane (i.e. adsorbent) properties. The properties are significantly dependent on both the synthesis method applied and the raw material used in the synthesis. Therefore, there is a clear demand for the formulation of a model that can predict membrane separation with minimal experimental data. Therefore, as a combination of the above-mentioned shortcomings, the following aims were set in the present work:

- to create *predictive and reliable* separation process models in different applications with minimum experimental data (Papers I - V),
- to apply the description of the *non-ideality* of the studied systems in the models created (Papers I, III and V), and
- to formulate and apply *robust* solution strategies for the process models (Papers I, III and V).

2 Separation process models

2.1 Membrane separation model

The selection of an appropriate membrane separation model is dependent on the phenomena prevailing in the application under investigation. The factors affecting the separation of a gas mixture by a zeolite can be categorized into three groups (Sircar and Myers 2003):

- size or steric exclusion of certain components from entering the zeolite pores, whereas the other components enter the pores and are adsorbed,
- thermodynamic selectivity: the preferential adsorption of certain components over others when all components can enter the pores,
- kinetic selectivity: the ability of certain components to enter the pores faster than other components.

Due to the differences between applications, the factors have different relative contributions to the separation capabilities of a zeolite membrane. The net result may be that the separation occurs as a combination of molecular sieving, physisorption and surface diffusion processes. In addition, the process conditions like the temperature, pressure and partial pressure of the permeating molecules have an effect on the relative importance of the factors. In addition, they change the separation selectivity of a zeolite membrane. 'Real' zeolite membranes have in practice flow-through defect pores in addition to the zeolite pores. All the defect pores have an influence on the achieved separation selectivity and permeation fluxes. The effects of the respective pores on membrane selectivity are illustrated in Fig. 1 in the context of H_2/CO_2 separation with an MFI membrane investigated in Paper I.

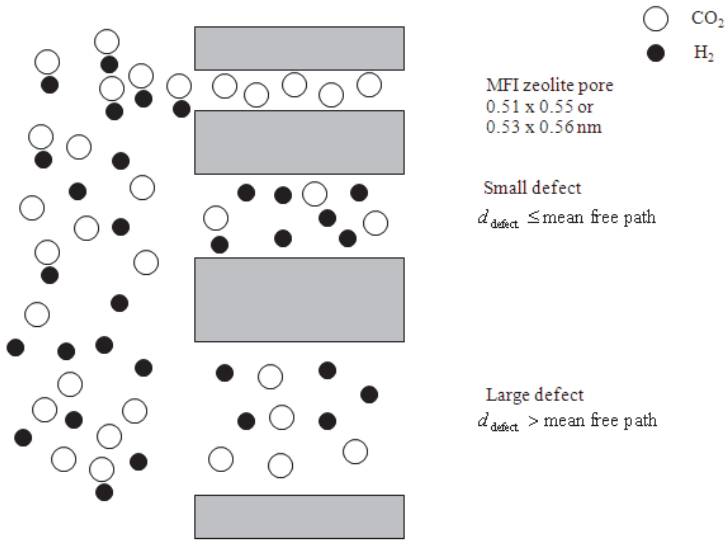

Fig. 1. Selectivity effect of different pores on the H_2/CO_2 separation capability of an MFI zeolite at low temperatures.

As can be seen in Fig. 1, CO_2 is preferentially adsorbed in the membrane and H_2 is essentially a weakly adsorbing permanent gas. In addition, H_2 has a smaller kinetic diameter than CO_2. At low temperatures, CO_2 blocks the permeance of H_2 in the smallest (zeolite) pores by adsorption. Both CO_2 and H_2 permeate through the zeolite pores with surface diffusion at low (room) temperatures. Typically, CO_2 molecules diffuse more slowly than H_2 through zeolite pores. The net result is that CO_2 slows down the diffusion of H_2 and H_2 in turn accelerates the diffusion of CO_2. Thus, due to the combination of adsorption and surface diffusivity, CO_2 permeates selectively through the zeolite pores.

In contrast, the small defects are selective with respect to H_2 due to the smaller kinetic diameter of H_2 and the fact that the defect diameter, d_{defect}, is smaller than the mean free path, λ, of a molecule in the situation depicted in Fig. 1. Therefore, Knudsen diffusion has a clear significance in these conditions. On the other hand, the larger defect pores are not selective, as the defect diameter is larger than the mean free path. Thus, Poiseuille flow dictates the mass transfer in the large defect pores.

In addition to the zeolite pores and flow-through defects, the zeolite has defects in the form of missing atoms in the structure and extra-framework gaps. The modelling of their contribution to mass transfer is generally difficult due to

the lack of appropriate data regarding their impact on mass transfer. Thus, their contribution is generally stated only implicitly in modelling (see e.g. Paper I).

The relative contribution of each pore type in Fig. 1 is dependent on the studied conditions and the relative proportions of each pore type of the total surface area. The proportion of the flow-through defects and the approximate defect diameters can be analyzed through permporometry studies. The main idea in permporometry studies, like the one performed in Paper I, is to follow the flux of a non-adsorbing component as the proportion of a strongly adsorbing component in the feed stream is increased. The strongly adsorbing component blocks the zeolite pores and the smallest defects, which decreases the flux of the non-adsorbing component. This decrease of the flux can be correlated with the size and relative amount of the flow-through defects. Further details of permporometry can be found e.g. in Hedlund *et al.* (2009).

The description of mass transfer through flow-through defects is well-established in the current literature. The mass transfer is generally modelled with the Dusty-Gas Model formulated by Mason and co-workers (see details e.g. from Mason and Malinauskas, 1983). Similarly, the surface diffusion inside the zeolite pores is frequently established in the usage of the Maxwell-Stefan formulation. However, the application of the Maxwell-Stefan formulation for different process conditions and permeating components demands further work. Thus, this formulation is investigated below in some depth.

2.1.1 Maxwell-Stefan modelling of surface diffusion of adsorbed components

The Maxwell-Stefan formulation provides a way to predict the surface diffusivity of a mixture using only data regarding single-component adsorption and diffusion. On the other hand, the prediction of the diffusivity of a multicomponent mixture is based on the pure component and correlation based binary diffusivities alone. Therefore, the application of the Maxwell-Stefan formulation to new objects is straightforward. In addition, the diffusivity coefficients are amenable to physical interpretation. (Krishna 1990, Krishna and Baur 2003) These are the key properties determining the benefits of the Maxwell-Stefan formulation in comparison with the Onsager approach. In the Maxwell-Stefan formulation, the dependence of the chemical potential gradients $\nabla\mu_i$ and the component surface fluxes N_i^s are connected as:

$$-\frac{\theta_i}{RT}\nabla\mu_i = \sum_{\substack{j=1 \\ j\neq i}}^{n} \frac{\theta_j N_i^{\mathrm{s}} - \theta_i N_j^{\mathrm{s}}}{\rho_{\mathrm{film}} q_i^{\mathrm{sat}} D_{i,j}^{\mathrm{s}}} + \frac{N_i^{\mathrm{s}}}{\rho_{\mathrm{film}} q_i^{\mathrm{sat}} D_i^{\mathrm{s}}}, \tag{1}$$

where $\theta_i = q_i / q_i^{\mathrm{sat}}$, n is the number of permeating components, ρ_{film} is the density of the zeolite film, D_i^{s} is the Maxwell-Stefan diffusivity for component *i* and $D_{i,j}^{\mathrm{s}}$ is the Maxwell-Stefan diffusivity describing the interchange between components *i* and *j*. The use of Eq. (1) requires that two different types of Maxwell-Stefan diffusivities have to be defined, i.e. $D_{i,j}^{\mathrm{s}}$ and D_i^{s} . $D_{i,j}^{\mathrm{s}}$ describes the adsorbate correlation effects, whereas D_i^{s} describes the adsorbate-adsorbent interaction. Generally, D_i^{s} is obtained from single-component permeation data and an interpolation formula is used to define $D_{i,j}^{\mathrm{s}}$. Eq. (1) can be revised in a matrix form by defining matrices $\mathbf{B}$ and $\mathbf{\Gamma}$. The elements of $\mathbf{B}$ are:

$$B_{i,i} = \frac{1}{D_i^{\mathrm{s}}} + \sum_{\substack{j=1 \\ j\neq i}}^{n} \frac{\theta_j}{D_{i,j}^{\mathrm{s}}}, B_{i,j} = -\frac{\theta_i}{D_{i,j}^{\mathrm{s}}}. \tag{2}$$

Assuming equilibrium between the adsorbent surface and the bulk fluid, the chemical potential in Eq. (1) may be expressed in terms of gradients of surface occupancy by introducing the thermodynamic factor matrix, $\mathbf{\Gamma}$. In addition, by assuming that chemical potential gradients exist only along the cross-sectional axis z of the membrane, i.e. the radial gradients are negligible, we obtain:

$$\frac{\theta_i}{RT}\frac{\partial\mu_i}{\partial z} = \sum_{j=1}^{n} \Gamma_{i,j}\frac{\partial\theta_j}{\partial z}, \text{ where } \Gamma_{i,j} = \theta_i \frac{\partial \ln f_i}{\partial \theta_j}, \tag{3}$$

where f_i is the fugacity of component *i* in bulk fluid. Now Eq. (1) can be represented in the matrix notation:

$$\mathbf{N}^{\mathrm{s}} = -\rho_{\mathrm{film}}\mathbf{q}^{\mathrm{sat}}\mathbf{B}^{-1}\mathbf{\Gamma}\frac{\partial\boldsymbol{\theta}}{\partial z}. \tag{4}$$

The evaluation of Eq. (4) requires both knowledge of the adsorption and the surface diffusivity behaviour of the permeating components.

2.1.2 Adsorption models

The physisorption of the studied components onto zeolites can be modelled with different approaches. The main alternatives are the usage of mixture adsorption data or the prediction of mixture adsorption based on pure component data. The latter alternative is more common in the current literature. In addition, the possibility to predict mixture adsorption based on pure component data is vital from the perspective of efficient separation process design as discussed previously. Thus, this approach is investigated in the following section.

Pure component adsorption models

Pure component adsorption behaviour is generally described with isotherms. Numerous adsorption isotherms have been presented in the literature depending on the adsorbent and the adsorbing component studied. Some frequently applied adsorption isotherms are shown in Table 1. In the literature, and in the original form, the isotherms are typically represented in the form, where $f_i = P$, but to emphasize the non-idealities present in the bulk phase this simplification has not been applied here.

Table 1. Adsorption isotherms for pure components.

Isotherm	Mathematical form
Henry's law	$\theta_i = b_{H,i}(T) f_i$
Single-site Langmuir	$\theta_i = \frac{b_{L,i}(T) f_i}{1 + b_{L,i}(T) f_i}$
Langmuir-Freundlich	$\theta_i = \frac{\left(b_{LF,i}(T) f_i\right)^{1/n_{LF,i}}}{1 + \left(b_{LF,i}(T) f_i\right)^{1/n_{LF,i}}}$
Dual-Langmuir-Sips	$q_i = q_{A,i}^{\text{sat}} \frac{b_{A,i}(T) f_i^{\nu_{A,i}}}{1 + b_{A,i}(T) f_i^{\nu_{A,i}}} + q_{B,i}^{\text{sat}} \frac{b_{B,i}(T) f_i^{\nu_{B,i}}}{1 + b_{B,i}(T) f_i^{\nu_{B,i}}}$
Nitta	$n_{Nit,i} b_{Nit,i}(T) f_i = \frac{\theta_i}{(1-\theta_i)^{n_{Nit,i}}} \exp\left(-\frac{n_{Nit,i} u}{kT}\right) \theta_i$
Tóth	$\theta_i = \frac{b_{T,i}(T) f_i}{\left[1 + \left(b_{T,i}(T) f_i\right)^t\right]^{1/t}}$

Isotherm	Mathematical form
BET	$\theta_i = \dfrac{b_{BET,i}(T)\left(f_i/f_i^0(T)\right)}{\left(1-f_i/f_i^0(T)\right)\left(1+\left[b_{BET,i}(T)-1\right]\left(f_i/f_i^0(T)\right)\right)}$
Dubinin-Radushkevich	$\theta_i = \exp\left[-\left(\dfrac{RT}{E_0\beta}\ln\left(\dfrac{f_i}{f_i^0(T)}\right)\right)^2\right]$
Dubinin-Astakhov	$\theta_i = \exp\left[-\left(\dfrac{RT}{E_0\beta}\ln\left(\dfrac{f_i}{f_i^0(T)}\right)\right)^{n_{DA,i}}\right]$

As can be seen in Table 1, certain isotherms include the standard state fugacity of a component f_i^0 in the model. In practice, the standard state fugacity can be assumed to be equal to the vapour pressure of the component, i.e. $f_i^0(T) = P_i^{\text{sat}}(T)$. Hence, the more well-known forms of the isotherms are discovered. The isotherms utilizing vapour pressure, i.e. a property of the bulk fluid phase, have been dedicated to the description of the adsorption of subcritical vapours onto microporous solids following a pore filling mechanism. Hence, the adsorbed components within the micropores are considered to behave as a liquid even though, due to the forces exerted by the adsorbent, the properties may differ from the corresponding properties of the bulk liquid at the same temperature (Ruthven 1984).

As shown in Table 1, the loading of an adsorbate onto an adsorbent is relative to the fugacity of the adsorbate in the bulk phase. Depending on the respective bulk phase, the conditions studied and the model used to describe the bulk phase properties, the fugacity of the adsorbate has different forms. The main alternative forms are shown in Table 2.

Table 2. Expressions of bulk phase fugacities according to different assumptions and models.

Expression of bulk phase fugacities	Main assumption	Application area
$f_i^V = p_i$	Ideal gas phase	Low pressure
$f_i^V = \phi_i^V\left(P,T,y_j\right)p_i$ †	Non-ideal gas phase	High pressure, i.e. over 10 bar, or e.g. carboxylic acids are present
$f_i^L = x_i P_i^{\mathrm{sat}}\left(T\right)$	Ideal liquid phase	Mixture contains only non-polar components, e.g. aliphatic hydrocarbons
$f_i^L = \gamma_i^L\left(T,x_j\right)x_i P_i^{\mathrm{sat}}\left(T\right)$ †	Non-ideal liquid phase, activity coefficients applied	Mixture contains e.g. polar components
$f_i^L = \phi_i^L\left(P,T,x_j\right)p_i$ †	Non-ideal liquid phase, equation of state applied	High pressure, or/and mixture contains e.g. polar components

† where ϕ_i^V and ϕ_i^L are the fugacity coefficients of component i in vapour and liquid respectively, γ_i^L is the activity coefficient of component i in liquid, $j = 1,\ldots,n$

Mixture adsorption models

The adsorption of mixtures can be predicted with e.g. multicomponent Langmuir, Nitta, Tóth, Langmuir-Freundlich adsorption isotherms (see e.g. Lito *et al.* 2011) and RAST or preferentially starting based on pure component adsorption isotherms (see Table 1) with, for example:

- IAST, ideal adsorbed solution theory (Wirawan *et al.* 2011, van den Broeke *et al.* 1999, Kapteijn *et al.* 2000, Zhu *et al.* 2006, Skoulidas *et al.* 2003),
- PRAST, predictive real adsorbed solution theory (Erto *et al.* 2011, Sakuth *et al.* 1998),
- VST, vacancy solution theory (Harlick and Tezel 2003) or
- MPTA, multicomponent potential theory of adsorption (Monsalvo and Shapiro 2007).

In principal, any of the above methods can be applied for the description of the mixtures studied. However, VST and MPTA have been used in the literature less than IAST and PRAST. According to Shapiro and Stenby (2002), the application of MPTA has been delayed due to the computational difficulties arising in the calculation of multicomponent distribution in the potential field emitted by the adsorbent, i.e. the adsorption potential. Hence, in this work the adsorption equilibrium of mixtures is determined using the IAST, RAST and PRAST adsorption theory models. On the other hand, PRAST has not been applied before

in the description of water-alcohol mixtures. Due to the capability of PRAST to predict mixture adsorption based on pure component adsorption data, it is also investigated in the present work.

RAST

RAST is derived from the adsorbed solution theory. The adsorbed solution theory was first presented by Myers and Prausnitz (1965). It can be seen as an analogy to the well-known flash calculation of vapour-liquid equilibrium. In the adsorbed solution theory, pure component adsorption data, i.e. usually in the form of an adsorption isotherm, is utilized to predict multi-component adsorption.

The basis of the treatment of Myers and Prausnitz (1965) is that the bulk fluid phase and the adsorbed phase are in thermodynamic equilibrium. Hence, the equilibrium can be represented by the chemical potentials of the phases and the following relation applies for a system having a general bulk fluid phase and non-ideal adsorbed phase:

$$f_i^{\text{fluid}} = f_i^0(\pi, T)\gamma_i^{\text{ads}}(x_j, T, \pi)x_i^{\text{ads}}, \tag{5}$$

where $f_i^0(\pi, T)$ is the bulk fluid phase fugacity exerted by the pure component i adsorbate at the same spreading pressure and temperature as the mixture, π is the spreading pressure of the system, $\gamma_i^{\text{ads}}(x_j, T, \pi)$ is the activity coefficient of component *i* in the adsorbed phase at the spreading pressure and temperature of the mixture and x_i^{ads} is the mole fraction of component *i* in the adsorbed phase.

Depending on the bulk fluid phase description (see Table 2), different forms of Eq. (5) are obtained. In RAST, the adsorbed phase is assumed to behave non-ideally, i.e. in Eq. (5) $\gamma_i^{\text{ads}} \neq 1$. The main drawback of using RAST is that the binary parameters between different adsorbates demanded for the adsorption model are not widely available in the literature and even a slight change in the adsorbent due to the variation of its synthesis procedure generally requires a change in the adsorption model parameters (Monsalvo and Shapiro 2007). Due to the requirement of the binary adsorbate parameters, the application of RAST to predict binary adsorption behaviour based on pure component adsorption data is not possible. The activity coefficients of the adsorbed phase in RAST can be estimated using the correlations developed for vapour-liquid equilibrium (e.g. NRTL and Wilson), but the approach is not generally thermodynamically consistent since the spreading pressure is not taken into account (Sochard *et al.*

2010). The presence of the solid adsorbent imposes a potential field upon the adsorbed phase. Hence, thermodynamic consistency in the context of adsorption requires that the adsorbed phase properties, and the activity coefficients, are dependent on spreading pressure. (Myers and Prausnitz 1965, Talu and Myers 1988) Only when the system under investigation is studied at constant spreading pressure are the correlations developed for vapour-liquid equilibrium applicable. Therefore, some activity coefficient models have been introduced that incorporate the spreading pressure dependence of the activity coefficients (see Talu and Myers 1988).

IAST

IAST is a simplified version of RAST. In the original form of IAST both the bulk phase and the adsorbed phase are assumed to be ideal. Basically, the selection of an adsorbed solution theory model denotes the selection of appropriate models for the adsorbed and bulk gas phase. However, the main distinctive factor of IAST in comparison with RAST is that the adsorbed phase is assumed to be ideal, i.e. $\gamma_i^{\mathrm{ads}} = 1$. In contrast, in IAST the bulk fluid phase can be described as ideal or non-ideal as previously shown in Table 2. The usage of fugacities instead of partial pressures is generally neglected in the literature, but is necessary if the bulk fluid mixture behaves non-ideally.

PRAST

PRAST is also based on RAST. The main difference between RAST and PRAST is that, essentially, PRAST demands no binary adsorption data. In PRAST mixture adsorption is predicted based on the infinite dilution activity coefficients. The infinite dilution activity coefficients can be predicted using pure adsorption isotherm data only. This, however, means that two simplifications have to be accepted. Firstly, the adsorbate phase mole fractions of the component *i* and *j* at $x_i \to 0$ and $x_j \to 0$, respectively should be calculable using (Sakuth *et al.* 1998)

$$\lim_{x_i \to 0} x_j = \frac{q_i(\pi)}{q_j(\pi)}; \tag{6}$$

$$\lim_{x_j \to 0} x_i = \frac{q_j(\pi)}{q_i(\pi)}. \tag{7}$$

Secondly, the corresponding values of q_i at $x_i \to 0$ and $q_j \;\; x_j \to 0$, should be approximated by pure component Henry coefficients (Sakuth *et al.* 1998)

$$\mathrm{k}_H = \lim_{f_i \to 0} \left(\frac{q_i^0}{f_i} \right)_T , \tag{8}$$

where q_i^0 is the pure component loading of component *i*. Finally, with the knowledge of the Henry coefficients, the infinite dilution activity coefficients $\gamma_i^{\mathrm{ads},\infty}$ of the adsorbed phase can be obtained from the following relation:

$$\gamma_i^{\mathrm{ads},\infty}(\pi) = \frac{q_j^0(\pi)}{\mathrm{k}_H f_i^0(\pi)} . \tag{9}$$

Similarly, to the VLE and LLE applications, $\gamma_i^{\mathrm{ads},\infty}$ can be used to calculate the interaction parameters for the activity coefficient model, even though the models are not thermodynamically consistent, due to the lack of the spreading pressure dependence, as stated previously. When the Wilson activity coefficient model,

$$\ln \gamma_i^{\mathrm{ads}} = -\ln\left(\sum_{j=1}^{n} x_j \Lambda_{i,j}^{\mathrm{ads}} \right) + 1 - \sum_{k=1}^{n} \frac{x_k \Lambda_{k,i}^{\mathrm{ads}}}{\sum_{\mathrm{j}=1}^{n} x_j \Lambda_{k,j}^{\mathrm{ads}}} , \tag{10}$$

is used, the interaction parameters $\Lambda_{i,j}^{\mathrm{ads}} = \Lambda_{i,j}^{\mathrm{ads}}(T)$ can be solved simultaneously for a binary mixture from the relations (Poling *et al.* 2001):

$$\ln \gamma_1^{\mathrm{ads},\infty} = -\ln \Lambda_{1,2}^{\mathrm{ads}} - \Lambda_{2,1}^{\mathrm{ads}} + 1 ; \tag{11}$$

$$\ln \gamma_2^{\mathrm{ads},\infty} = -\ln \Lambda_{2,1}^{\mathrm{ads}} - \Lambda_{1,2}^{\mathrm{ads}} + 1 . \tag{12}$$

Next, let us investigate the selection of a mixture adsorption model based on the applications investigated in this thesis.

Gas mixtures

Adsorption of gases is generally performed at low pressures and near (or below) room temperature. However, in the gas mixture applications studied in this work the pressure is elevated. Thus, in the description of gas mixture adsorption, like that of H_2 and CO_2, bulk gas phase fugacities should be used as is illustrated in Fig. 2.

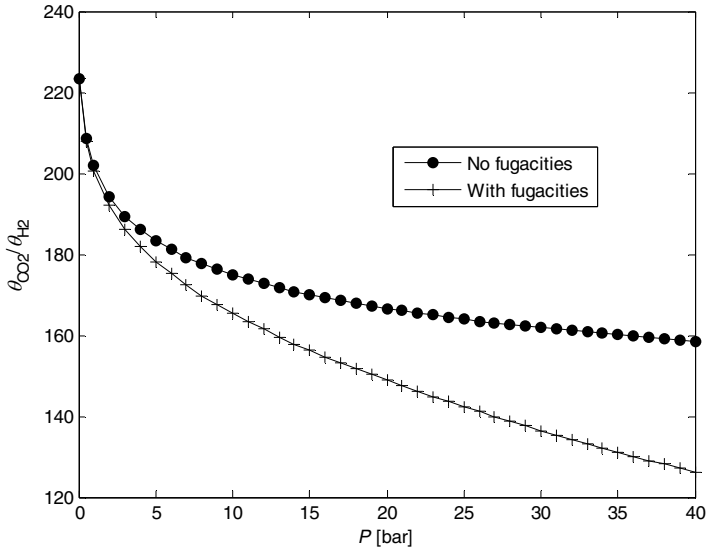

Fig. 2. Adsorption selectivity of an equimolar mixture of hydrogen and carbon dioxide at different system pressures with (+) and without (•) bulk gas phase fugacity coefficients. Both H_2 and CO_2 adsorption are described with the single-site Langmuir adsorption isotherm. The mixture adsorption was calculated with IAST. Pure component adsorption parameters were taken from Bakker *et al.* (1997). The temperature was 22°C. (Paper I, published by permission of Elsevier).

As shown in Fig. 2, the adsorption selectivity is decreased due to the introduction of the fugacity coefficients. On the other hand, it is a good first guess to assume that the adsorbed phase behaves ideally. In addition, appropriate experimental binary adsorption data is not generally available to estimate the adsorbed phase interaction parameters. In certain cases, IAST can be applied successfully. As an example, Krishna and van Baten (2011) applied IAST successfully for H_2/CO_2 adsorption at high pressure. The reference fugacity of a component can be calculated from $f_i^0(\pi) = P_i^0(\pi)$ if the reference state corresponds to the pure adsorbent spreading pressure at T (Myers and Prausnitz 1965). Thus, Eq. (5) is transformed into (Paper I):

$$Py_i\varphi_i^V = P_i^0(\pi)x_i^{\text{ads}}. \tag{13}$$

Water-alcohol mixtures

Generally, adsorption measurements with water-alcohol mixtures are performed either at low pressure with gaseous components or at normal pressure with liquid mixtures. The temperature is generally in the vicinity of room temperature. Therefore, in the description of water and alcohol (e.g. methanol or ethanol) mixtures, the bulk fluid phase is either an ideal gas mixture or a non-ideal liquid mixture in the conditions studied. In the first case, Eq. (5) is transformed into:

$$y_i P = f_i^0(\pi)\gamma_i^{\text{ads}} x_i^{\text{ads}}, \tag{14}$$

as the reference state is the pure component spreading fugacity at the given temperature. In the latter case, Eq. (5) is transformed into:

$$\gamma_i^L x_i P_i^{\text{sat}} = P_i^0(\pi) x_i^{\text{ads}}, \tag{15}$$

as the reference state is a pure component spreading pressure at a given temperature.

Common relations of the adsorbed solution theory models

In addition to the phase equilibrium relations for each of the adsorbed solution theory based models, IAST, RAST or PRAST, other relations also hold in the system. According to the adsorption solution theory, the spreading pressure of each component has to be equal:

$$\pi\left(f_i^0\right) = \pi\left(f_j^0\right),\ i \neq j\,. \tag{16}$$

The spreading pressures in Eq. (16) can be calculated from the pure component adsorption isotherms with:

$$\pi\left(f_i^0\right) = \frac{RT}{A}\int_0^{f_i^0} q_i^0(s)\, d\ln s\,, \tag{17}$$

where A is the surface area of the adsorbent and s is the integration variable. It is worth noting in Eq. (17) that the integral is evaluated from 0 to the reference state fugacity of the component. Thus, the pure component loading data should be applicable throughout the whole integration range. In practice, however, performing adsorption measurements in the region of Henry's law is not easy especially for strongly adsorbing components, which have a Henry's law region

that may be confined to extremely low pressures (Gamba *et al.* 1989). On the other hand, some adsorption models fail to describe the adsorption behaviour at low pressure. The adsorption isotherm should have a finite and positive limiting slope at low pressure. This requirement is not fulfilled with e.g. the Dubinin-Radushkevich isotherm as the limiting slope of the isotherm is zero. (Talu and Myers 1988) In contrast, the Langmuir isotherm for example has a finite limiting slope and can be used to calculate the spreading pressure. Depending on the adsorption isotherm and the reference state used, different forms for the integral are obtained as shown in Table 3.

Table 3. Analytical solutions of the integral in Eq. (17) with different adsorption isotherms.

Pure component isotherm	Reference state	$\frac{\pi\left(f_i^0\right)A}{RT}$
Langmuir	$f_i^0 = P_i^0$	$q_i^{\text{sat}} \ln\left(1+b_{L,i}P_i^0\right)$
Single-site Langmuir-Freundlich	$f_i^0 = P_i^0$	$n_{LF,i}q_i^{\text{sat}} \ln\left(1+\left[b_{LF,i}P_i^0\right]^{1/n_{LF,i}}\right)$
Dual-site Langmuir-Freundlich	$f_i^0 = f_i^0$	$n_{LFA,i}q_{A,i}^{\text{sat}} \ln\left(1+\left[b_{LFA,i}f_i^0\right]^{1/n_{LFA,i}}\right)+$ $n_{LFB,i}q_{B,i}^{\text{sat}} \ln\left(1+\left[b_{LFB,i}f_i^0\right]^{1/n_{LFB,i}}\right)$

The possibility of an analytical solution of the integral in Eq. (17) is important due to the fact that the alternative, i.e. a numerical solution, increases the solving time and may induce error in the solution.

In addition to the phase equilibrium and spreading pressure equality equations, the mole fraction summation equations have to be, naturally, fulfilled in both the bulk and adsorbed phases:

$$\sum_{i=1}^{n} y_i = 1; \tag{18}$$

$$\sum_{i=1}^{n} x_i^{\text{ads}} = 1. \tag{19}$$

Calculation of the absolute amount adsorbed

In addition to the calculation of the relative amounts of adsorbed components at the thermodynamic equilibrium, the knowledge of the absolute amounts is also an important factor e.g. in the prediction of membrane separation behaviour. The absolute amount adsorbed of each component can be calculated rigorously with (Talu and Myers 1986)

$$\frac{1}{q^{\mathrm{tot}}} = \sum_{i=1}^{n} \frac{x_i^{\mathrm{ads}}}{q_i^0} + \frac{RT}{A} \sum_{i=1}^{n} x_i^{\mathrm{ads}} \left[\frac{\partial \ln \gamma_i^{\mathrm{ads}}(\pi)}{\partial \pi} \right]_{T, x_i^{\mathrm{ads}}} . \tag{20}$$

However, if the adsorbate-adsorbate interactions prevail with respect to the adsorbate-adsorbent interaction or IAST is employed in the description of mixture adsorption, the second term on the right, i.e. $\left(\partial \ln \gamma_i^{\mathrm{ads}}(\pi)/\partial \pi\right)_{T, x_i^{\mathrm{ads}}}$, can be neglected. Hence, in that case the loadings can be calculated with:

$$\frac{1}{q^{\mathrm{tot}}} = \sum_{i=1}^{n} \frac{x_i^{\mathrm{ads}}}{q_i^0} . \tag{21}$$

Thermodynamic factor

Adsorption and the thermodynamic factor are closely related as the thermodynamic factor is dependent on the occupancy fractions. The chemical potential in the Maxwell-Stefan formulation, Eq. (3), is expressed in terms of gradients of surface occupancy by introducing the thermodynamic factor matrix. The thermodynamic factor matrix elements include the partial derivative of fugacity with respect to the occupancy fraction. From the perspective of model solution it is beneficial to have the values evaluated analytically. The analytical solution is typically possible, if pure gaseous component permeation at low pressures is studied or if the mixture adsorption is described with a suitable model, like the multicomponent Langmuir isotherm, as can be seen in Table 4.

Table 4. Thermodynamic factors for certain adsorption models.[1]

Adsorption model	Thermodynamic factor
Pure component	
Henry's law	$\Gamma_i = 1$
Langmuir	$\Gamma_i = \frac{1}{1-\theta_i}$
Tóth	$\Gamma_i = \frac{\theta_i^{-t_i}}{\theta_i^{-t_i}-1}$
Multicomponent	
Multicomponent Langmuir	$\Gamma_{i,j} = \frac{q_i^{\mathrm{sat}}}{q_j^{\mathrm{sat}}}\left(\delta_{i,j} + \frac{\theta_i}{1-\sum_{k=1}^{n}\theta_k}\right)$
IAST, RAST, PRAST	$\Gamma_{i,j} = \theta_i \frac{\partial \ln f_i^{\mathrm{fluid}}}{\partial \theta_j}$

[1] Additional thermodynamic factors for different adsorption models can be found e.g. from Lito *et al.* (2011).

In contrast, if the bulk fluid behaves non-ideally or the adsorption isotherms have been fitted with respect to partial pressure rather than with respect to fugacity, an analytical solution is not generally possible. Similarly, the usage of IAST, PRAST or RAST for mixture adsorption results in a demand for the numerical evaluation of thermodynamic factor elements. In practice, the partial derivative elements have to be calculated by solving the adsorption equilibrium several times at the given conditions.

It is also worth noting that the thermodynamic factor in common increases as the occupancy fraction of components increases as can be seen in Table 4. The exception to this rule is Henry's law, which predicts a constant value for the thermodynamic factor. Henry's law is based on the assumption that the adsorption behaviour of the adsorbates is not influenced by other adsorbates. This occurs only at the limit of zero coverage, but is sufficient in the description of weakly adsorbing molecules like hydrogen at low coverages, i.e. low pressure or high temperature. The thermodynamic factor, and naturally adsorption, is dependent on the temperature. Hence, the effects of the temperature dependence of adsorption are discussed next.

2.1.3 Temperature dependence of adsorption

The temperature dependence of adsorption isotherms is frequently represented with the adsorption equilibrium parameter, $b_i(T)$, as shown in Table 1. The temperature-dependence of b_i can be represented with the van't-Hoff type expression (Zhu *et al.* 2006):

$$b_i(T) = b_{0,i} \exp\left(-\frac{\Delta H_i^{\text{ads}}}{RT} \right), \tag{22}$$

where ΔH_i^{ads} is the heat of adsorption of component *i*. As Eq. (22) shows, the extent of the temperature dependence is related to the heat of adsorption. Since adsorption is exothermic, the value of the heat of adsorption is negative. Hence, the adsorbed loading decreases as the temperature increases. The heat of adsorption is a combination of electrostatic and dispersion energies. For small polar molecules, such as H_2O, the electrostatic energy contribution is dominant only at low coverages on zeolites. (Ruthven 1984)

In addition to the temperature dependence of b_i, the saturation loading of the adsorbate q_i^{sat} may also exhibit temperature dependency. Malek and Farooq (1996) state that the temperature dependency of saturation loading is generally thought to account for the thermal expansion of the adsorbed phase, which results in a decrease in the monolayer coverage at high temperatures. In addition, Malek and Farooq (1996) state that the exact form of the temperature dependency of saturated surface coverage is not well validated.

However, it is a widely accepted approach to assume that the saturation loading is independent of the temperature, e.g. in the studies regarding zeolite adsorption by Zhu *et al.* (2006) and Pera-Titus *et al.* (2008). In addition, Zhu *et al.* (2006) state that the saturation loading should remain constant and independent of the operating temperature. In addition, Do (1998) states that the saturation loading can be taken as constant or it can take an arbitrary form of temperaturedependency. In addition, Do (1998) takes a case example where a temperature-dependent form of the Sips isotherm value is used for propane adsorption on activated carbon at three temperatures. The fitting of the Sips isotherm parameters provides results where the saturation loading at different temperatures is in fact the same as at the reference temperature, i.e. saturation loading is independent of temperature.

Similarly, Helminen *et al.* (2000) compared different sorbents, e.g. zeolites, and isotherm models for ammonia-gas separation by adsorption. Based on their study, Helminen *et al.* (2000) concluded that the functional form of the saturation loading equation has a very small effect. Similarly, Do and Do (1997) stated that the saturation capacity is almost independent of temperature when studying the adsorption of hydrocarbons, CO_2 and hydrogen sulphide on different sorbents. Hence, in this thesis the saturation loading temperature dependence is omitted.

In contrast, the mixture adsorption models also include adsorbate-adsorbate interactions. In PRAST and RAST, the adsorbate-adsorbate interactions are described through the activity coefficients. Basically, the activity coefficients are also dependent on temperature. However, their impact on the model predictions is omitted in this thesis due to the lack of data.

The adsorbed and bulk continuous fluid phase properties differ due to the presence of the adsorbent, i.e. the solid phase, in the system. The interaction between the solid and the adsorbed phase dictate the adsorption behaviour on the surface of the adsorbent. However, quantities linked to the continuous fluid phases can be used to describe the adsorption behaviour. In the BET isotherm, the multilayer adsorption is described by considering the second and subsequent layers to behave essentially as saturated liquid. Thus, as shown in Table 1, the BET includes the ratio of fugacity to the saturation fugacity of the component *i*, $f/f_i^{\mathrm{sat}}(T)$.

Similarly, the ratio is included in Dubinin-Radushkevich (D-R) and Dubinin-Astakhov (D-A) isotherms. The basis of having the term in the D-R and D-A isotherms is the concept of the adsorption potential theory originally presented by Polanyi, and further developed by Dubinin. The theory states that the adsorbed amount of a component is a function of the adsorption potential, ε, (Ruthven 1984; Wood 2001):

$$q_i = \eta(\varepsilon) = \eta\left(-RT\ln\left[\frac{f}{f_i^{\mathrm{sat}}}\right]\right) = \eta\left(RT\ln\left[\frac{P_i^{\mathrm{sat}}(T)}{P}\right]\right). \tag{23}$$

The adsorption potential is defined as the work done by the adsorption forces in delivering the molecules from the bulk phase to the adsorbed phase on the adsorbent surface (Zhang *et al.* 2012). As can be seen from Table 1 and Eq. (23), the adsorption potential of a component decreases as the system pressure approaches the vapour pressure of the component, and at the saturation pressure the work is decreased to zero. The adsorption potential can be used to predict the

adsorption at different temperatures once the characteristic curve is obtained (Zhang *et al.* 2012). The characteristic curve is defined here as the curve formed when q_i is plotted versus $RT\ln\left(f_i^{\text{sat}}/f\right)$. According to the Polanyi theory, and the assumptions included in the theory, the characteristic curve should capture the temperature dependence of adsorption. This is theoretically possible only if the energy of adsorption is entirely formed from temperature-independent van der Waals forces, and the entropy term contribution to the adsorption potential is negligible. These terms are generally fulfilled only by nonpolar systems. (Ruthven 1984) Nevertheless, the ratio of fugacity to the saturation fugacity of the component i, $f/f_i^{\text{sat}}(T)$, can be applied even to the description of the temperature dependence of adsorption in a number of polar systems, as shown in Paper IV.

2.1.4 Surface diffusivity models

Generally, it can be stated that the surface diffusivity of a component is dependent on the prevailing conditions, temperature and pressure (fugacity), and on the interaction of:

- the adsorbent, i.e. surface, and the adsorbate, i.e. the diffusing component *i*,
- the molecules of the diffusing component *i*, and
- the molecules of the diffusing components *i* and *j*.

Due to these interactions, the description of surface diffusivity in the adsorbent is not simple. Firstly and principally, creating a model to predict mixture surface diffusion, demands reliable data on pure component diffusion from zero coverage to saturation loading. Then a suitable mixing rule is required to predict binary- and multi-component diffusion in the adsorbent. On the other hand, the surface diffusion is dependent on the adsorption behaviour through the occupancy fractions. Therefore, the Maxwell-Stefan formulation for surface diffusion, Eq. (1), on a zeolite introduces two different Maxwell-Stefan diffusivities, $D_{i,j}^{\text{s}}$ and D_i^{s}. $D_{i,j}^{\text{s}}$ describes the adsorbate correlation effects, whereas D_i^{s} describes the adsorbate-adsorbent interaction.

Adsorbate-adsorbent interaction

The surface diffusion is an activated process and for the movement of a molecule it has to cross the potential barrier (Krishna 1990; Krishna and Paschek 2000).

Thus, the temperature dependence of D_i^s can be represented with the Arrhenius dependence:

$$D_i^s(T) = D_{0,i}^s \exp\left(-E_{a,i}/RT\right), \tag{24}$$

where $E_{a,i}$ is the activation energy of component *i*. The dependence of surface diffusion on bulk phase fugacities is indirectly induced through the occupancy fractions and the adsorption equilibrium. Mechanistically, the Maxwell-Stefan diffusivity D_i^s can be related to the displacement of the adsorbed molecular species, λ, and the jump frequency, ν, which can be seen to be dependent on the coverage of the diffusing components (Krishna and Paschek 2000; Reed and Ehrlich 1981):

$$D_i^s = \frac{1}{z}\lambda^2 \nu\,, \tag{25}$$

where z is the number of neighbour sites. It is expected that the jump frequency will decrease as a function of occupancy. In addition, if it is assumed that one molecule can move from one site to another only if the site is free, the probability of a molecule moving is a function of the number of unoccupied sites. Therefore, Maxwell-Stefan diffusivity D_i^s can be presented as (Krishna and Paschek 2000):

$$D_i^s = D_i^s(0)\kappa(\theta_V)\,, \tag{26}$$

where $D_i^s(0)$ is the Maxwell-Stefan diffusivity in the limit of zero loading and $\kappa(\theta_V)$ is a function of the unoccupied site fraction. Hence, if the diffusivity is assumed to be independent of the occupancy fraction, $\kappa(\theta_V)=1$ and Eq. (26) is transformed into:

$$D_i^s = D_i^s(0)\,. \tag{27}$$

Eq. (27) is typical for weakly confined molecules in zeolite hosts (Krishna and Baur 2003). Skoulidas and Sholl (2002) have observed that Eq. (27) is valid for He, Ar, and Ne in MFI. The assumption of having D_i^s independent of occupancy, i.e. the component behaves according to Eq. (27), is frequently employed in the literature (see e.g. Wirawan *et al.* 2011; Kapteijn *et al.* 2000; Zhu *et al.* 2006; Krishna and Paschek 2000). Generally, the reason for employing the weak confinement scenario is the lack of reliable data regarding surface diffusivity loading dependence. In contrast, for strongly confined molecules, the loading dependency can be described with (Krishna *et al.* 2004):

$$D_i^s = D_i^s(0)(1-\theta_i). \tag{28}$$

Occupancy dependencies that are even more severe than Eq. (28) have been observed. According to Krishna and Paschek (2000), the experimental data of *n*-heptane in 13X appears to follow:

$$D_i^s = D_i^s(0)(1-\theta_i)^8. \tag{29}$$

Reed and Ehrlich (1981) have proposed a more general occupancy dependence model, describing the diffusion of interacting atoms on a square lattice of binding sites. In their approach, adsorbed atoms interact with each other through the nearest adatoms only. Finally, a relation is formed for the loading dependency of Maxwell-Stefan diffusivity:

$$D_i^s = D_i^s(0)\frac{(1+\varepsilon_i)^{z-1}}{(1+\varepsilon_i/\eta_i)^z}, \tag{30}$$

where $\eta_i = \exp(\delta E_i/RT)$, $\varepsilon_i = (\beta_i - 1 + 2\theta_i)\eta_i / [2(1-\theta_i)]$, and $\beta_i = \sqrt{1-4\theta_i(1-\theta_i)(1-1/\eta_i)}$.

It is worth noting that unless the system energy is significantly changed as the adatom is added to a neighbouring site, δE_i will become vanishingly small in Eq. (30). Thus, both η_i and β_i are equal to 1. Hence, by substituting η_i and β_i in Eq. (30), the occupancy dependence in Eq. (30) is simplified to the strong confinement scenario presented in Eq. (28). In addition, the weak confinement scenario Eq. (27) cannot be obtained with any combination of the parameters. This is due to the fact that the movement of an adatom is dependent on the vacancy (Krishna *et al.* 2004). Krishna and van Baten (2005) performed KMC (Kinetic Monte Carlo) simulations to model the surface diffusivity loading dependence in MFI using the Reed-Ehrlich approach. Lee (2007) predicted CO_2 and CH_4 permeation in silicalite-1 based on the occupancy fraction dependence of Reed-Ehrlich. Recently, Krishna and van Baten (2011) used molecular dynamics simulation data to estimate the unknown parameters in the Reed-Ehrlich approach and thereon predicted both single and binary surface diffusivities for a number of gaseous components, including CO_2 and H_2, in different adsorbent structures. Eqs. (27) and (28) were applied in Paper I.

Recently, van den Bergh *et al.* (2009) proposed the relevant site model for describing the occupancy dependence of diffusion in zeolites. In their model, the sites are divided into sites that are relevant and irrelevant for diffusion. The distinction of the sites can be performed e.g. based on the categorization of

window and cage sites as relevant and irrelevant sites, respectively. The Maxwell-Stefan diffusivity is represented with the relevant site model with (van den Bergh *et al.* 2009):

$$D_i^s = D_i^s(0)(1-\theta_i)\frac{\theta_i^*}{\theta_i}\frac{b_{L,i}}{b_{L,i}^*}, \tag{31}$$

where $b_{L,i}^*$ represents the relevant site adsorption equilibrium constant for the single-site Langmuir isotherm, and θ_i^* is the relevant site occupancy fraction. As can be seen in Eq. (31), when the relevant site occupancy fraction equals the total occupancy fraction, the strong confinement scenario is discovered. The occupancy dependence of D_i^s with different scenarios is illustrated in Fig. 3.

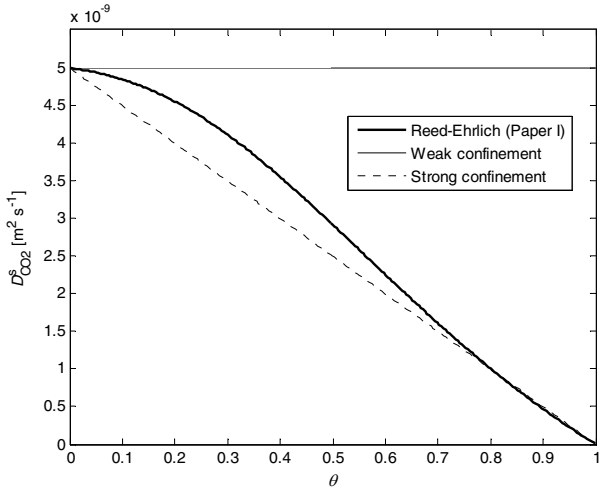

Fig. 3. Maxwell-Stefan surface diffusivity of CO_2, $D_{CO_2}^s$, as a function of occupancy fraction. $D_{CO_2}^s(0) = 4.9904 \cdot 10^{-9}\ m^2\ s^{-1}$. The zero-loading surface diffusivity value is taken from Paper I.

Fig. 3 shows that the surface diffusivities are, naturally, the same at zero coverage. On the other hand the strong confinement scenario and the Reed-Ehrlich scenario coincide as the occupancy fraction reaches 1. In contrast, the weak confinement scenario is constant throughout the occupancy fraction space. This is not a feasible scenario that is usable in a general case, as the movement of a molecule from one site to another is dependent on the number of vacant neighbouring sites. Thus, the application of the weak confinement scenario, e.g. to the rigorous description of CO_2 surface diffusivity on a wide occupancy fraction domain, is

not appropriate, as was concluded in Paper I. The extent of the effect of the different scenarios on the permeation of CO_2 on an MFI-type high-silica zeolite supported membrane can be seen in Fig. 4.

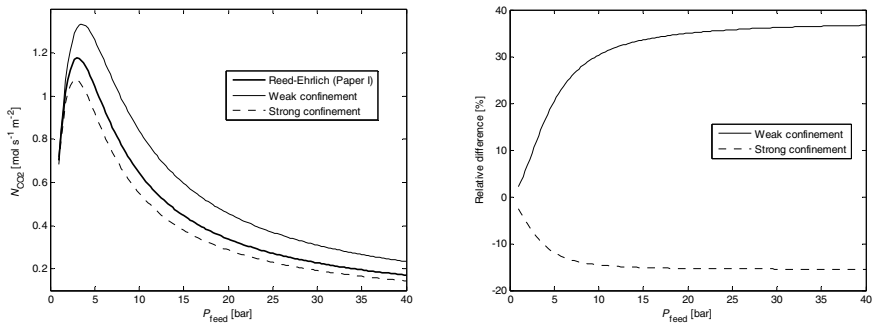

a) b)

Fig. 4. a) Permeation flux of CO_2 as a function of feed pressure with different surface diffusivity scenarios and b) the relative difference between the Reed-Ehrlich model and the weak and strong confinement scenarios. Pressure difference across the membrane is 0.999 bar. $T = 22\ ^{o}\mathrm{C}$ **. The membrane model used is presented in Paper I.**

As can be seen in Fig. 4a, the scenario selected for surface diffusivity has a clear influence on the predicted permeation flux of CO_2. The relative difference between the scenarios increases as the occupancy fraction increases, as shown in Fig. 4b. It is also worth noting that the permeation flux profiles approach each other at low pressure as is to be expected due to the same $D_{\mathrm{CO}_2}^{\mathrm{s}}(0)$ value of the scenarios.

As a whole, it can be stated that there are multiple scenarios that the surface diffusivity of a component may follow. The determination of the appropriate scenario for each case is dependent both on the degree of confinement within the adsorbent, and on the characteristics of the adsorbate *i* - adsorbate *i* interactions (Krishna and Baur 2003; Skoulidas *et al.* 2003).

Adsorbate-adsorbate interaction

The binary exchange coefficients $D_{i,j}^{\mathrm{s}}$, or adsorbate interaction diffusivities, can be interpreted as the capability of an adsorbate *j* to replace an adsorbate *i* on a sorption site. Generally, the consequence of this interaction is that the faster diffusing adsorbate is slowed down by the slower moving adsorbate as

demonstrated in Paper I. Even mutual slowing down effects have been observed with water-methanol and water-ethanol mixtures (Krishna and van Baten 2010c). However, the literature models assume that the mutual slowing effects can be neglected, which has been shown to apply e.g. in gas mixtures.

Krishna and van Baten (2011) noticed that based on molecular dynamics simulations, regardless of the topology of the studied adsorbent, the correlation effects increase with increasing pore concentrations, i.e. the magnitude of $D_{i,j}^{\mathrm{s}}$ is reduced significantly. In addition, the movement of the slower moving adsorbate is accelerated. In the case of a single adsorbed component diffusing, D_i^{s} is equivalent to the 'corrected' diffusivity $D_{i,j}^{\mathrm{s}}$ (Skoulidas *et al.* 2003). This can also be deduced from the Maxwell-Stefan formulation, Eq. (1), for single-component permeation.

Because there are no fundamental models as yet to predict the binary exchange coefficients, $D_{i,j}^{\mathrm{s}}$ is generally estimated with different models (Krishna and Paschek 2000). The literature attempts to describe binary exchange coefficients can be summarized to include the following dependence:

$$D_{i,j}^{s} = \eta\left(T, q_i^{\mathrm{sat}}, q_j^{\mathrm{sat}}, D_{i,i}^{\mathrm{s}}, D_{j,j}^{\mathrm{s}}, \frac{\theta_i}{\theta_i+\theta_j}, \frac{\theta_j}{\theta_i+\theta_j}\right). \tag{32}$$

As can be seen in Eq. (32), the binary exchange coefficients are dependent on the saturation loadings, the self-exchange coefficients of the pure species, i.e. $D_{i,i}^{\mathrm{s}}$ and $D_{j,j}^{\mathrm{s}}$, and their compositions in the adsorbed mixture at a given temperature. Note that the Onsager reciprocal relations demand that $D_{i,j}^{\mathrm{s}} = D_{j,i}^{\mathrm{s}}$ (Krishna and Paschek 2002). In practice a relationship that strictly follows Eq. (32) is difficult to apply, due to the self-exchange coefficient dependence of the relation.

Self-exchange coefficients

Self-exchange coefficients can be determined based on D_i^{s} and $D_{i,\mathrm{self}}$, providing that they are known independently (Skoulidas *et al.* 2003). Krishna and Paschek (2002) derived a relation between D_i^{s} and $D_{i,\mathrm{self}}$ for a binary mixture with tagged and untagged species, both having identical D_i^{s}:

$$D_{i,\mathrm{self}} = \frac{1}{\dfrac{1}{D_i^{\mathrm{s}}} + \dfrac{\theta_i}{D_{i,i}^{\mathrm{s}}}}. \tag{33}$$

Next, based on the data on the self-diffusivity $D_{i,\mathrm{self}}$ and surface diffusivity D_i^{s} of the species the self-exchange coefficients $D_{i,i}^{\mathrm{s}}$ can be calculated. Skoulidas *et al.* (2003) noticed that the dependence follows the empirical expression:

$$D_{i,i}^{\mathrm{s}} = D_i^{\mathrm{s}}\left[\alpha_i \exp\left(-\beta_i\theta_i\right)\right], \tag{34}$$

where α_i and β_i are fitted parameters dependent on both the component *i* and the topology of the particular adsorbent. The ratio $D_i^{\mathrm{s}}/D_{i,i}^{\mathrm{s}}$ can be seen as a measure of the degree of correlation for the unary diffusion of component *i*. $D_i^{\mathrm{s}}/D_{i,i}^{\mathrm{s}}$ increases as the pore concentration increases, i.e. the movement of individual molecules become increasingly correlated. (Krishna and van Baten 2011) Later on, e.g. Krishna and van Baten (2005) and Lee (2007) applied Eq. (34) in the description of permeation in zeolites. Recently, based on MD-simulated data, Krishna and van Baten (2011) fitted the degree of correlation for unary diffusion with the expression

$$\frac{D_i^{\mathrm{s}}}{D_{i,i}^{\mathrm{s}}} = a_i + b_i\theta_i + c_i\theta_i^2\,, \tag{35}$$

where a_i, b_i and c_i are fitted constants dependent on the studied component *i* and the adsorbent properties. The degree of correlation can be viewed in detail in Fig. 5.

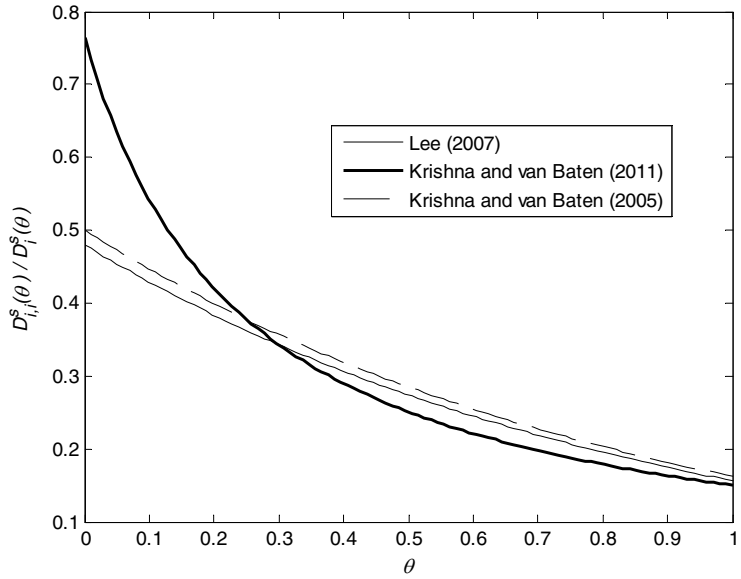

Fig. 5. $D^{\mathrm{s}}_{i,i}(\theta) \approx D^{\mathrm{s}}_{i}(\theta)$ **of CO_2 in MFI at the temperature of 300 K as a function of occupancy fraction.** $q^{\mathrm{sat}}_{\mathrm{CO_2}} = 5.1876 \ \mathrm{mol\ kg^{-1}}$**. The literature models are based on MD simulation studies.**

As shown in Fig. 5, $D^{\mathrm{s}}_{i,i}(\theta) / D^{\mathrm{s}}_{i}(\theta)$ decreases as the occupancy fraction of CO_2 increases. The decrease means in turn that the degree of correlation increases as the pore concentration increases, as expected. The practical consequence of the decrease in the ratio is that the predicted binary exchange coefficients have smaller values and the movement of the components is slowed down even from the values calculated based on D^{s}_{i}. In addition, Fig. 5 shows that the ratio approaches the value of 1 as the occupancy fraction approaches zero. On the other hand, it is common that the ratio cannot be determined due to the insufficiency of available data on the system. Therefore, the approximation $D^{\mathrm{s}}_{i,i}(\theta) \approx D^{\mathrm{s}}_{i}(\theta)$ is frequently applied.

Binary exchange coefficients

Binary correlation effects can be predicted with relationships originally developed for the description of diffusion in bulk liquid mixtures by Vignes (1966):

$$D_{i,j} = \left(D^{\infty}_{i,j}\right)^{x_j} \left(D^{\infty}_{j,i}\right)^{x_i}, \tag{36}$$

where $D_{i,j}^{\infty}$ and $D_{j,i}^{\infty}$ are the infinite dilution diffusion coefficient of *i* and *j*, respectively. Similarly, inspired by the bulk liquid diffusivity descriptions, linear and square root interpolation formulas for surface diffusion binary exchange coefficients have also been suggested (Krishna and Paschek 2002). However, the linear and square root interpolation formulas have not been applied widely in conjunction with surface diffusion.

In the Vignes relationship, Eq. (36), the binary exchange diffusivities are exponentially related to the mole fraction of each component. However, the mole fraction is not very suitable as a measure of the adsorbed species proportion on an adsorbent. Thus, Krishna (1990) generalized the Vignes relationship to the diffusion of adsorbed species with the usage of occupancy fractions instead of mole fractions:

$$D_{i,j}^{\mathrm{s}} = \left[D_i^{\mathrm{s}}\right]^{\theta_i/(\theta_i+\theta_j)}\left[D_j^{\mathrm{s}}\right]^{\theta_j/(\theta_i+\theta_j)}. \tag{37}$$

On the other hand, if the saturation loading of each component is equal or mole fractions are usable, Eq. (37) transforms into (Skoulidas *et al.* 2003):

$$D_{i,j}^{\mathrm{s}} = \left[D_i^{\mathrm{s}}\right]^{q_i/(q_i+q_j)}\left[D_j^{\mathrm{s}}\right]^{q_j/(q_i+q_j)}. \tag{38}$$

Assuming that we have obtained the self-exchange diffusivities $D_{i,i}^{\mathrm{s}}$ independently from Maxwell-Stefan diffusivities D_i^{s}, a relationship based on Eq. (32) can be formulated as proposed by Skoulidas *et al.* (2003):

$$q_j^{\mathrm{sat}} D_{i,j}^{\mathrm{s}} = \left[q_j^{\mathrm{sat}} D_{i,i}^{\mathrm{s}}\right]^{q_i/(q_i+q_j)}\left[q_i^{\mathrm{sat}} D_{j,j}^{\mathrm{s}}\right]^{q_j/(q_i+q_j)}. \tag{39}$$

Skoulidas *et al.* (2003) successfully applied the interpolation formula, Eq. (39), to predict the diffusivities of a mixture of CH_4/CF_4. Recently, van den Bergh *et al.* (2010) applied Eq. (39) in conjunction with the relevant site model to model the diffusion of light gases in zeolites. It is worth noting that Eq. (39) returns to the form of Eq. (38) if the saturation loadings of the perspective components are equal and $D_{i,i}^{\mathrm{s}} = D_i^{\mathrm{s}}$. The main drawback of Eq. (39) in general is that the saturation loadings are required. In Paper I, a Vignes-type interpolation formula including the self-exchange correlations:

$$D_{i,j}^{\mathrm{s}} = \left[D_{i,i}^{\mathrm{s}}\right]^{\theta_i/(\theta_i+\theta_j)}\left[D_{j,j}^{\mathrm{s}}\right]^{\theta_j/(\theta_i+\theta_j)} \tag{40}$$

was used due to the availability of data on the degree of correlation for unary diffusion from Krishna and van Baten (2011). Krishna and van Baten (2009, 2011)

also proposed that the mole fractions could be used instead of occupancy fractions in Eq. (40). The differences between the predictions of the proposed binary exchange correlation formulas can be observed in Fig. 6.

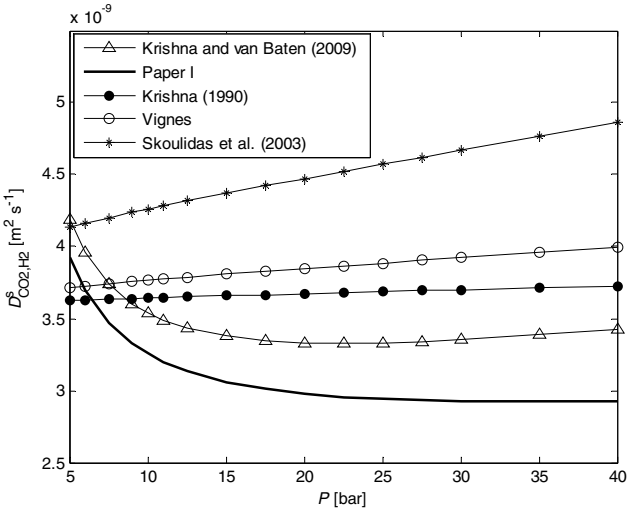

Fig. 6. Binary exchange surface diffusivities with different literature formulas for diffusion of equimolar bulk phase mixtures of H_2 and CO_2 at 23°C as a function of the bulk gas phase pressure. The adsorption and diffusivity parameters used are from Paper I.

As can be seen in Fig. 6, the selection of the binary exchange formula is relevant, especially at high pressure. However, all the formulas predict surface diffusivities with the same order of magnitude. The reason for this is the strong effect of CO_2 on the binary exchange diffusivity. The proportion of CO_2 adsorbed is clearly higher than the proportion of H_2. Thus, $D^{s}_{CO_2,H_2} \approx D^{s}_{CO_2}$ or $D^{s}_{CO_2,H_2} \approx D^{s}_{CO_2,CO_2}$ depending on the formula in question. Essentially, self-exchange diffusivities decline as pressure increases, but the adsorption equilibrium shifts at the same time slightly towards preferring hydrogen adsorption in comparison with carbon dioxide. This interplay between the effects means that in Fig. 6 the trends between the formulas differ, i.e. also qualitatively. As a whole, the usage of self-exchange diffusivities is a more theoretically sound approach. Nevertheless, the selection between the formulas using self-exchange diffusivities is not self-evident, and demands further investigation in the future.

Although the above mentioned models for *predicting* the binary exchange diffusivities of the adsorbate have been shown to apply to the description of a multitude of mixtures, there is still work to be done in different applications. One important application, where the models fail, is the surface diffusion of water-alcohol mixtures as shown by Krishna and van Baten (2010a, 2010b, 2010c). The failure is due to the hydrogen bonding between water-alcohol molecules.

2.2 Liquid-liquid phase separation

Modelling liquid-liquid phase separation can be performed starting from the description of the liquid-liquid equilibrium. The phase equilibrium can be described with the thermodynamic potentials. A general liquid-liquid equilibrium problem consists of finding the correct number and types of phases and their corresponding equilibrium compositions such that the Gibbs free energy of the system is at the minimum. A considerable number of methods and algorithms have been formulated to solve the phase equilibrium problem. Generally, the basis of the algorithms is to solve a sequence of sub-problems. The algorithms can be separated into two groups: equation-solving and Gibbs free energy minimization approaches (Wakeham and Stateva 2004; Rangaiah 2001).

2.2.1 Equation-solving approach

The equation-solving approaches solve a set of nonlinear equations, based on the component mass balances and phase equilibrium relations. In practice, the equation set formed in the equation-solving approach describes the liquid-liquid phase separation equipment operating isothermally or/and it is assumed that the energy changes attributed to the phase changes are negligible.

Let us first assume a mixture of n components with molar amounts (N_1,N_2,...,N_n). In addition, let us assume that the mixture may split into F liquid phases. Then the following group of equations can be solved to obtain the equilibrium compositions and relative amounts of the phases at temperature T and pressure P:

$$\sum_{j=1}^{F} \beta_j x_{i,j} = N_i \ , \ i = 1,2,..., n, \tag{41}$$

$$x_{i,1}\gamma_{i,1}^{L} = x_{i,2}\gamma_{i,2}^{L} = ... = x_{i,F}\gamma_{i,F}^{L} \ , \ i = 1,2,...,n, \tag{42}$$

$$\sum_{i=1}^{n} x_{i,j} = 1, j = 1,2,..., F, \tag{43}$$

where β_j is the total amount of phase j. It is worth noting that the activity coefficients are temperature-dependent. Thus, Eqs. (41)-(43) have to be solved again or an energy balance for the system has to be introduced, if the energy changes related to the phase appearance or disappearance are significant and the temperature of the system changes significantly. On the other hand, Eqs. (41)-(43) fulfil only the *necessary* conditions of equality of the chemical potential of every component in each phase. Hence, Eqs. (41)-(43) are always fulfilled when the composition of each phase is the same, i.e. even when the actual phase configuration and compositions are different. However, they do not ensure that the *sufficient* condition of phase equilibrium is satisfied (Baker *et al.* 1982; Cairns and Furzer 1990; Rangaiah 2001; Michelsen and Mollerup 2007). The *sufficient* condition refers here to the fact that the phase configuration of the system is fulfilled only when the Gibbs energy of the resulting system is at minimum.

In practice, the insufficiency of the approach may signify that the solved compositions and relative amounts do not correspond to the actual phase configuration. In addition, the straightforward application of the equation set in Eqs. (41)-(43) demands knowledge of the possible number of phases. Therefore, the approach is generally used only in conjunction with short-cut calculation routines and when a considerable amount of problem-dependent data is available.

2.2.2 Minimization of Gibbs energy

The second approach of minimizing the Gibbs energy yields both the *necessary* and *sufficient* conditions of phase equilibrium (Tolsma and Barton 2000a). Thus, the Gibbs free energy minimization approach is more preferable than the equation-solving approach in the robust evaluation of phase equilibrium conditions. The core of the Gibbs energy minimization approaches is to evaluate the multicomponent and multiphase equilibrium based on the global minimum of the Gibbs free energy of the system (Baker *et al.* 1982). Fundamentally, there are two routes that can be followed to obtain or verify that an equilibrium solution corresponds to the global minimum of the Gibbs free energy. The two optimization problems associated with these approaches are the direct minimization of the Gibbs free energy and the minimization of the tangent plane distance function (TPDF). In this thesis, the minimization of TPDF is considered.

Therefore, only issues regarding TPDF are discussed in depth. More can be found on the direct minimization of the Gibbs free energy e.g. in the review by Wakeham and Stateva (2004).

2.2.3 Phase stability analysis

The stability of a phase can be determined by using the Gibbs tangent plane criterion (Michelsen 1982). The mixture is stable at temperature T and pressure P if and only if the total Gibbs energy of the system is at its global minimum. Let us consider a phase with a composition $\mathbf{z}$ and chemical potential $\mu(\mathbf{z})$. Assume that an infinitesimal amount δe of a new phase of molar composition $\mathbf{x}$ and chemical potential $\mu(\mathbf{z})$ is formed. The Gibbs energy change δG related with the formation of the new phase is then (Michelsen and Mollerup 2007):

$$\delta G = \delta e \sum_{i=1}^{n} x_i \left(\mu_i(\mathbf{x}) - \mu_i(\mathbf{z}) \right). \tag{44}$$

One *necessary* and *sufficient* condition for the stability of a phase with the composition $\mathbf{z}$ is that $\delta G \geq 0$ for any positive δe and for any composition $\mathbf{x}$ (Michelsen and Mollerup 2007), i.e.

$$\delta G(\mathbf{x}) = \sum_{i=1}^{n} x_i \left(\mu_i(\mathbf{x}) - \mu_i(\mathbf{z}) \right) \geq 0 . \tag{45}$$

Note that $x_i \in [0,1]$ and $\sum x_i = 1$. As it is more convenient to use fugacities instead of chemical potential and excess Gibbs energy models are applied, Eq. (45) can be reformulated into the form:

$$D(\mathbf{x}) = \sum_{i=1}^{n} x_i \left(\ln x_i + \ln \gamma_i^L(\mathbf{x}) - \ln z_i - \ln \gamma_i^L(\mathbf{z}) \right), \tag{46}$$

where $D(\mathbf{x}) = \delta G(\mathbf{x}) / RT$ is the tangent plane distance function (TPDF). In other words, the Gibbs tangent plane criterion states that the phase is unstable if its molar Gibbs mixing energy surface, $m(\mathbf{x})$, is below the tangent plane to the surface at any composition (Michelsen 1982). Schematically the analysis can be viewed for a water-aniline mixture in Fig. 7.

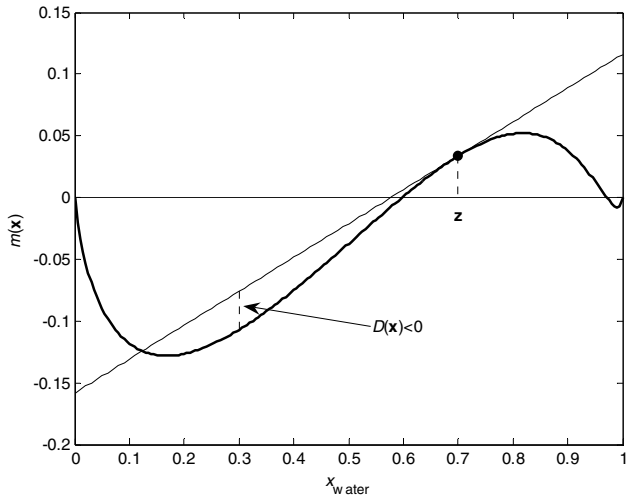

a)

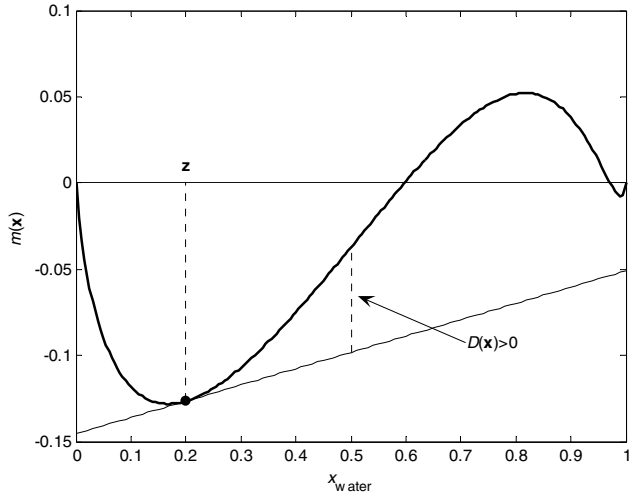

b)

Fig. 7. Gibbs mixing surface and tangent plane to the surface of a water (1) – aniline (2) mixture at a) $\mathbf{z} = [0.7 \;\; 0.3]$ **and b)** $\mathbf{z} = [0.2 \;\; 0.8]$.

As shown in Fig. 7, the Gibbs mixing surface falls below the tangent plane in Fig. 7a. Instead, in Fig. 7b the tangent plane is below the Gibbs mixing surface at all compositions. Thus, according to the tangent plane distance criterion, the mixture is unstable in Fig. 7a and stable in Fig. 7b at the given *T* and *P*. Numerically, the

phase stability can be analyzed by checking if the distance of the tangent plane to the molar Gibbs mixing energy surface, $D(\mathbf{x})$:

$$D(\mathbf{x}) = m(\mathbf{x}) - m_0 - \sum_{i=1}^{n} \left(\frac{\partial m}{\partial x_i} \right)_0 (x_i - z_i) \tag{47}$$

is negative (Tessier *et al.* 2000). Therefore, a phase with composition **z** is unstable in these conditions and will split into two or more phases. In Eq. (47), **x** is the mole fraction vector, n is the number of components and $m(\mathbf{x})$ is the reduced Gibbs energy of mixing. The subscript zero stands for the evaluation at $\mathbf{x} = \mathbf{z}$. The reduced Gibbs energy of mixing is given by:

$$m(\mathbf{x}) = \sum_{i=1}^{n} x_i \ln x_i + G^E(\mathbf{x}) = \sum_{i=1}^{n} x_i \ln\left(\gamma_i^L x_i\right) \tag{48}$$

as excess Gibbs energy models are used. The first term on the right in Eq. (48) is convex and the second term, i.e. the contribution of the mixture non-ideality, is nonconvex. The activity coefficient values in Eq. (48) can be calculated with different excess Gibbs energy, i.e. activity coefficient, models such as NRTL and UNIQUAC. When using NRTL, the excess Gibbs energy is evaluated with (Tessier *et al.* 2000)

$$G^E(\mathbf{x}) = \sum_{k=1}^{n} x_k \frac{\left(\overline{\tau G}\right)_k}{\overline{G}_k}, \tag{49}$$

where the weighted molar averages $\left(\overline{\tau G}\right)_k$ and $\overline{G}_k$ are given by:

$$\left(\overline{\tau G}\right)_k = \sum_{i=1}^{n} \tau_{i,k} G_{i,k} x_i, \tag{50}$$

$$\overline{G_k} = \sum_{i=1}^{n} G_{i,k} x_i, \tag{51}$$

in which $G_{i,k} = \exp\left(-\alpha_{i,k}\tau_{i,k}\right)$. $\alpha_{i,k}$ and $\tau_{i,k}$ are experimentally defined parameters of the NRTL activity coefficient model. Fig. 8 presents an example of $m(\mathbf{x})$ for a liquid-liquid equilibrium ternary component system.

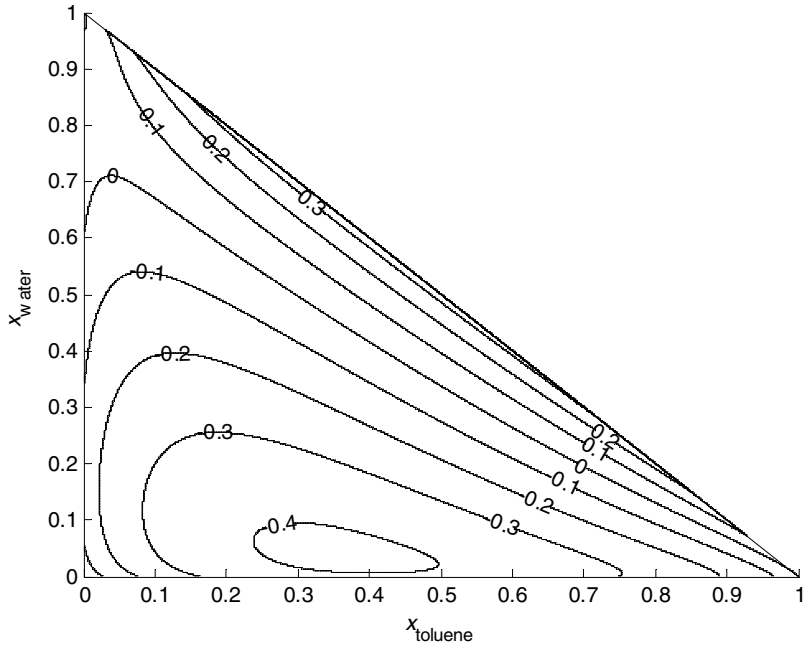

Fig. 8. Reduced Gibbs energy of mixing for Case 3 in Paper V. $x_{\text{aniline}} = 1 - x_{\text{water}} - x_{\text{toluene}}$.

The main difficulties in the minimization of $D(\mathbf{x})$ arise in general from the non-convex term in Eq. (48). The Gibbs tangent plane criterion is generally checked by minimizing $D(\mathbf{x})$ with a mole fraction restriction. This minimization problem can either be solved directly or by solving an equivalent set of nonlinear equations for the stationary points of $D(\mathbf{x})$ (Tessier *et al.* 2000). An example of the $D(\mathbf{x})$ surface can be seen in Fig. 9.

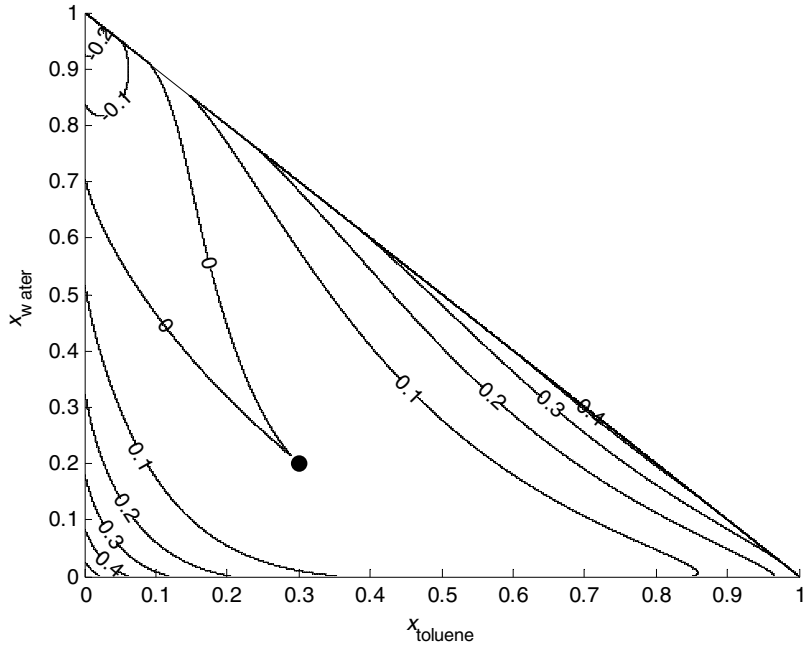

Fig. 9. The tangent plane distance contour plot for Case 3 in Paper V. The mixture studied is $\mathbf{z} = [0.29989,\ 0.20006,\ 0.50005]$ and marked with '•'.

In Fig. 9 with certain test compositions, $D(\mathbf{x})$ is negative, indicating that the mixture at composition $\mathbf{z}$ is unstable and will split into two or more phases depending on the subsequent flash calculations. Hence, in many cases the knowledge of phase splitting can be obtained efficiently with local solving methods. However, in order to obtain feasible estimates for the individual phase compositions for the subsequent flash calculations, at least the global minimum of D should be sought, which cannot be ascertained with local solving methods.

The global minimum of TPDF and all the other roots of the problem can be solved by directly minimizing the TPDF or creating a set of nonlinear equations for the stationary points of $D(\mathbf{x})$. Schematically, the solution of the stationary points can be seen in Fig. 10.

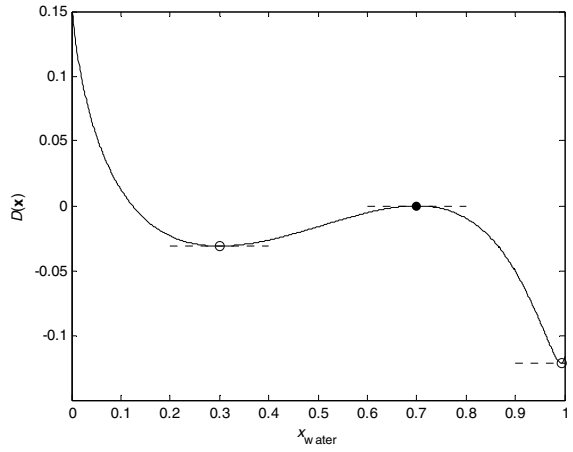

a)

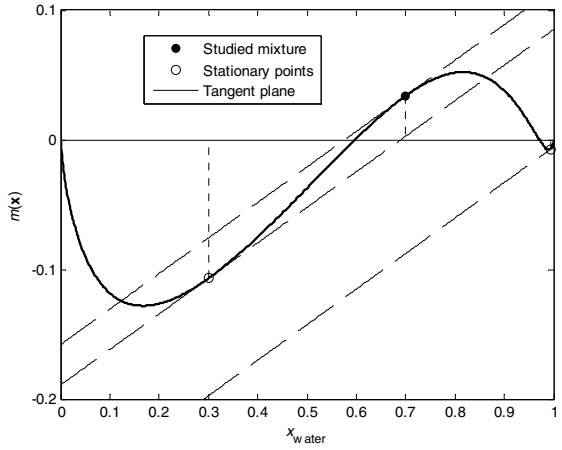

b)

Fig. 10. a) Tangent plane distance function and b) Gibbs mixing surface of a water-aniline mixture $z = [0.7 \;\; 0.3]$ including stationary points and respective tangent planes.

A number of issues can be seen in Fig. 10. The binary mixture of water and aniline is unstable at the studied composition because the tangent plane distance function value is negative at two stationary points in Fig. 10a. Note that only one stationary point with a negative $D(\mathbf{x})$ is required to verify instability. Secondly, the studied mixture is a local maximum on the $D(\mathbf{x})$ curve as can be seen in Fig.

10a. Therefore, the instability of the studied mixture can be determined with the evaluation of $D(\mathbf{x})$ at a composition infinitesimally close to the composition. However, this evaluation will not supply a good initial guess for the subsequent phase equilibrium calculations. Instead, the stationary points with a negative $D(\mathbf{x})$ value can be used to initiate the phase equilibrium calculations efficiently.

To obtain the locations of all the stationary points, the following equation set is solved (Tessier *et al.* 2000):

$$\left[\left(\frac{\partial m}{\partial x_i}\right)-\left(\frac{\partial m}{\partial x_n}\right)\right]-\left[\left(\frac{\partial m}{\partial x_i}\right)-\left(\frac{\partial m}{\partial x_n}\right)\right]_0 = 0\,,\ i = 1,\ldots,\ n-1; \tag{52}$$

$$1-\sum_{i=1}^{n} x_i = 0\,. \tag{53}$$

It is also noteworthy that at all the stationary points the tangent planes evaluated on the basis of $m(\mathbf{x})$ are parallel in Fig. 10b as expected, when applying Eqs. (52)-(53) for a binary mixture. The set of equations, Eqs. (52)-(53), can be reformulated by using Eq. (48) into

$$\ln\left(\frac{x_i}{x_n}\right)-\ln\left(\frac{z_i}{z_n}\right)+s_i(\mathbf{x})-s_i(\mathbf{z}) = 0\,,\ i = 1,\ldots,\ n-1; \tag{54}$$

$$1-\sum_{i=1}^{n} x_i = 0\,, \tag{55}$$

where $s_i(\mathbf{x})$ is represented by:

$$s_i(x) = \frac{(\overline{\tau G})_i}{\overline{G}_i}-\frac{(\overline{\tau G})_n}{\overline{G}_n}+\sum_{k=1}^{n} x_k\left[\frac{\tau_{i,k}G_{i,k}-\tau_{n,k}G_{n,k}}{\overline{G}_k}+\frac{(\overline{\tau G})_k\left(-G_{i,k}+G_{n,k}\right)}{\overline{G}_k^2}\right], \tag{56}$$

if NRTL is used to describe the liquid phase activity coefficients. The equation set, Eqs. (54) and (55), has a trivial root, which corresponds to the composition of the inspected mixture ($\mathbf{x} = \mathbf{z}$). The equation set may also have multiple non-trivial feasible roots, i.e. mixture compositions that fulfil Eqs. (54) and (55) and the condition, $x_i \in [0,1]$, as was shown in Fig. 10. Thus, the problem can be termed a multiplicity problem. The number of roots depends on the case studied, i.e. the components, conditions, and the location of the mixture composition with respect to phase splitting, and the thermodynamic model used to describe the phase equilibrium.

Finding only one root out of many or a negative TPDF value is not sufficient to assure both accurate phase stability analysis and feasible estimates for subsequent phase splitting calculations (Nichita and Gomez 2009). The problem may have several roots giving negative $D(\mathbf{x})$ values and the smallest $D(\mathbf{x})$ value corresponds to the global minimum. If the system is found to be unstable, the global minimum gives an initial estimate for the subsequent flash calculation (Michelsen 1982). The global minimum and the other located stationary points can be used together to initiate the phase splitting calculations efficiently (see e.g. Sofyan *et al.* 2003). The issue is illustrated in Fig. 11.

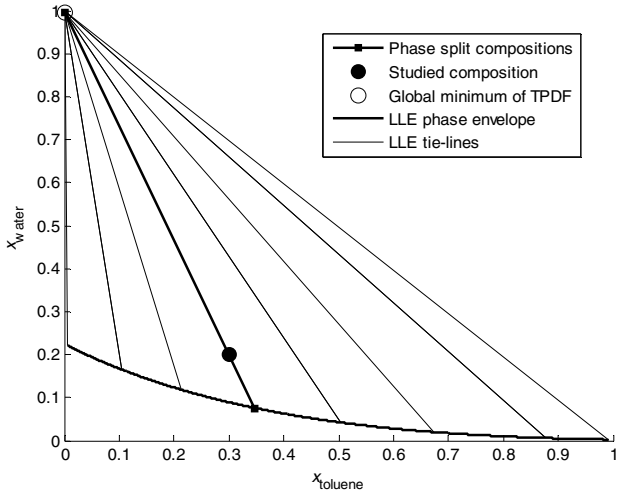

Fig. 11. Phase equilibrium behaviour of a component system consisting of toluene, water and aniline. Studied composition, $\mathbf{z} = [0.29989, 0.20006, 0.50005]$. The composition corresponding to the global minimum of $D(\mathbf{x})$ is $[6.6937 \cdot 10^{-5}$ 0.996865 0.003068]. The case investigated is Case 3 in Paper V.

As can be seen from Fig. 11, the global minimum of TPDF is extremely close to the composition of one of the liquid phases that is formed. Similarly, the studied composition, the local minimum of $D(\mathbf{x})$, is close to the other liquid phase composition. Therefore, the subsequent phase splitting solving in Case 3 (Paper V) can be initiated efficiently using the global and local minimum compositions as starting points. Fig. 11 also shows that the relative amounts of the forming liquid phases can be approximated relatively well, based on the location of the minima of TPDF and the mass balance equation.

Verification of finding a consistent number of feasible solutions

The correct number and type of solutions of TPDF are not known beforehand. Thus, it is evident that the knowledge that all the feasible solutions of the problem have been found is in practice vital to ascertain the *robustness* of the problem solving. Currently, there is no tool available that can either verify that all the solutions have been found or evaluate the relative number of solutions before solving the problem. However, Wasylkiewicz *et al.* (1996) have presented the topological criterion, which can be used to verify the consistency of the stationary points found with respect to the TPDF surface topology. The criterion was applied in Papers III and V to verify that the number of feasible solutions found is consistent. The criterion states that, for an n component mixture:

$$N_{\max} + (-1)^d N_{\min} + N_{\text{sad}}^{\text{even}} - N_{\text{sad}}^{\text{odd}} = (-1)^d , \tag{57}$$

where $d = n-1$, $N_{\max}$ is the number of maxima of $D(\mathbf{x})$, $N_{\min}$ is the number of minima, $N_{\text{sad}}^{\text{even}}$ is the number of saddles with an even number of negative eigenvalues, and $N_{\text{sad}}^{\text{odd}}$ is the number of saddles with an odd number of negative eigenvalues of the Hessian matrix $\mathbf{H}(D(\hat{\mathbf{x}}))$, where $\hat{\mathbf{x}}$ is a mole fraction vector with $n-1$ elements of vector $\mathbf{x}$. The type of stationary point $\hat{\mathbf{x}}$ can be determined from the eigenvalues, e_i, $i = 1,...,n-1$, of the Hessian matrix $\mathbf{H}(D(\hat{\mathbf{x}}))$ as follows:

- If all the eigenvalues are positive, the stationary point is a minimum.
- If all the eigenvalues are negative, the stationary point is a maximum.
- If $d \geq 2$ and there is at least one negative eigenvalue and at least one positive eigenvalue, the stationary point is a saddle.

3 Separation process model solution methods

Separation process model formulation is dependent on multiple issues. From the perspective of solving the model, the existence of possible temporal- and location- dependent gradients, i.e. $\partial \mathbf{c}/\partial t$ or $\partial \mathbf{c}/\partial r$, inside the process equipment dictates to a great extent the selection of the solution strategy. Table 5 shows a selection of solution strategies used in process model solution.

Table 5. Selected mathematical solution strategies for different process models.

Model	Mathematical type of model	Solution strategies	Reference
Gas-liquid reactor models			
DADM with FPM[1]	$\frac{\partial \mathbf{c}}{\partial t}, \frac{\partial^2 \mathbf{c}}{\partial l^2}, \frac{\partial \mathbf{c}}{\partial l}, \frac{\partial \mathbf{c}}{\partial r}, \mathbf{c}^{\dagger}$ $\frac{\partial \mathbf{c}}{\partial t}, \frac{\partial^2 \mathbf{c}}{\partial r^2}, \mathbf{c}$	PDE + PDE discretize *r* and *l* and integrate *t*	Romanainen (1994)
SADM with FM[1]	$\frac{\partial^2 \mathbf{c}}{\partial l^2}, \frac{\partial \mathbf{c}}{\partial l}, \frac{\partial \mathbf{c}}{\partial r}, \mathbf{c}$	PDE + BVP discretize *r*/*l* and solve *l*/*r* discretize *r* and *l* and solve NLE	Romanainen (1994)
STS with FM[1]	$\frac{\partial \mathbf{c}}{\partial r}, \mathbf{c}\frac{\partial^2 \mathbf{c}}{\partial r^2}, \mathbf{c}$	ODE + BVP discretize *r* and solve NLE include STS to FM and solve BVP	Romanainen (1994)
Automotive catalytic converter	$\frac{\partial \mathbf{y}}{\partial t}, \frac{\partial^2 \mathbf{y}}{\partial l^2}, \frac{\partial \mathbf{y}}{\partial l}, \mathbf{y}$ $\frac{\partial \mathbf{T_g}}{\partial t}, \frac{\partial^2 \mathbf{T_g}}{\partial l^2}, \frac{\partial \mathbf{T_g}}{\partial l}, \mathbf{T_g}^{\dagger}$ $\frac{\partial \mathbf{T_s}}{\partial t}, \frac{\partial^2 \mathbf{T_s}}{\partial l^2}, \mathbf{T_s}^{\dagger}$	PDE discretize *l* and integrate *t*	Kangas *et al.* (2002)

Model	Mathematical type of model	Solution strategies	Reference
Membrane separation			
with support, finite $D_{i,j}$	$\frac{\partial \boldsymbol{\theta}}{\partial z}, \boldsymbol{\theta}$	ODE discretize z and solve NLE	Paper I
no support, pure component permeation	$\frac{\partial \boldsymbol{\theta}}{\partial z}, \boldsymbol{\theta}$	ODE integrate z	Sandström *et al.* (2011)
no support, infinite $D_{i,j}$	$\frac{\partial \boldsymbol{\theta}}{\partial z}, \boldsymbol{\theta}$	Analytic solution	Krishna and Baur (2004)
Decanter	$\mathbf{f}(\mathbf{x}) = \mathbf{0}$	NLE solve NLE	Paper V
Mixture adsorption equilibrium			Papers I and II
Thermally-coupled distillation columns			Malinen and Tanskanen (2009)

[1]Dynamic bubble column with axial dispersion (DADM), Film model (FM), Film-penetration model (FPM), Steady state bubble column with axial dispersion model (SADM), Steady state tanks-in-series model (STS). † **c** is the vector of component concentrations, T_s is the vector of the solid temperature, T_g is the vector of gas phase temperatures, r and l are the radial and length coordinates, respectively.

As can be seen in Table 5, it is common to convert a process model composed of an ODE set into the form of an NLE set by first discretizing along the physical coordinates and then solving the resulting NLE set. This is especially true when the steady-state behaviour of a process is being studied. However, even after the conversion of the problem to an NLE set, the solving of the problem is not certain. The solving of an NLE set is difficult for various reasons:

- Some of the functions can be undefined for certain variable values, which creates a discontinuity (see e.g. Shacham and Brauner (2002)) or a boundary across the solution path.
- The equation set may have solutions that are not physically feasible.
- The functions may be highly nonlinear and/or badly scaled.
- The feasible selection of the starting (or initial) point may be difficult.

In addition, in separation process models, like the heterogeneous distillation column and membrane separation models, the number of equations and variables in the formed NLE set may be high and the Jacobian of the equation set may be sparse, i.e. the Jacobian matrix has a large portion of elements having a value of zero. This is illustrated in Fig. 12.

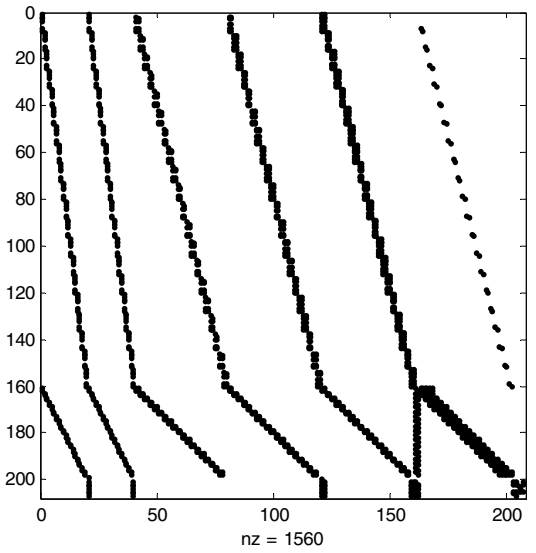

Fig. 12. Numerical sparsity pattern of the Jacobian of the membrane separation model used in Paper I. The number of axial elements along the zeolite film is 20. The sparsity pattern of the Jacobian was evaluated using MATLAB. The number of non-zero elements (•) is 1560.

A sparse Jacobian in turn may cause the solving of the NLE set to be inefficient unless the Jacobian matrix can be determined analytically or the Jacobian matrix structure is taken into account in the numerical Jacobian matrix approximation.

NLE sets are frequently solved iteratively with Newton-Raphson based solution methods. The Newton and quasi-Newton methods are widely used local methods because they are simple and, theoretically at least, superlinearly convergent. These methods will not converge generally unless an initial guess is supplied that is reasonably close to the solution. In addition, these methods typically achieve only one solution from one initial point.

3.1 Solution of the membrane separation model

In the case of a membrane separation process model as described in Paper I, it is important to note that the model has only one solution and a reasonably good initial guess can be supplied by using application-dependent knowledge and a simplified membrane model. Thus, a successful solution with Newton-based solving methods can be ascertained. However, the solution may still travel outside

the feasible problem domain without using variables mapping, for instance. Therefore, the variables mapping was applied in the solution of the membrane and mixture adsorption equilibrium models in Paper I.

The application of a Newton-based local solving method demands first that the Maxwell-Stefan equations representing the membrane separation through the zeolite pores, Eq. (4), are modified into a form compatible with NLE equations, as shown in Table 5, i.e. in the form $\mathbf{f}(\mathbf{x})=\mathbf{0}$. This can be performed with the discretization of the zeolite film into elements as applied in Paper I. The film was discretized into 21 spatially uniform grid points, i.e. equalling 20 elements. In the literature, 50 or even more elements have been used (Wirawan *et al.* 2011; Graaf 1999), but the selected number of elements was adequate for this application as the occupancy fraction profiles were relatively linear across the zeolite film. One reason for the relatively linear gradients is that the surface diffusivities have only mild occupancy dependences in the domain investigated. Otherwise, the implementation of Eq. (29), for instance, in a membrane separation model would have a clear effect on the gradients. This is due to the severity of the occupancy dependence in Eq. (29). Similarly, the occupancy dependence has an effect on the selection of a method to evaluate the elements of $\partial\boldsymbol{\theta}/\partial z$.

In this context it is worth noting that the selection of a method to evaluate numerically the elements of $\partial\boldsymbol{\theta}/\partial z$ has an effect on the robustness of the solving strategy. In Paper I, the terms of $\partial\boldsymbol{\theta}/\partial z$ in Eq. (4) were then approximated with classical three-point, second-order finite differences. In addition, the selection of a numerical method to approximate the gradients is not straightforward. The finite differences can easily be formulated although the number of grid points should be large. On the other hand, when the problem has steep gradients, the finite difference or the finite element method could be preferred. However, if the problem is relatively easy to solve and the problem solution is smooth, a weighted residuals method should be preferred. (Finlayson 1980) It is difficult to determine the steepness of the gradients in the membrane model beforehand. Hence, the finite difference method was selected in this work.

After discretization and implementation in the Matlab environment, the *fsolve* function of Matlab can be applied in the model solution. In addition to the upper level solving of the equation set, an iterative solution of the adsorption equilibrium is required as the relation of occupancy fractions and partial pressures/fugacities is calculated in the thermodynamic factor matrix, as presented in Eq. (3). The iterative solution of the thermodynamic factors based on IAST is the main factor that determines solution time. Note however that the

iterative solution of the thermodynamic factor matrix is demanded when studying mixture separation, not when investigating pure component permeation. Hence, in Paper I, the following solution strategy was applied as depicted in Fig. 13.

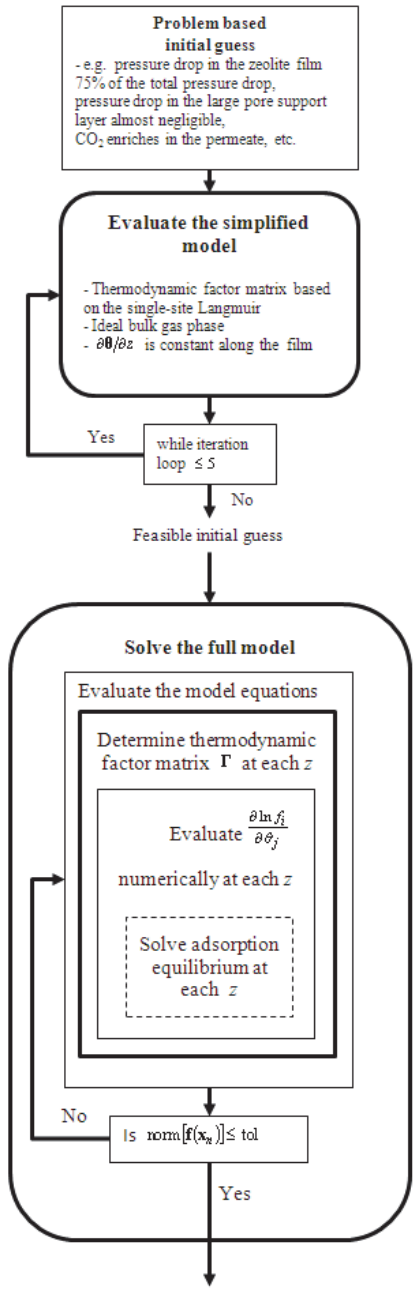

Fig. 13. Solution strategy of the membrane separation model built in Paper I.

As can be seen in Fig. 13, the solution of the membrane model demanded a relatively large amount of problem-dependent knowledge. In addition, the solution time was extensive due to the iterative solution of the sub-problem, i.e. the evaluation of the thermodynamic factor matrix elements. However, the solution strategy guaranteed that the model was solved robustly.

3.2 Solution of a phase stability analysis problem

In contrast, the solution of a phase stability analysis problem, as formulated in Section 2.2.3, requires advanced solving strategies preferentially in the form of a robust solving method. However, solving strategies with application-dependent knowledge utilizing local solution methods have also been proposed in the literature. The main features of a phase stability analysis problem that cause difficulties during the solution of the problem are:

- all the feasible solutions of the equation set have to be discovered,
- the equation set is highly nonlinear,
- all the variables have strict physically determined boundaries,
- the equation set includes logarithmic terms,
- the Jacobian of the equation set is full, and
- the trivial solution of the equation set cannot be avoided.

Thus, due to the considerable problems caused by the features, the usage of local solving methods demands heuristics (see e.g. Michelsen 1982) in terms of choosing the initial guess, and in practice, multiple initial guesses. However, even with the use of numerous starting points along with heuristics it cannot be guaranteed that all the minima of TPDF will be found (Wasylkiewicz *et al.* 1996). Therefore, e.g. Michelsen and Mollerup (2007) set a more modest target for the solution of the problem: ”*A less ambitious approach is to perform the search for local minima with a number of judiciously selected initial estimates in the hope that these searches will uncover at least all the negative minima.*” Thus, the formulation of a robust solving strategy is vital to enable robust phase stability analysis. Hence, it is not surprising that the usage of global solution methods in phase stability analysis has been intensive in the literature during recent two decades. In order to determine *robustly* if a phase is stable or not, several numerical techniques, global solving methods, have been proposed during the years to solve the problem, as shown in Table 6.

Table 6. Global solution methods in phase stability analysis.

Solution method	Main solution stages	References
Stochastic methods	Generation of a group of initial guesses Selection of promising initial guesses Creation of a new generation Repetition of the previous stages until convergence	Balogh *et al.* (2003); Bhargava *et al.* (2013); Bonilla-Petriciolet *et al.*, (2006); Fateen *et al.* (2012); Rangaiah (2001); Srinivas and Rangaiah (2007); Zhang *et al.* (2011); Zhu *et al.* (2000); Zhu and Xu (1999b)
Interval Newton methods	Division of the variable domain into intervals Updating the intervals with Newton-based methods Selection of the intervals including $\mathbf{f}(\mathbf{x}^*) = \mathbf{0}$ Convergence when interval(s) sufficiently narrow	Gecegormez and Demirel (2005); Hua *et al.* (1996, 1998); Staudt *et al.* (2013); Tessier *et al.* (2000); Xu *et al.* (2005)
Branch and bound methods	Partitioning the initial feasible region into subdomains Construction of a convex envelope for the subdomains to provide underestimators Sequence of nondecreasing lower bounds is generated until convergence is obtained	McDonald and Floudas (1995a, 1995b, 1997), Zhu and Xu (1999a)
Tunneling method	Locating a local minimum of the objective function from one or multiple initial guesses Use of a tunneling function to locate another valley of the function solved	Nichita *et al.* (2002); Nichita and Gomez (2009)
Terrain method	Surface of the problem is tracked along the ridges and valleys to locate all the solutions	Lucia *et al.* (2005)
Homotopy methods	An initial point is selected or solved Path from the initial point is tracked with a homotopy parameter Convergence is obtained when the homotopy parameter receives the value of one	Bausa and Marquardt (2000); Jalali-Farahani and Seader (2000); Jalali and Seader (1999); Kangas *et al.* (Paper V); Khaleghi and Jalali (2007); Malinen *et al.* (Paper III); Sun and Seider (1995)

As Table 6 shows, the majority of the literature studies use stochastic methods. However, the application of stochastic methods in chemical process simulation software has not progressed significantly. The main reasons for the slow progress in the application of stochastic methods, and in fact of all the global solving methods, are the failures of finding all the roots of TPDF and the considerable solving time of the methods. The solving time becomes impractical especially when the number of components (variables) increases in the studied system.

In addition, homotopy methods have attracted considerable interest, as shown in Table 6. The main issue to be tackled with the homotopy methods is that only some roots of TPDF are obtained from a single initial guess. Homotopy methods are also generally used in the field of phase behaviour analysis to solve NLE sets and the methods have already been applied in commercial chemical simulation software such as ASPENPlus. The literature regarding homotopy methods in phase equilibrium studies can be divided into the use of either problem-dependent or problem-independent homotopies.

3.2.1 Problem-dependent homotopies

The emphasis in the literature is to take application properties into account (see e.g. Fidkowski *et al.* (1993), Eckert and Kubicek (1997), Tolsma and Barton (2000a, 2000b), Wasylkiewicz *et al.* (1999), Wang *et al.* (1999) or Aslam and Sunol (2006)). Thus, the homotopy is reformed frequently into a problem-dependent form. The problem dependency of a homotopy can be defined to include one or several of the options below:

- usage of a problem variable in place of an artificial homotopy parameter,
- change in the properties of the problem along the homotopy path, e.g. the non-ideality of the mixture increases from Raoult's law behaviour to actual non-ideal behaviour as the value of the homotopy parameter is increased,
- usage of the homotopy parameter only for certain equations of the problem.

3.2.2 Problem-independent homotopies

Problem-independent homotopies have also been used in the place of problem-dependent homotopies. In this approach, a phase stability analysis problem is investigated with the help of an artificial homotopy parameter. However, some heuristics regarding the problem properties are usually utilized in order to ensure

that a feasible starting point is chosen (see e.g. Sun and Seider 1995, Bausa and Marquardt 2000). Similarly, in Paper V, heuristics regarding the selection of the starting point were investigated. The second alternative to enable the robust solving of a phase stability analysis problem is to relax the calculations to a complex space (see Khaleghi and Jalali (2007)). However, the approach is not trouble-free as the relaxation to the complex space is not applicable unless the equations can be converted to include complex variables (Jalali *et al.* 2008).

The literature studies of problem-independent homotopies in phase stability analysis concentrate on the usage of either fixed-point (see Khaleghi and Jalali 2007 or Sun and Seider 1995) or Newton (see Jalali-Farahani and Seader 2000 or Jalali and Seader 1999) homotopies. In contrast, the affine homotopy as applied in Paper V is not generally used. One reason for the omission of the affine homotopy is the high nonlinearity of the functions, according to Jalali and Seader (1999). Therefore, the calculation of function derivatives is problematic with the (scale-invariant) affine homotopy. On the other hand, the fixed-point homotopy may have a scaling problem, which is an important issue in computations. However, according to Khaleghi and Jalali (2007), the main benefit of fixed-point homotopy is that it is sensitive to the selection of a starting point. All the homotopy methods investigated in this thesis (Papers III and V) are problem-independent. Thus, only problem-independent homotopies are considered herein in more depth.

3.3 Formulation of problem-independent homotopies

Problem-independent homotopies are formed as a combination of the original problem function, $\mathbf{f}(\mathbf{x})$, and an auxiliary function, $\mathbf{g}(\mathbf{x})$. The $\mathbf{g}(\mathbf{x})$ and $\mathbf{f}(\mathbf{x})$ are embedded with the help of a homotopy parameter, θ, to form a homotopy function $\mathbf{h}(\mathbf{x},\theta)$. The first advantage of embedding is that the initial guess for $\mathbf{h}(\mathbf{x},\theta)$ at $\theta = 0$, i.e. the solution of $\mathbf{g}(\mathbf{x})$, may be obtained with a system of equations for which a solution is known or is easily obtained (Wayburn and Seader 1987). Secondly, a continuous blend between the starting point and the solution(s) of the original problem $\mathbf{f}(\mathbf{x})$ is created. The principle of homotopy (continuation) methods is illustrated in Fig. 14.

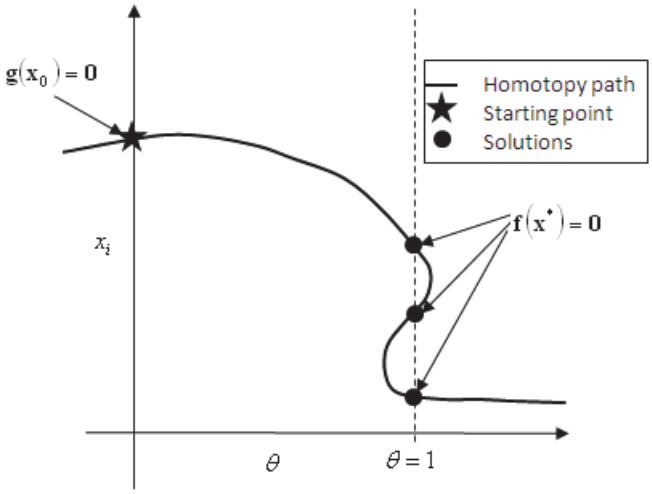

Fig. 14. Schematic homotopy path of an unbounded problem-independent homotopy.

As can be seen in Fig. 14, the homotopy path is tracked with the help of the homotopy parameter from a known solution $\mathbf{x}_0$ at $\theta = 0$ to unknown solutions $\mathbf{x}^*$ at $\theta = 1$. The homotopy path is formed based on usage of the following homotopy equation:

$$\mathbf{h}(\mathbf{x}, \theta) = \theta \mathbf{f}(\mathbf{x}) + (1 - \theta)\mathbf{g}(\mathbf{x}) = \mathbf{0} \,. \tag{58}$$

The auxiliary function $\mathbf{g}(\mathbf{x})$ in Eq. (58) is generally defined as (Seader *et al.* 1990):

$$\mathbf{g}(\mathbf{x}) = (\mathbf{x} - \mathbf{x}_0) \,, \tag{59}$$

$$\mathbf{g}(\mathbf{x}) = (\mathbf{f}(\mathbf{x}) - \mathbf{f}(\mathbf{x}_0)) \,, \tag{60}$$

$$\mathbf{g}(\mathbf{x}) = \mathbf{f}'(\mathbf{x}_0)(\mathbf{x} - \mathbf{x}_0) \,. \tag{61}$$

$\mathbf{g}(\mathbf{x})$ forms, when substituted in Eq. (58), homotopies called as fixed-point, Newton, and scale-invariant affine homotopies, respectively. $\mathbf{f}'(\mathbf{x}_0)$ in Eq. (61) is the Jacobian of the original problem $\mathbf{f}(\mathbf{x})$ evaluated at the starting point $\mathbf{x}_0$.

All the homotopies in Eqs. (59)-(61) have their own benefits and shortcomings. The fixed-point and scale-invariant affine homotopies have the advantage that only one root satisfies $\mathbf{h}(\mathbf{x}, \theta) = \mathbf{0}$ at $\theta = 0$. Therefore, no starting point multiplicities exist. However, the path can consist of branches that are only connected at the opposite infinities or branches in a complex domain.

Newton homotopy, on the other hand, has the advantage that a closed path for $\mathbf{x}$ on θ may exist within a finite domain, which in turn is also a consequence of the appearance of starting point multiplicities. The main drawback of Newton homotopy is that the homotopy path may have multiple roots at $\theta = 0$ and thus more than one homotopy path branch may exist (Seader *et al.* 1990). In addition, the possibility of a starting point multiplicity may imply that the path will return to $\theta = 0$ before reaching the first root, i.e. a starting point isola is formed. This is unproductive in relation to computational efficiency, as the appearance of the starting point isola demands the selection of either a new initial guess or a different homotopy.

The homotopy methods are particularly useful in solving problems in which sufficiently good starting guesses for the unknown variable values cannot be given. The homotopy methods presented by e.g. Allgower and Georg (1980), Wayburn and Seader (1987), Seader *et al.* (1990), and Sun and Seider (1995) have in theory the property of global convergence, but they have their own shortcomings.

One challenge is that the homotopy path may run partly or completely outside the feasible problem domain. Outside the domain, a problem may rise if the physico-chemical properties of the system under study have to be evaluated and the procedure for doing so does not accept values outside a feasible domain. A typical example of this is the calculation of thermodynamic properties using the thermodynamic relations built into process simulators. Thus, the computer subroutines evaluating e.g. the phase equilibrium constants and enthalpies may generate fatal errors (Wayburn and Seader 1987).

Another challenge encountered frequently in chemical engineering is boundary striking in the numerical solution of NLE sets. Boundary striking may occur if the solution path runs in the vicinity of the domain boundary without crossing it. Even though the correct solution path does not cross the domain boundary, the numerical predictor-corrector path-tracking algorithm may predict variable values outside the feasible domain. Boundary crossing usually occurs in homotopy methods because of an unacceptably long predictor step. In some cases, these problems can be tackled with the use of absolute value functions (Wayburn and Seader 1987), and different mapping techniques (see e.g. Seader *et al.* 1990). The homotopy methods also have other shortcomings. The fundamental causes of failure of homotopy methods and proposed remedies to address these failures are listed in Table 7.

Table 7. Fundamental causes of failure of homotopy methods and solutions proposed in the literature (adapted from Malinen 2010).

Failure	Proposed solutions
The Jacobian of $\mathbf{h}(\mathbf{x},\theta)$ becomes singular at the turning points of the homotopy path	arc length path tracking
The homotopy path strikes an interior boundary of the problem variable domain, i.e. *interior boundary striking*.	variables bounding variables mapping
The homotopy path exceeds the variable definition domain, i.e. *exterior boundary striking*.	variables bounding variables mapping
The homotopy path becomes totally unbounded, i.e. runs towards +/- infinity.	toroidal and boomerang mapping branch jumping techniques
Multiple solutions exist for $\mathbf{g}(\mathbf{x})$, i.e. a starting point multiplicity problem.	select another homotopy function
Occurrence of isolated solutions.	application of complex space arithmetic homotopy parameter bounding

As can be seen in Table 7, the problem of boundary striking can be solved by using variables bounding and mapping. Boundary striking is encountered frequently in process modelling. Thus, a robust solving method should include a remedy for the problem.

3.3.1 Bounded homotopies

A promising proposal for overcoming the problems of the exterior boundary striking of a homotopy path with respect to problem variables is the class of bounded homotopy methods presented by Paloschi (1995). Bounded homotopy methods can be expressed in the form:

$$\mathbf{h}_b(\mathbf{x},\theta) = \pi(\mathbf{x})\mathbf{h}(\mathbf{x},\theta) + \mathbf{v}(\mathbf{x}) - \mathbf{v}(\mathbf{x}^b) = \mathbf{0} \,. \tag{62}$$

The purpose of $\pi(\mathbf{x})$ is to annihilate the 'original' homotopy $\mathbf{h}(\mathbf{x},\theta)$ when the homotopy path enters the bounding zone. The effect is that the homotopy path is bounded within a predefined variable domain.

Paloschi (1997) has also extended the capabilities of bounded homotopies to handle sparse problems. The difference compared to Eq. (62) is that the single penalty function value $\pi(\mathbf{x})$ has been replaced with a penalty matrix $\mathbf{P}(\mathbf{x})$. The proposed methods yield a bounded homotopy path that preserves a Jacobian with the same sparsity pattern as the original problem. Thus, the possibility of exploiting sparse matrix techniques is maintained. This is important from an efficiency point of view.

The main shortcoming of the bounded homotopies presented by Paloschi (1995, 1997) is that the tracking of the homotopy path inside the narrow bounding zone is numerically challenging. For example, a predicted step may fall outside the problem domain. In addition, the capability of the bounded homotopy methods to keep the homotopy path strictly bounded with respect to the problem variables is questionable in the form proposed by Paloschi. These weaknesses can be overcome using the modified bounded homotopies proposed by Malinen and Tanskanen (2007, 2008, 2010).

3.3.2 Modified bounded homotopies

In Paper V, the modified bounded homotopy presented in Malinen and Tanskanen (2007, 2008):

$$\mathbf{h}_b^{\mathrm{mod}}\left(\mathbf{x}^{\mathrm{inf}},\theta\right)=\pi\left(\mathbf{x}^{\mathrm{inf}}\right)\mathbf{h}\left(\mathbf{x}^{\mathrm{inf}},\theta\right)+\mathbf{v}\left(\mathbf{x}^{\mathrm{inf}}\right)-\mathbf{v}\left(\mathbf{x}^{b,\mathrm{inf}}\right)=\mathbf{0}\,, \tag{63}$$

where $\mathbf{v}\left(\mathbf{x}^{\mathrm{inf}}\right)=\mathbf{f}'\left(\mathbf{x}_0^{\mathrm{inf}}\right)\left(\mathbf{x}^{\mathrm{inf}}-\mathbf{x}_0^{\mathrm{inf}}\right)$, was applied to investigate the first root attraction domains with different homotopy functions. The modified bounded homotopy Eq. (63) enables the constraining of the homotopy path within feasible variable values, i.e. the mole fractions can be kept within the physically relevant domain of [0 1], thus avoiding fatal errors caused by unfeasible variable values in thermodynamic subroutines. In addition, the application of variables mapping assists in homotopy path tracking in the vicinity of variable domain boundaries. These issues are illustrated in Fig. 15.

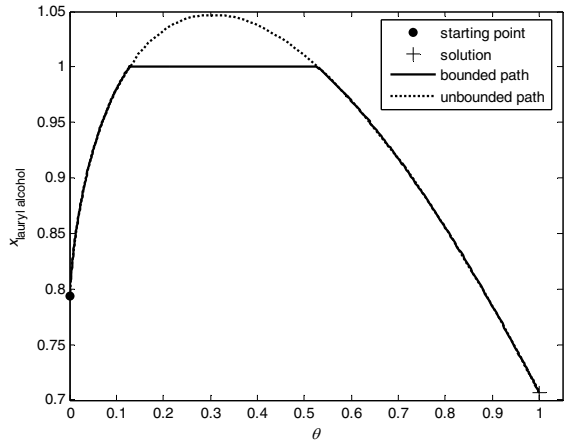

a)

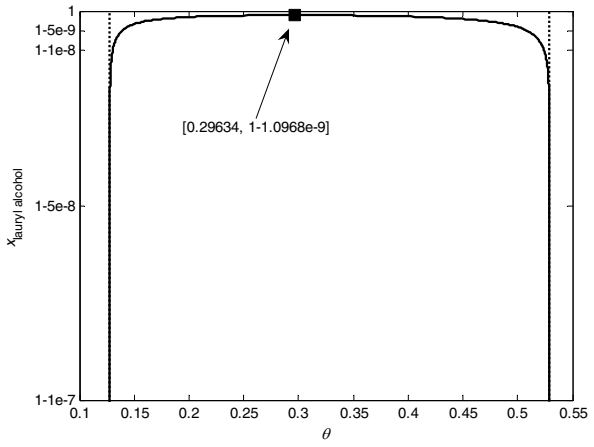

b)

Fig. 15. a) The bounded Eq. (63) and unbounded homotopy Eq. (60) paths from the starting point to the first solution in an unmapped domain. b) A magnification of the bounding domain. The width of the bounding domain is $1 \cdot 10^{-7}$ for Case 1 presented in Paper V. The mixture composition studied is z = [0.2030, 0.7071, 0.0899]. The starting point in the unmapped variable space is x_0 = [0.7455, 0.7932, 0.8746].

Undeniably, as can be seen in Fig. 15, application of the homotopy presented in Eq. (63) bounds the homotopy path with respect to the variables. In addition, the homotopy path can be tracked within a narrow bounding zone without crossing the defined boundary. The applicability of the homotopy presented in Eq. (63) for large-scale problems can be improved using the replacement of the penalty function π with penalty matrix Π, as proposed by Malinen and Tanskanen (2008). However, the targeted applications in the present work focus on small-scale problems for which the usage of the single value penalty function is sufficient. In addition, it is worth noting that the Jacobian of the investigated equation set, Eqs. (54)-(55), has no zero elements. Therefore, the sparsity pattern of the original equation set cannot be exploited to improve the homotopy path tracking. This fact also diminishes the benefits of using the penalty matrix instead of the penalty function.

In Paper III, Eq. (63) was combined with the concept of homotopy parameter bounding as presented in Malinen and Tanskanen (2010):

$$\mathbf{h}_{b\theta}(\mathbf{x},\theta) = \boldsymbol{\pi}(\theta)\mathbf{h}(\mathbf{x},\theta) + \mathbf{v}_{\theta}(\theta) - \mathbf{v}_{\theta}(\theta^{b}) = \mathbf{0}, \tag{64}$$

where $\mathbf{v}_{\theta}(\theta) = M\theta\mathbf{e}$, to reach all the feasible solutions for a TPDF problem. As pointed out in Malinen and Tanskanen (2010), Eq. (64) is capable, at least in some cases, of forcing separate homotopy path branches to connect, thus resulting in a continuous homotopy path connecting the roots of the problem. It is worth noting that homotopy parameter bounding can also be used to disconnect a homotopy path branch, as demonstrated in Malinen and Tanskanen (2010). This property is useful especially when a starting point isola appears.

The combination of the homotopy parameter and variables bounding features in Eqs. (63) and (64) together with variables mapping results in the following homotopy:

$$\mathbf{h}^{\mathrm{mod}}_{bx\theta}(\mathbf{x}^{\mathrm{inf}},\theta) = \pi(\mathbf{x}^{\mathrm{inf}},\theta)\mathbf{h}(\mathbf{x}^{\mathrm{inf}},\theta) + \mathbf{f}'(\mathbf{x}_0^{\mathrm{inf}})(\mathbf{x}^{\mathrm{inf}} - \mathbf{x}^{b,\mathrm{inf}}) + M(\theta - \theta^{b})\mathbf{e} = \mathbf{0}. \tag{65}$$

In addition, as shown in Paper III, also applying the knowledge of the location of the trivial root results in a solving tool that is capable of determining all the roots of Eqs. (54) and (55) in the phase stability analysis robustly. The trivial root of the problem, $\mathbf{x} = \mathbf{z}$ and $\mathbf{f}(\mathbf{z}) = \mathbf{0}$, is used as a starting point in the solving method. Thus, the Newton homotopy, Eq. (60), is reformulated in mapped variables to $\mathbf{h}(\mathbf{x}^{\mathrm{inf}},\theta) = \mathbf{f}(\mathbf{x}^{\mathrm{inf}})$. Finally, the Newton homotopy method with both the homotopy

parameter and variable bounding, together with the trivial root as the starting point, can be defined by:

$$\mathbf{h}_{bx\theta}^{\mathrm{mod}}\left(\mathbf{x}^{\mathrm{inf}},\theta\right)=\pi\left(\mathbf{x}^{\mathrm{inf}},\theta\right)\mathbf{f}\left(\mathbf{x}^{\mathrm{inf}}\right)+\mathbf{f}'\left(\mathbf{z}^{\mathrm{inf}}\right)\left(\mathbf{x}^{\mathrm{inf}}-\mathbf{x}^{b,\mathrm{inf}}\right)+M\left(\theta-\theta^{b}\right)\mathbf{e}=\mathbf{0}\,. \qquad (66)$$

The properties of different modified bounded homotopies, Eqs. (63)-(66), in an optimal case are illustrated in Fig. 16. The term 'optimal' indicates here that all the feasible solutions are found from a single starting point.

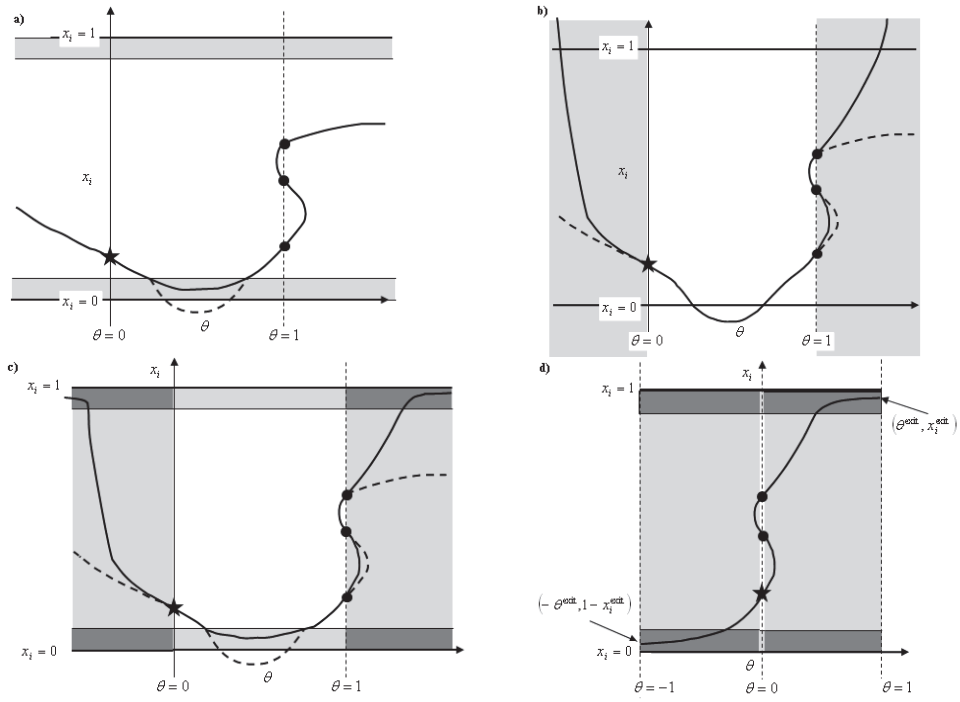

Fig. 16. Homotopy path of a) a variable bounded (Eq. (63)), b) a homotopy parameter bounded (Eq. (64)), c) both variable and homotopy bounded (Eq. (65)), and d) trivial root applying both variable and homotopy bounded (Eq. (66)) homotopy. The star and the circles indicate the starting point and the feasible solutions, respectively. In the light grey domain, either variable or homotopy parameter bounding is in force. In the dark grey domain, there is both the variable and homotopy parameter in force. The dashed path indicates an unbounded path.

Some general observations can be made based on Fig. 16:

- Unbounded and only homotopy parameter bounded (Fig. 16b) homotopy paths enter the non-physical variable domain,
- Bounding the variables or/and the homotopy parameter (Fig. 16a-d) results in a shorter homotopy path than with unbounded homotopy (Fig. 16a),
- Application of the trivial root and bounding both variables and the homotopy parameter (Fig. 16d) results in the shortest homotopy path,
- Appropriate selection of the relative importance of the variables bounding and homotopy parameter results in a path that exits the domain inside the bounding zone where both bounding factors are in force, and more importantly with respect to the homotopy parameter. (Fig. 16d)
- Only the trivial root applying homotopy has interception points $\left(\theta^{\text{exit}}, x_i^{\text{exit}}\right)$ located in such a way that the homotopy path can be continued in the same direction from $\left(-\theta^{\text{exit}}, 1-x_i^{\text{exit}}\right)$. (Fig. 16d)

On the whole, the observations based on Fig. 16d imply that the application of the trivial root is the best alternative for solving the TPDF problem. However, the direct application of the method in Eq. (65) for solving a general chemical engineering problem is hindered due to the fact that it is rare that one solution of the problem is known before the start of the solution. However, in the case of solving the TPDF problem, the method works well, as the trivial root is known beforehand as demonstrated in Paper III.

In the following sections, various issues related to modified bounded homotopies are discussed in more detail. Illustrative examples of the use and properties of the proposed methods are given in Section 4.3.3.

Variables mapping

In order to facilitate variables bounding within a narrow bounding zone while still enabling accurate and flexible path tracking with bounded homotopy methods, the variables mapping presented first in conjunction with homotopies by Malinen and Tanskanen (2007, 2008, 2010) has been applied. Note that in Paper I variables mapping has also been applied in conjunction with local solving methods when solving membrane separation or the mixture adsorption equilibrium models.

Even though the homotopy path defined by modified bounded homotopies is tracked in the mapped variable space, i.e. in what is termed the infinite variable space, the variables are mapped into finite variable space before substituting them

into the equations describing the original problem. The maximum $b_i^{\max}$ and minimum $b_i^{\min}$ values are set separately for each problem variable x_i. Based on the selected boundary values, mapping from a finite space into an infinite space can be carried out as follows:

$$x_i^{\inf} = \log_{10}\left(\frac{2\cdot\left(x_i - b_i^{\min}\right)}{b_i^{\max} - b_i^{\min}}\right), \text{ when } x_i < 0.5\cdot\left(b_i^{\max} + b_i^{\min}\right), \tag{67}$$

$$x_i^{\inf} = \log_{10}\left(\frac{0.5\cdot\left(b_i^{\max} - b_i^{\min}\right)}{b_i^{\max} - x_i}\right), \text{ when } x_i \geq 0.5\cdot\left(b_i^{\max} + b_i^{\min}\right). \tag{68}$$

and the mapping from an infinite space into a finite space as:

$$x_i = b_i^{\min} + 0.5\cdot\left(b_i^{\max} - b_i^{\min}\right)\cdot 10^{x_i^{\inf}}, \text{ when } x_i^{\inf} < 0, \tag{69}$$

$$x_i = b_i^{\max} - 0.5\cdot\frac{\left(b_i^{\max} - b_i^{\min}\right)}{10^{x_i^{\inf}}}, \text{ when } x_i^{\inf} \geq 0. \tag{70}$$

The minimum, $b_i^{\min}$, and maximum, $b_i^{\max}$, values are realized as the domain boundary values. In the case of mole fractions, the boundary values are, naturally, $b_i^{\min} = 0$ and $b_i^{\max} = 1$ (Papers III and V).

Homotopy parameter bounding

The homotopy parameter bounding is achieved with the auxiliary function $\mathbf{v}_\theta(\theta)$. As Eq. (64) is applied the auxiliary function is in the form $M\left(\theta - \theta^b\right)\mathbf{e}$, where $\mathbf{e}$ is a $n\times 1$ vector, in which every element has the value of one. The purpose of parameter $M \in \left]-\infty\ +\infty\right[$ is to scale the elements of vector $\mathbf{e}$ properly. In addition, parameter M can be used as a weighting factor when applying Eq. (65) or (66). Based on the value of M, the homotopy path will exit the feasible domain either with respect to the variables or the homotopy parameter. Parameter θ^b is defined as:

$$\theta^b = \theta\left(1 - \left[6\cdot|\theta|^5 - 15\cdot|\theta|^4 + 10\cdot|\theta|^3\right]\right). \tag{71}$$

The definition in Eq. (71) differs slightly from the form presented by Malinen and Tanskanen (2010):

$$\theta^b = \theta - \left(6\cdot\left|\theta - \theta^{b'}\right|^5 - 15\cdot\left|\theta - \theta^{b'}\right|^4 + 10\cdot\left|\theta - \theta^{b'}\right|^3\right)\cdot\left[\theta - \theta^{b'}\right]. \tag{72}$$

The difference is due to the change in the homotopy that was used. In Malinen and Tanskanen (2010), homotopy parameter bounding was used in the domain $\theta \in [-1, 0[\cup]1, 2]$. In contrast, in the present work, the bounding is in force when $\theta \in [-1, 0[\cup]0, 1]$. In other words, only at $\theta = 0$ the parameter $\theta^b = 0$. Thus, at this point, the auxiliary function $M(\theta - \theta^b)\mathbf{e} = \mathbf{0}$. In practice, this fact means that homotopy parameter bounding is in force throughout the θ domain, the $\theta = 0$ plane being the only exception.

Variables bounding

The bounding of the variables is achieved with the usage of the auxiliary function $\mathbf{v}(\mathbf{x}^{\inf})$. When Eq. (66) is applied, as in Paper III, the auxiliary function is defined as $\mathbf{f}'(\mathbf{z}^{\inf})(\mathbf{x}^{\inf} - \mathbf{x}^{b,\inf})$. $\mathbf{f}'(\mathbf{z}^{\inf})$ is Jacobian matrix expressed in terms of the mapped variables determined at the starting point of homotopy path tracking, i.e. at the trivial root, $\mathbf{x} = \mathbf{z}$. The elements in vector $\mathbf{x}^{b,\inf}$ are obtained from:

$$x_i^{b,\inf} = x_i^{\inf} - \rho_2\left(W_{ii}\left(x_i^{\inf} - x_i^{b',\inf}\right), \delta\right)\left(x_i^{\inf} - x_i^{b',\inf}\right), \tag{73}$$

and the elements in the diagonal weighting matrix $\mathbf{W}$ as:

$$W_{ii} = \frac{1}{u_i^{\inf} - l_i^{\inf}}, \tag{74}$$

where the upper and lower constraints, i.e. $u_i^{\inf}$ and $l_i^{\inf}$, form the inner boundaries for the bounding zone in the mapped variable space. The higher the absolute values of the constraints, the narrower the bounding zone in the finite variable space. In the case of sharp phase splitting, where mole fractions close to 0 and/or 1 exist, the upper and lower constraints must be defined so that the feasible solutions do not fall into the bounding zone. In Paper III, the choices of $u_i^{\inf} = 4$ and $l_i^{\inf} = -4$ were successfully applied. This denotes that variables bounding is in effect when $x_i \in \left[0\ 5 \cdot 10^{-5}\right[$ or $x_i \in \left]1 - 5 \cdot 10^{-5}\ 1\right]$. On the other hand, an even narrower bounding zone was applied in Paper V. Based on the selected $u_i^{\inf}$ and $l_i^{\inf}$, $x_i^{b',\inf}$ in Eq. (74) is defined as:

$$x_i^{b',\inf} = \begin{cases} l_i^{\inf}, & x_i^{\inf} < l_i^{\inf}, \\ x_i^{\inf}, & l_i^{\inf} \le x_i^{\inf} \le u_i^{\inf}, \\ u_i^{\inf}, & x_i^{\inf} > u_i^{\inf}. \end{cases} \tag{75}$$

Penalty function

The purpose of the penalty function π is to annihilate the term corresponding to $\mathbf{h}(\mathbf{x},\theta)$ whenever the homotopy path enters the bounding zone. The annihilation may occur with respect to the variables or/and the homotopy parameter. If both the homotopy parameter and variables are bound, the penalty function depends on both the vector of the mapped variables, $\mathbf{x}^{\inf}$, and the homotopy parameter, θ, i.e. $\pi = \pi(\mathbf{x}^{\inf},\theta)$. In this case, the penalty function is determined as:

$$\pi(\mathbf{x}^{\inf},\theta) = \left\| \mathbf{e} - \begin{bmatrix} \boldsymbol{\pi}(\mathbf{x}^{\inf}) \\ \pi(\theta) \end{bmatrix} \right\|_{\infty}, \tag{76}$$

in which $\mathbf{e}$ is a $(n + 1) \times 1$ vector, where each element has the value of one. The elements in the function vector, $\boldsymbol{\pi}(\mathbf{x}^{\inf})$, and $\pi(\theta)$ are specified as:

$$\pi_i(x_i^{\inf}) = \rho_1(|W_{ii}(x_i^{\inf} - x_i^{b,\inf})|,\delta), \tag{77}$$

$$\pi(\theta) = 1 - \rho_1(|\theta - \theta^b|,1). \tag{78}$$

The functions ρ_1 and ρ_2 in Eqs. (73), (77) and (78) are defined as:

$$\rho_1(\xi,\delta) = \begin{cases} a_5\xi^5 + a_4\xi^4 + a_3\xi^3, & 0 \le \xi \le \delta, \\ 1, & \xi > \delta, \end{cases} \tag{79}$$

$$\rho_2(\xi,\delta) = \rho_1(|\xi|,\delta). \tag{80}$$

The parameters a_5, a_4 and a_3 are specified as $6/\delta^5$, $-15/\delta^4$ and $10/\delta^3$, respectively. Thus, the functions ρ_1 and ρ_2 are twice continuously differentiable (Paloschi 1995). The positive constant δ is a relative measure of how close to the actual domain boundary the bounded homotopy path may run in the finite variable space. In Papers III and V, the value $\delta = 0.5$ was applied.

4 Results and discussion

4.1 Prediction of H_2/CO_2 membrane separation

Paper I considers membrane separation with a supported disc-shaped membrane. The membrane separation is modelled at steady-state conditions. During the model formulation, a number of assumptions regarding both membrane uniformity and the conditions prevailing both inside and external to the membrane are required. In Paper I, the following assumptions were made:

- external mass transfer effects are insignificant,
- bulk gas phase chemical reactions do not occur,
- only physisorption is considered,
- the zeolite film is considered to have uniform properties, i.e. both the defects and the adsorption sites are scattered along the film evenly,
- radial concentration and pressure gradients are negligible, and
- temperature is constant throughout the membrane.

Diffusion inside the zeolite film is assumed to occur through the surface diffusion mechanism. Recently, Wirawan *et al.* (2011) modelled H_2/CO_2 separation at low pressure with a similar approach, but added the effect of gas translational diffusion based on Xiao and Wei (1992). Wirawan *et al.* (2011) observed that the effect of gas translational diffusion is relatively small at low temperatures (e.g. at room temperature), but the proportion of gas translational diffusion flux increases strongly as the temperature increases. In the present study, the separation of a H_2/CO_2 mixture was studied at low temperatures, i.e. near room temperature. Therefore, the gas translational diffusion mechanism is omitted.

4.1.1 Supported zeolite membrane

In Paper I the separation of H_2/CO_2 mixtures was performed with a supported MFI zeolite. MFI can be prepared with different Si/Al ratios, and the pure silica polymorph is called as silicalite-1. In the present study, the zeolite under investigation has a Si/Al ratio of 139 (Sandström *et al.* 2010). Hence, the zeolite is generally called as high-silica MFI. The aluminium in the structure is originally from the support material. The MFI structure has straight pores running in one direction and sinusoidal pores in the other, and the pore openings are 0.51 × 0.55 or 0.53 × 0.56 nm (Baerlocher *et al.* 2007).

The zeolite membrane film studied in this work is relatively thin (about 0.71 μm), which enables high permeation fluxes, as shown in Sandström *et al.* (2011) for the separation of $H_2/CO/CO_2$ mixtures at high pressure and low temperatures. On the other hand, the proportion of the defects, and especially flow-through defects, has an effect on the membrane selectivity. The selective zeolite film is supported on a porous, graded α-alumina support disc, which was supplied by Fraunhofer IKTS (Germany). The support is 25 mm in diameter and 3 mm thick, and consists of two layers with different pore sizes. The top layer with small pores (100 nm pore size) is in contact with the zeolite film, while the thicker layer has larger pores and provides the membrane with mechanical strength. A representation of the investigated membrane and phenomena included in the model is shown in Fig. 17.

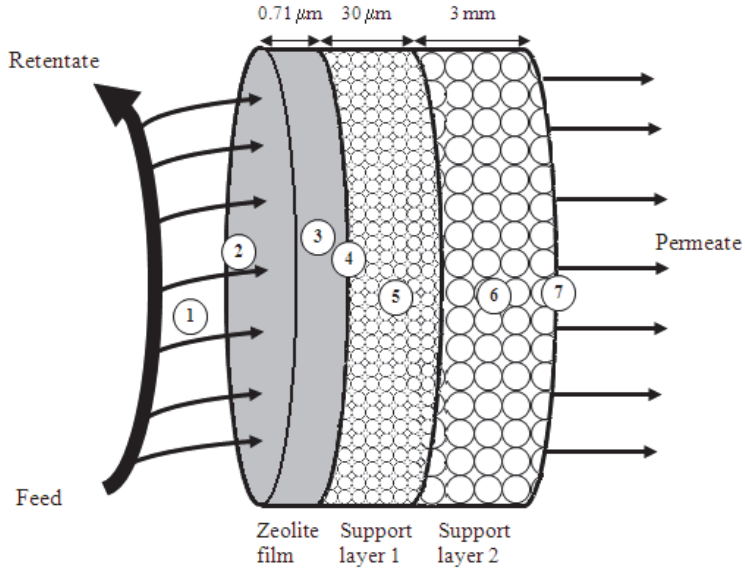

1. Mass transfer onto the zeolite film surface
2. Adsorption on the zeolite surface or entering defects
3. a. Surface diffusion in zeolite pores, or
   b. Poiseuille flow or Knudsen diffusion in defects
4. a. Desorption off the zeolite surface, or
   b. Entering support pores
5. Poiseuille flow or Knudsen diffusion in support pores
6. Poiseuille flow in support pores
7. Mass transfer off the support layer

Fig. 17. Schematic drawing of the supported MFI membrane investigated in this work.

Based on Fig. 17, it can be concluded that the main membrane-related factors limiting flux and separation selectivity, if external factors can be neglected, are as follows:

- zeolite film adsorption behaviour,
- zeolite film diffusivity characteristics,
- film thickness,
- defects in the zeolite film, and
- support layer properties.

The key property of the Maxwell-Stefan formulation is the possibility to *predict* multicomponent separation behaviour based *only* on pure component data. In addition, the Maxwell-Stefan formulation can be extended to the description of multicomponent permeation. These properties increase the number of applications where Maxwell-Stefan based models can be utilized. The *predictive* capability of the models has been demonstrated earlier, e.g. at low pressure for H_2-CO_2 mixtures with a supported high-silica MFI membrane (Wirawan *et al.* 2011). In Paper I, a Maxwell-Stefan based model was created for a high-pressure separation of H_2-CO_2 mixtures with a high-silica MFI membrane.

4.1.2 Pure component permeation

First, the pure component diffusivities were fitted based on the pure component permeation measurements, as shown in Fig. 18 for H_2 and in Fig. 19 for CO_2. In the case of H_2, the literature data regarding adsorption on silicalite-1 was observed to be scarce. Thus, the adsorption coefficient was fitted simultaneously in Paper I. In addition, due to the low occupancy fraction of H_2 in the conditions under study, it was assumed that the surface diffusion of H_2 follows the weak confinement scenario, i.e. $D_{\mathrm{H_2}}^{\mathrm{s}}(\theta) = D_{\mathrm{H_2}}^{\mathrm{s}}(0)$.

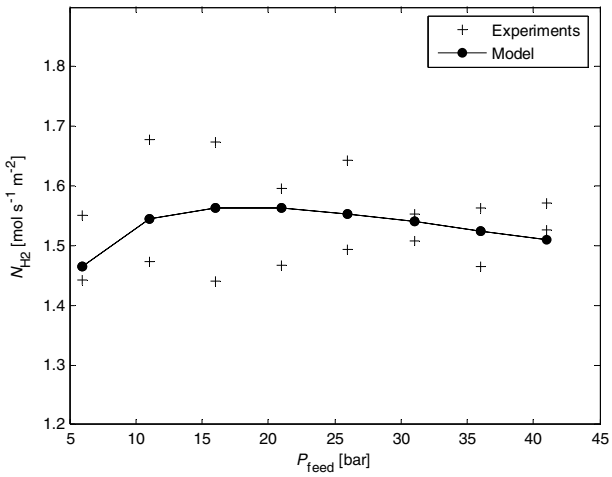

Fig. 18. Pure hydrogen permeation through the MFI membrane in experiments and based on the model predictions. The pressure difference across the membrane was 1 bar and the temperature was 22°C. (Paper I, published by permission of Elsevier)

Fig. 18 shows that the model in Paper I is capable of predicting experimental fluxes. However, it is worth noting that the experimental data in Fig. 18 is scattered to a relatively great extent at low feed pressures. The most probable origins of the scattering behaviour, i.e. other than experimental errors like measurement and control of experimental conditions, are:

- impurities in the feed gas have accumulated during the experiments on the zeolite film, thus blocking the permeation of H_2 in later experiments,
- the hysteresis effect in adsorption of H_2 on the zeolite. Müller and Unger (1988) have noticed that the hysteresis behaviour occurs with different ZSM-5 zeolites for nitrogen. Hence, the adsorption behaviour of a high-silica MFI may be slightly different going first from low pressure to high pressure and back to low pressure, or
- the zeolite film properties change slightly during the experiments due to some irreversible processes like chemical reactions between H_2 and zeolite.

Hence, the scattering may originate from a number of sources, which should be investigated in more detail in the future work. The scattering induces uncertainty to the estimated parameter values and the possibility of cross-correlation between the estimated parameters. Nevertheless, it is important to note that both the fitted

surface diffusivity and the Langmuir adsorption isotherm coefficient values were in-line with the literature values as discussed in Paper I.

The permeation of CO_2 was studied with two models in Paper I. In the first model, the occupancy dependence was omitted. Thus, it was assumed that the weak confinement scenario, Eq. (27) was applicable. In the second model, the occupancy fraction dependence was included through the Reed-Ehrlich approach, Eq. (30). Basically due to the high occupancy fraction of CO_2 in the studied conditions, the inclusion of the occupancy was demanded as discussed in Section 2.1.4. However, this was also tested in the given application.

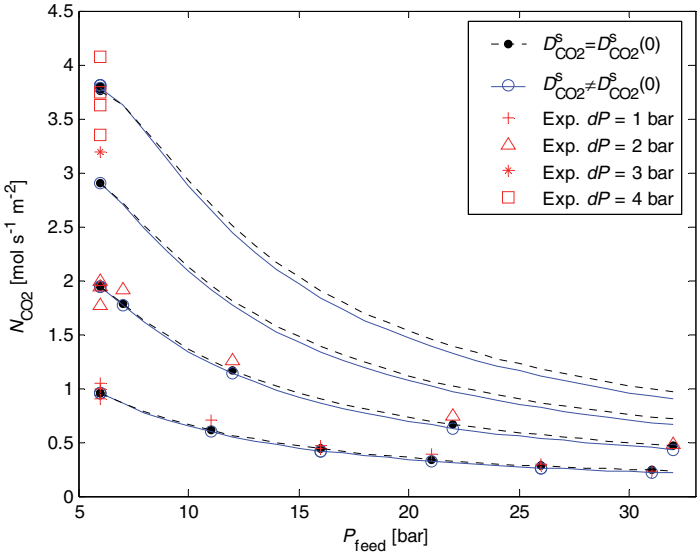

Fig. 19. Pure CO_2 permeation through an MFI membrane in experiments and using the membrane model presented in Paper I either with occupancy dependence, $D^s_{CO_2}(\theta) \neq D^s_{CO_2}(0)$, or without, $D^s_{CO_2}(\theta) = D^s_{CO_2}(0)$. The temperature in the experiments was between 20–22°C. (Paper I, published by permission by Elsevier).

As can be observed in Fig. 19, the application of the occupancy dependence did not have a considerable effect on the fit of the model to the experimental data. However, the value of the fitted surface diffusivity, $D^s_{CO_2}(0)$, differs considerably from the value obtained with the model including the occupancy dependence. To investigate further which of the two models is more realistic, a comparison with the literature models is shown in Fig. 20.

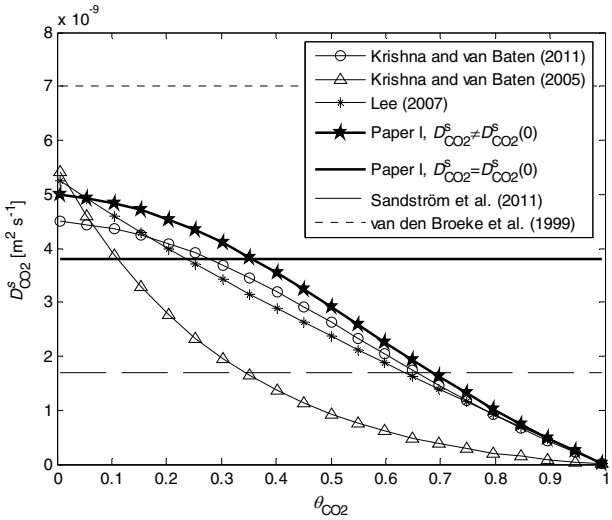

Fig. 20. CO_2 surface diffusivity as a function of the occupancy fraction of CO_2. Sandström *et al.* (2011), van den Broeke *et al.* (1999) and the present study models, '$D^s_{CO_2}(\theta) \neq D^s_{CO_2}(0)$' and '$D^s_{CO_2}(\theta) = D^s_{CO_2}(0)$', are based on experimental data. Krishna and van Baten (2005, 2011) and Lee (2007) are based on molecular dynamics simulation calculations. The temperature in all the references is in the range of 19–27°C. (Paper I, published by permission by Elsevier).

As shown in Fig. 20, the estimated zero coverage surface diffusivity values of both models in Paper I are well inside the range of the molecular dynamics simulation values. In addition, the values are relatively close to the literature values obtained from permeation experiments. On the other hand, according to the MD simulations presented in Fig. 20, $D^s_{CO_2}(0)$ varies in the range of $4.5 - 5.5 \cdot 10^{-9}$ m^2 s^{-1}. Hence, the fitted zero-coverage surface diffusivity parameter value in the Reed-Ehrlich approach, Eq. (30), appears to be realistic in the context. In contrast, the value of $D^s_{CO_2}(0)$ with the weak confinement scenario, i.e. $D^s_{CO_2}(\theta) = D^s_{CO_2}(0)$, is clearly below the corresponding values in MD simulation studies in the literature. However, a final conclusion between the models is not possible without further investigation.

4.1.3 Mixture separation

Finally, as both the surface diffusivity and adsorption behaviour of pure components have been determined, the mixture separation can be predicted using the models presented in Paper I. The results of the separation of an equimolar

H_2/CO_2 mixture with a supported MFI membrane at high feed pressure and low temperatures are shown in Fig. 21.

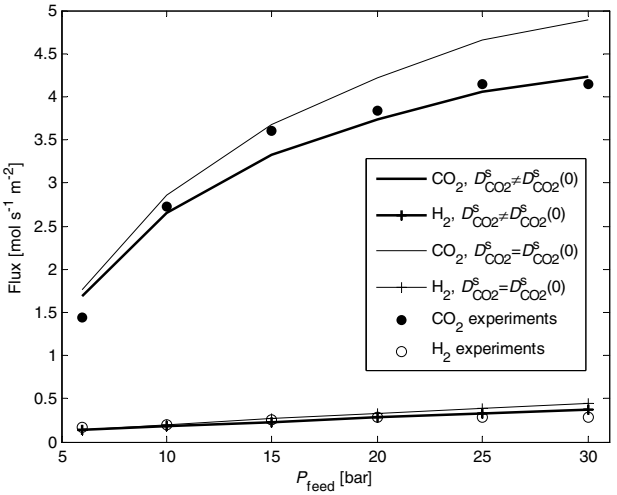

Fig. 21. Model predictions and experimental fluxes of H_2 and CO_2 as a function of feed pressure both with and without the occupancy dependence of $D^{s}_{CO_2}(\theta)$. $P_{perm} = 1/5\, P_{feed}$ at a temperature of 23°C. Data is from Paper I.

Based on Fig. 21, it can be stated that the flux of hydrogen is slightly underestimated at low pressure and slightly overestimated at high pressure with both models. However, it is evident that adding the occupancy dependence of CO_2 and the effect of correlations for unary diffusion with Eq. (35) for both components results in better prediction of the experimental component fluxes. Usage of the dependence clearly decreases the flux of CO_2, i.e. $D^{s}_{CO_2}$, at high pressures, reflecting high occupancy fractions. At the same time, the smaller surface diffusivity of CO_2 decreases the diffusivity of H_2 through the self-exchange diffusivity term, $D^{s}_{CO_2,CO_2}$, and naturally the binary exchange term, $D^{s}_{i,j}$.

Effects of the defects and the support

Even though the Maxwell-Stefan based models are predictive in nature, the prediction of mixture separation also demands three important factors to be taken into account:

- the effect of the flow-through defects on permeation,
- the effect of the support, and
- assumptions regarding external phenomena.

It is common in laboratory experiments that the majority of the membrane external phenomena have only a minor effect. This is usually made possible by designing the experiments appropriately. In contrast, the effects of the defects and the support cannot be neglected if a *predictive* model is created. The magnitude of the effects of the support and the flow-through defects can be observed in Fig. 22 and Fig. 23, respectively.

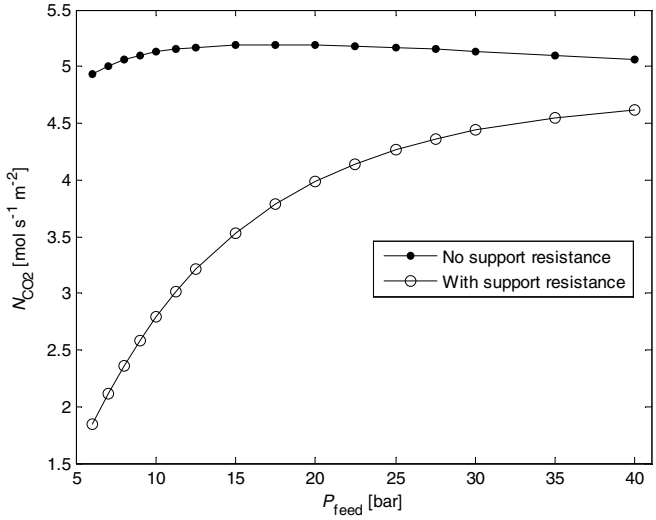

Fig. 22. Flux of CO_2 with and without the support mass transfer resistance with equimolar feed composition. Temperature is 23°C and $P_{perm} = 1/5\, P_{feed}$. (Paper I, published by permission of Elsevier).

As can be seen in Fig. 22, the flux of CO_2 is considerably slowed down by the presence of the support, especially at low pressures. As shown in Paper I, the support has a significant mass transfer resistance through the pressure gradient across the support, which results in the trends shown in Fig. 22. The support also causes the membrane selectivity to decrease, mainly due to the decrease of the pressure gradient across the zeolite film, which also indirectly decreases the chemical potential gradient across the zeolite film. Both the mass transfer and

selectivity effects of the support decrease as the feed pressure increases. The situation is the opposite with the defects as shown in Fig. 23.

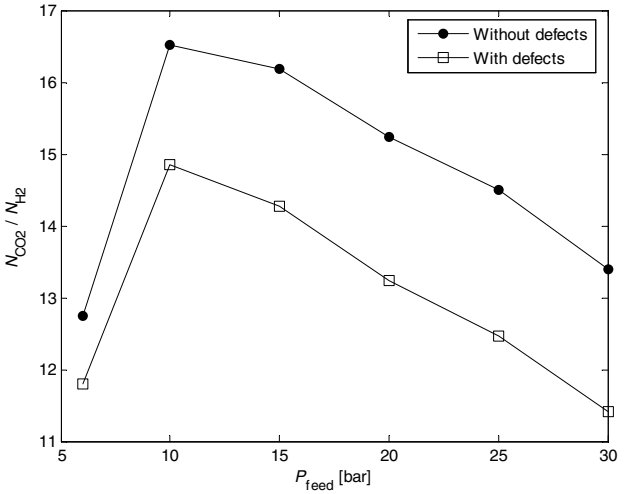

Fig. 23. Component flux ratio at different feed pressures both with and without defects in the zeolite film in the mixture separation conditions. Temperature is 23°C and $P_{\text{perm}} = 1/5\, P_{\text{feed}}$. (Paper I, published by permission of Elsevier)

The curves showing the flux ratio with and without the defects diverge from each other as a function of feed pressure, as shown in Fig. 23. Thus, the importance of defects increases considerably as the feed pressure is increased. It can be concluded that both the support and the defects have a considerable effect on membrane behaviour and have to be included to enable the formulation of a model with predictive capabilities.

4.2 Prediction of adsorption behaviour

4.2.1 Pure component

The usage of the knowledge of the $f/f_i^{\text{sat}}(T)$ dependence of certain components adsorption in the prediction of the temperature dependence of adsorption has been limited in the literature. Even though the behaviour has been noticed in the literature especially in the conjunction of the Polanyi theory, predicting the adsorption behaviour at different temperatures using the vapour pressure

temperature dependency has not been studied before the present work. The behaviour is illustrated in the case of water adsorption in Fig. 24 for a 4A zeolite and in Fig. 25 for a silicalite-1 zeolite.

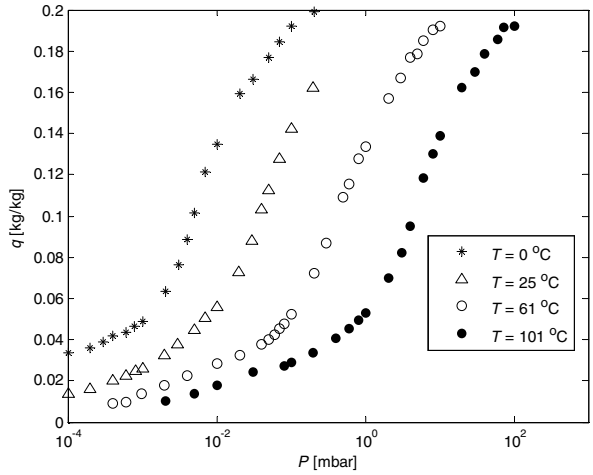

a)

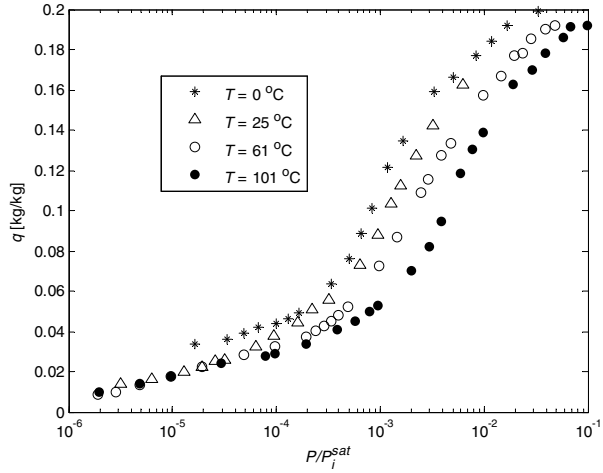

b)

Fig. 24. Adsorbed loading of water vapour on zeolite 4A as a function of a) the system pressure and b) P/P_i^{sat} based on the experimental data presented in Gorbach *et al.* (2004).

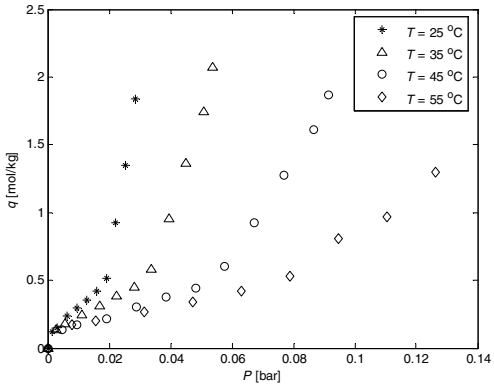

a)

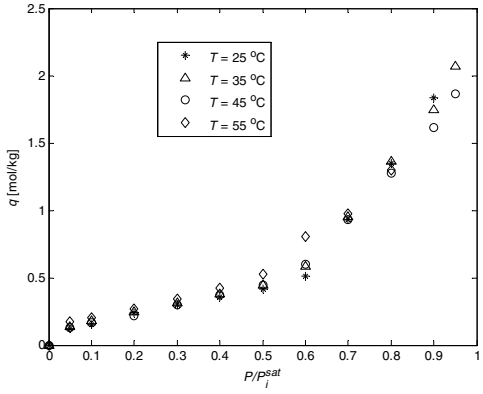

b)

Fig. 25. Adsorbed loading of water vapour on silicalite-1 (OH^-) as a function of a) the system pressure and b) P/P_i^{sat} based on the experimental data presented in Zhang *et al.* (2012).

As can be seen in Fig. 24 and Fig. 25, the application of the P/P_i^{sat} dependence results in the overlapping of water loading data at different temperatures. Therefore, in Paper IV, the temperature dependence of vapour pressure was applied successfully in the description of adsorption on different zeolites. Thus, on the basis of Fig. 24, Fig. 25 and Paper IV it can be concluded that especially for water and alcohols, the temperature dependence of adsorption on zeolites can be described with vapour pressure temperature dependence. It is worth noting that, essentially, the saturation loading is not a function of temperature. However, it is common to fit the saturation loading for each temperature separately in the

literature (see e.g. Loughlin 2009). This can be avoided in multiple applications with the application of the P_i^{sat} temperature dependence (Paper IV). The P_i^{sat} temperature dependence approach can be applied to any adsorption isotherm model by simply replacing f_i with f_i/P_i^{sat} , i.e. $q_i = \eta(f_i)$ is replaced with $q_i = \eta\left(f_i/P_i^{sat}\right)$, as shown in Paper IV. In addition, as the first guess, the temperature dependence of all other adsorption parameters, i.e. typically $b_i(T)$, can be neglected after the replacement. The practical implementation of the P_i^{sat} temperature dependence approach is also easy due to the wide availability of vapour pressure data in the literature, and principally only adsorption data at one temperature is demanded to predict the adsorption behaviour at any temperature. The main practical limit of the approach with respect to temperature is the validity range of the vapour pressure. This is especially true if supercritical conditions are studied. However, on the whole, the approach is a valuable tool from the perspective of engineering work, as concluded in Paper IV.

4.2.2 Mixture

The P_i^{sat} temperature dependence approach can be applied to the description of mixture adsorption in conjunction with the appropriate mixture adsorption model. The basic idea is to fit adsorption parameters at one temperature for each component with a suitable pure component adsorption isotherm, applying the f_i/P_i^{sat} ratio. It is then assumed that data regarding the temperature dependence of adsorption, e.g. the heat of adsorption, is not available, or the measurement is not possible within the available time frame for the studied system. Then the multicomponent adsorption is predicted (at another temperature) with an appropriate multicomponent adsorption model, e.g. the multicomponent Langmuir isotherm, IAST, PRAST or RAST.

The usage of the approach to predict mixture adsorption is illustrated with water-ethanol vapour mixture adsorption on an NaA zeolite. The vapour mixture can be assumed to behave ideally, thus $f_i/P_i^{sat} = P/P_i^{sat}$. Thus, applying the vapour pressure temperature dependence, and using the Langmuir adsorption isotherm as the base model, the following modified Langmuir model is applied to describe the pure component adsorption (Paper II):

$$q_i = q_{\mathrm{i}}^{\mathrm{sat}} \frac{b_i^* \dfrac{P}{P_i^{\mathrm{sat}}(T)}}{1 + b_i^* \dfrac{P}{P_i^{\mathrm{sat}}(T)}}, \tag{81}$$

where b_i^* is the temperature-independent adsorption equilibrium parameter. The pure component adsorption parameters have been fitted at 305 K, whereas the mixture adsorption is predicted at 333 K. The fitted pure component adsorption parameters are presented in Paper II (see Table 4 in Paper II). The fit of the model to water and ethanol adsorption data is shown in Fig. 26.

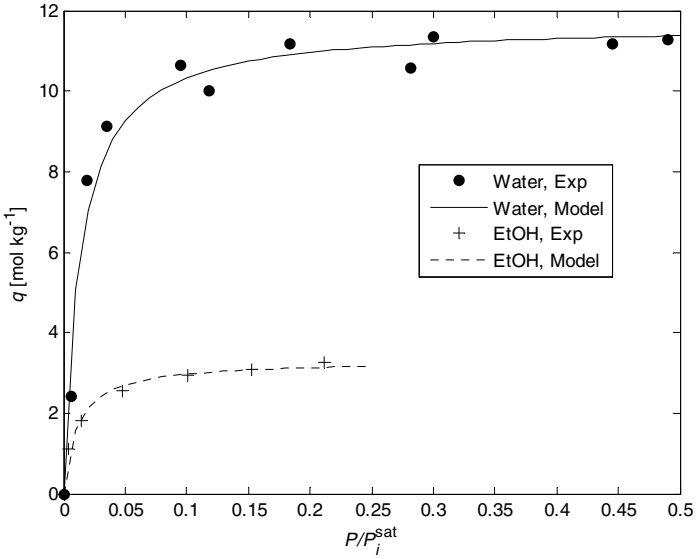

Fig. 26. Pure water and ethanol adsorption on NaA at 305 K predicted by the modified Langmuir model, 'Model'. Experimental data, 'Exp', is from Pera-Titus *et al.* (2008).

As can be seen in Fig. 26, the modified Langmuir model describes the adsorption of pure water and ethanol on NaA at 305 K well. Now, let us compare the prediction of mixture adsorption at 333 K with different models. The results with different mixture adsorption models are shown in Fig. 27.

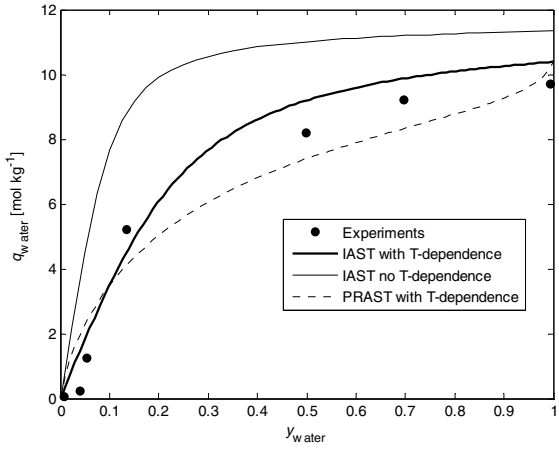

a)

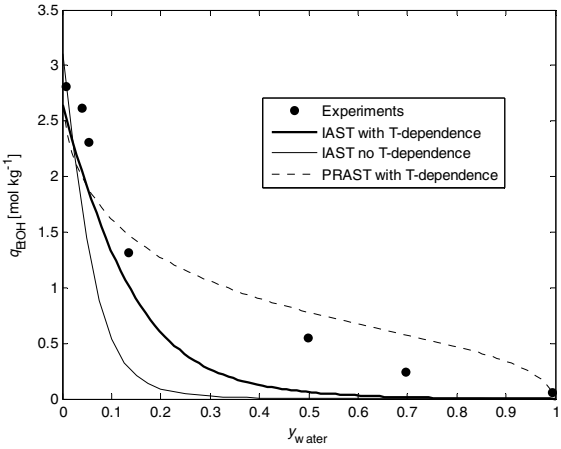

b)

Fig. 27. a) Water and b) ethanol mixture adsorption loadings on NaA at 333 K and 2.1 kPa based on the experiments, IAST model predictions both with the vapour pressure temperature dependence approach and without temperature dependence (Paper II), and PRAST model predictions. The experimental data is taken from Pera-Titus *et al.* (2008).

As can be seen in Fig. 27, the models with vapour pressure temperature dependence predict the adsorbed loadings relatively well. In contrast, IAST

without temperature dependence clearly over-predicts the loading of water and under-predicts the loading of ethanol. The best selectivity predictions as a whole can be achieved by using PRAST. In Fig. 27, the differences between the predictions of different mixture adsorption models are partly, i.e. in addition to the temperature dependence, caused by the different formulation of the respective models. Based on Fig. 27 and Paper II, it can be concluded that the P_i^{sat} temperature dependence approach is a feasible approach in the description of pure component adsorption and reasonably good mixture adsorption predictions can be achieved using the approach in conjunction with an appropriate mixture adsorption model.

4.3 Prediction of phase stability

The prediction of phase stability can be performed by finding all the stationary points of the tangent plane distance function (TPDF). The stationary points can be found by solving Eqs. (54)-(55). Eqs. (54)-(55) form a non-linear equation set, which can be solved with homotopy methods applied in Papers III and V.

4.3.1 Finding the first root

The main peculiarity of TPDF is that one solution of the problem, i.e. the trivial root, is known in advance. This property of the TPDF problem distinguishes it from other process models, and related numerical problems that exhibit multiple solutions. The trivial root is a major problem for both local and global solution methods, which concentrate on finding only the first root of a problem. The importance of the issue in the context of TPDF problem solving, Eqs. (52) and (53), can be viewed in Table 8.

Table 8. The proportion [%] of first root types with Newton modified bounded homotopy, Eq. (63), and *fsolve* routine of Matlab for Case 3 presented in Paper V with starting point restriction. 1000 randomly (with the *rand* function of Matlab) selected starting points were studied. The mixture under investigation was z = [0.29989, 0.20006, 0.50005].

Root	Homotopy	*fsolve* routine of Matlab
Isola[1]	13.7	-
Trivial (Local minimum)	13.4	48.1
Saddle point	42.4	51.7
Global minimum	13.5	0.2
Unfeasible	0.1	-
No root[2]	16.9	-

[1] No root found, a starting point isola detected, [2] No root, the path crosses. $\theta = -20$.

As can be seen in Table 8, the trivial root is found with a high probability as a first root with both Newton modified bounded homotopy, i.e. Eq. (63) with Newton homotopy, and the local solver of Matlab. With a homotopy this is not so detrimental, as the homotopy path can be tracked forward after the first root has been found. In contrast, with the local solver a new starting point has to be selected to find a new root, and even then it is possible to end up with the same root. The main distinctive drawbacks of different modified bounded homotopies, Eq. (63), in finding the first root of TPDF solution are (Paper V):

- with the affine homotopy function, unfeasible roots are frequently obtained as the first root,
- with the fixed-point homotopy function, some of the roots are unattainable as the first root regardless of the starting point, and
- with the Newton homotopy function, no roots are found due to the frequent appearance of starting point isolas and multiplicities.

However, in the cases studied in Paper V, the unattainable roots were classified as saddle points, not as the global minimum or local minima. Hence, this is not detrimental with respect to the overall solving progress. The unfeasible roots, fortunately, are easily separated from feasible roots, as they do not fulfil the original TPDF equation set, Eqs. (54) and (55). In contrast, the appearance of a starting point isola cannot be circumvented with the Newton modified bounded homotopy Eq. (63). The drawbacks stated can be tackled e.g. by

1. selecting a new starting point,
2. selecting another homotopy,
3. modifying the problem equation set,
4. modifying the homotopy, or
5. using knowledge of the location of the trivial root.

The first two options are self-evident alternatives applicable to the solution of any problem, whereas the third option of modifying the problem equation set demands more knowledge of the problem properties.

Especially due to the appearance of starting point isolas with the Newton homotopy function and the study of the attraction domain maps of the first root for different homotopies, the following solution strategy was proposed in Paper V:

- use modified bounded fixed-point homotopy, in particular, if the trivial root is a saddle point,
- start the solution sequentially from each vertex point of the composition domain, and
- track the homotopy paths until the first root is obtained.

However, as acknowledged in Paper V, the proposed solution strategy can only verify the phase stability/instability of a liquid mixture into several liquid phases along with feasible initial estimates for the subsequent phase splitting calculation with *a high degree of certainty, not robustly*. Thus, the fourth (modify the homotopy) and fifth (use the trivial root) alternatives should be investigated further. The utilization of the trivial root to our advantage is discussed next. The combined effect of utilizing the trivial root and the modification of the homotopy to create a more robust solving method is studied later on in Section 4.3.3.

4.3.2 Utilization of the trivial root of TPDF

The starting point isola that is formed can be circumvented by continuing path tracking from the trivial root after the isola has been obtained. In this situation, the starting point and the trivial root are on different homotopy branches, as can be seen in Fig. 28.

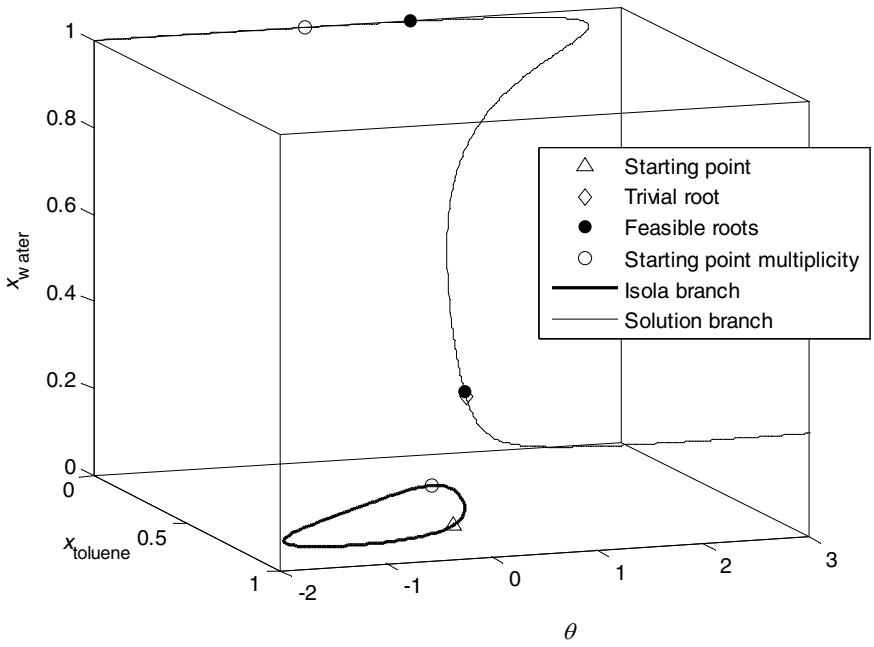

Fig. 28. Homotopy branches with the Newton modified bounded homotopy, Eq. (63), in the component system of toluene-water-aniline (see Case 3 of Paper V). The starting point is $\mathbf{x}_0 = \begin{bmatrix} 0.80 & 0.03 & 0.17 \end{bmatrix}$.

The option of continuing from the trivial root after noticing that a starting point isola has appeared adds complexity to the resulting solving algorithm. In addition, the solving algorithm is still dependent on the starting point selection as continuing from the trivial root cannot guarantee that all the feasible roots are on the same homotopy branch. Thus, other options should also be investigated. Therefore, the modification of the homotopy is discussed next.

4.3.3 Modification of the bounded homotopy

The homotopy can be modified by introducing homotopy parameter bounding, Eq. (65). The bounding can be utilized both to connect separate homotopy branches and disconnect homotopy branches. In the case of a starting point isola being formed, the application of homotopy parameter bounding can be used to break the isola. This is illustrated in Fig. 29.

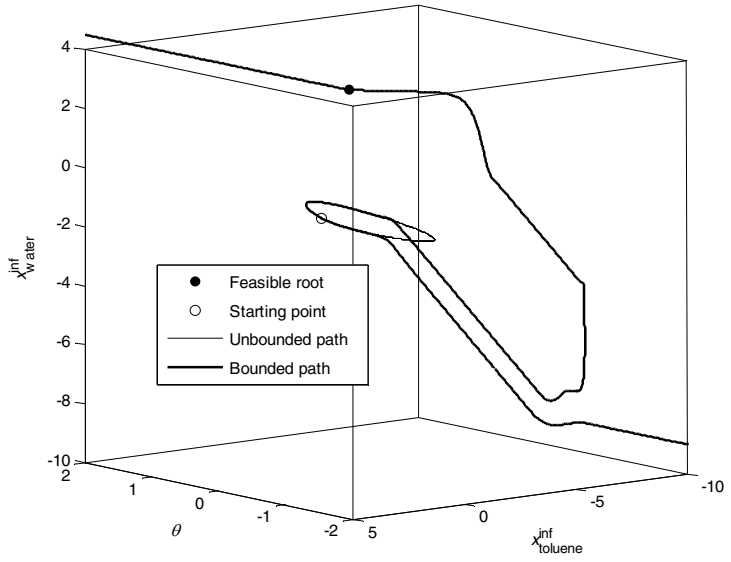

Fig. 29. Homotopy path with the Newton modified bounded homotopy with, Eq. (65) and without homotopy parameter bounding, Eq. (63), in a mapped variable space, indicated with 'Bounded path' and 'Unbounded path' respectively. The starting point is $\mathbf{x}_0^{\inf} = [0.3979 \;\; -1.2218 \;\; -0.4685]$. $M = 0.001$. The case is Case 3 of Paper V.

As can be seen in Fig. 29, the application of homotopy parameter bounding breaks the isola and the homotopy path that is formed travels through one of the original problem roots. However, the two other feasible roots are not obtained. This is the principal problem with Newton bounded homotopy, Eq. (65), combining both variable and homotopy parameter bounding. It is also worth noting that bounding the homotopy path to travel within a defined $[\theta, \mathbf{x}]$ domain is not possible. However, by selecting a suitable value for parameter M, it can be ascertained that the path will exit the domain with respect to the homotopy parameter. In addition, the formed path is continuous if both the variables and the homotopy parameter are bounded.

As originally presented in Paper III, bounded homotopies can be modified to form a homotopy path that is continuous and also to include all the feasible roots of a TPDF problem. The bounding of the homotopy parameter is used to connect the separate homotopy branches. It is worth noting that in all the cases presented

in Paper III the value of M was set to 0.001. The performance of the homotopy, Eq. (66), is illustrated in Fig. 30.

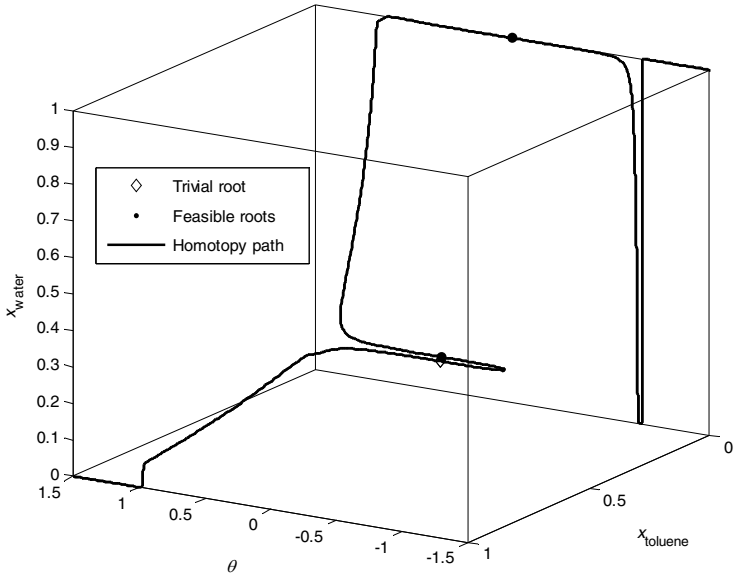

Fig. 30. The homotopy path with the trivial root utilizing Newton modified homotopy, Eq. (66) in the component system of toluene-water-aniline (see Case 3 of Paper V). $u_i = 1 - 5 \cdot 10^{-9}$ **and** $l_i = 5 \cdot 10^{-9}$**.** $M = 0.001$**.**

As can be seen in Fig. 30, all the feasible roots are found from a single starting point. In the studied component system, the global minimum exists close to the feasible problem domain boundaries. When mole fractions close to 0 and/or 1 exist, the upper and lower constraints must be defined so that the feasible solutions do not fall in the bounding zone, i.e. the width of the bounding zone should be narrow.

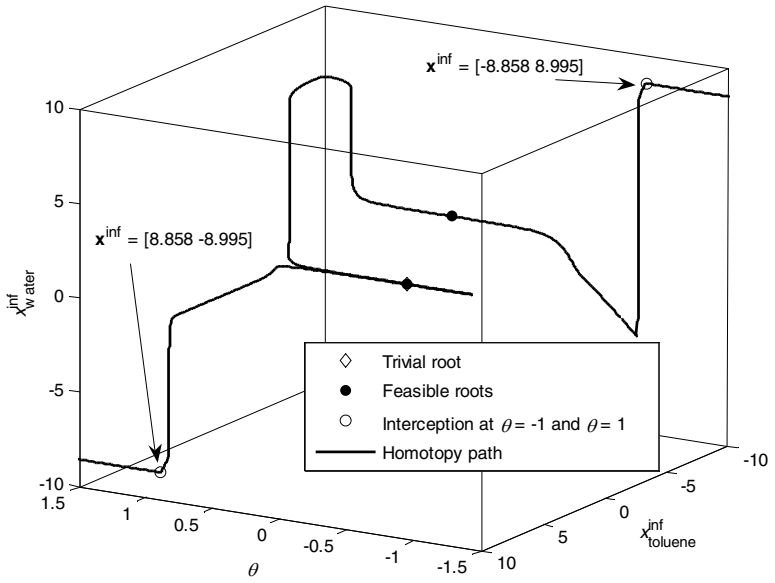

Fig. 31. Homotopy path with the trivial root utilizing Newton modified homotopy, Eq. (66) in mapped variable space in the component system of toluene-water-aniline (see Case 3 of Paper V) $u_i^{\inf} = 8$ **and** $l_i^{\inf} = -8$ **.** $M = 0.001$ **.**

Fig. 31 shows that the homotopy path intercepts the $\theta = -1$ and $\theta = 1$ planes at the points where the variables have the same values as the opposite signs, i.e. at the points $\left(\theta^{\text{exit}}, \mathbf{x}^{\text{exit,inf}}\right) = \left[-1\ -8.858\ 8.995;\ 1\ 8.858\ -8.995\right]$. It is important to note that the interception takes place inside the bounding zone where both the homotopy parameter and variables bounding features are in force. On the other hand, the interception locations of the homotopy path enable the alternative of continuing path tracking in the same direction from $\left(-\theta^{\text{exit}}, -\mathbf{x}^{\text{exit,inf}}\right)$ instead of starting again from $\left(0, \mathbf{z}^{\inf}\right)$ backwards.

Finally, it is possible to evaluate the consistency of the obtained roots according to the values presented in Table 9 with the topology criterion of Wasylkiewicz *et al.* (1996).

Table 9. The feasible stationary points and corresponding values of *D* for toluene (1) – water (2) – aniline (3) composition z = [0.29989, 0.20006, 0.50005]. (Paper V, published by permission of ACS Publications)

Root, [x_1 x_2 x_3]	Type	*D*
0.29989 0.20006 0.50005	Trivial, Local minimum	0
0.29255 0.209041 0.498409	Saddle point (odd)	$2.9698 \cdot 10^{-7}$
$6.6937 \cdot 10^{-5}$ 0.996865 $3.068 \cdot 10^{-3}$	Global minimum	-0.29454

As shown in Table 9, $d = 2$, $N_{\max} = 0$, $N_{\min} = 2$, $N_{\text{sad}}^{\text{even}} = 0$ and $N_{\text{sad}}^{\text{odd}} = 1$. Thus, $N_{\max} + N_{\min} + N_{\text{sad}}^{\text{even}} - N_{\text{sad}}^{\text{odd}} = 1$. Hence, according to the topology criterion, Eq. (57), the number of stationary points is consistent. Although the criterion only yields knowledge of the consistency of the *relative* number of stationary points, in Paper III it was demonstrated that the proposed solution strategy was able to find all the feasible stationary points in all the cases studied. In addition, the topology criterion was fulfilled in all the cases. The mixture under investigation is unstable in the given conditions and splits into two liquid phases as shown in Table 10.

Table 10. LLE compositions and phase fractions for toluene (1) – water (2) – aniline (3) composition z = [0.29989, 0.20006, 0.50005]. At a temperature of 295 K and P = 1 atm. (Paper V, published by permission of ACS Publications)

Liquid phase	Phase fraction	L, [x_1 x_2 x_3]		
L_1	0.86485	0.34674	0.07584	0.57742
L_2	0.13515	$9.13 \cdot 10^{-5}$	0.9949475	$4.9612 \cdot 10^{-3}$

As can be noticed by comparing Table 9 and Table 10, the global minimum composition is the composition of one of the resulting liquid phases. Thus, LLE solving can be initiated efficiently based on phase stability analysis solutions. This can be performed even with a local solving method, for instance, due to the close proximity of the initial guess and the solution of the LLE equation set.

5 Conclusions and suggestions for future research

As illustrated in Papers I, III and V, the formulation of a *predictive* process model demands both a *robust* solving strategy and a process model with a firm phenomenon base. The robustness of the solving strategy can be improved either by extensively applying problem-dependent knowledge (Paper I) or by utilizing a global solving method (Papers III and V).

However, the usage of a global solving method without any exploitation of the problem properties cannot guarantee that all the feasible solutions are found. Rather, as shown in Paper III, finding all the feasible solutions of the phase stability analysis problem *robustly* also requires the utilization of the trivial root of the problem. The trivial root of a phase stability analysis problem is a special case among the class of process models. Generally, no solutions of the process model are known before the start of the solution. It is common that both the local solving methods and the modified bounded homotopies presented by Malinen and Tanskanen (2008) find the trivial root first, as shown in Paper V, for multiple liquid-liquid phase equilibrium cases. On the other hand, finding all the feasible solutions necessitates modifying the existing modified bounded homotopies presented by Malinen and Tanskanen (2008, 2010) appropriately. For that purpose, a combination of variables and homotopy parameter bounding features was utilized for the first time (Paper III).

Finding all the feasible solutions of a process model robustly is an ambitious goal especially when applied to a general process model. There is as yet no tool for the purpose. However, the application of the solution strategy proposed in Paper III has yielded promising results in the endeavours towards this goal. Therefore, the solution strategy should be applied to a wider class of process models. If the same concept as that in Paper III could be applied in the solution of the models, it would undoubtedly be extremely useful in the field of process systems engineering.

Formulation of a predictive process model in connection with membrane separation can be achieved with the Maxwell-Stefan approach. Usage of the Maxwell-Stefan approach means that pure component surface diffusivities and binary exchange diffusivities are used to predict multicomponent membrane separation. However, the accuracy of the predictions is dependent on the adopted model for pure component surface diffusion and the underlying assumptions performed regarding the adsorption phenomena characteristics. In Paper I, it was

illustrated that the experimental H_2/CO_2 separation data at high pressure can be predicted well on the basis of pure component permeation data and adsorption data. However, prediction results are considerably dependent on the self-exchange and binary exchange correlations used. Similarly, prediction of mixture adsorption demands the usage of a suitable predictive model. Adsorbed solution theory models were applied successfully for this purpose in Papers I and II.

Further studies should include the rigorous application of the occupancy fraction dependence of surface diffusion to verify its general applicability in conjunction with experimental data. The verification of the correct occupancy dependence demands experimental data from a wide occupancy fraction domain, i.e. from low to high fugacity/pressure. This data is not generally available for many adsorbate-adsorbent pairs. Similarly, no comprehensive description exists for the correlation of self-exchange and binary exchange surface diffusivities.

Molecular dynamics simulation appears to be a feasible tool for determining surface diffusivities in membrane separation based on pure component permeation data as shown in Paper I. Thus, MD simulation could be used as a predictive method to predict 'real' surface diffusivity behaviour. Therefore, the application of an MD-based surface diffusivity and adsorption behaviour more widely in the description of both adsorption and surface diffusion on zeolites could be beneficial to the overall progress of membrane research. Even though the usage of MD also definitely has particular uncertainties, such as how in practice a high-silica MFI instead of silicalite-1 can be treated with MD, these limits should be sought in future research.

In conclusion, it can be stated that the combination of a model with a clear phenomenon base and a robust solution strategy results in the improvement of the predictive capabilities of the investigated separation process models. In addition, the usability of the models in separation process design is enhanced.

References

Allgower E & Georg K (1980) Simplicial and Continuation Methods for Approximating Fixed Points and Solutions to Systems of Equations. SIAM Rev 22: 28–85.

Aslam N & Sunol AK (2006) Sensitivity of azeotropic states to activity coefficient model parameters and system variables. Fluid Phase Equilibr 240: 1–14.

Baerlocher C, McCusker LB & Olson, DH (2007) Atlas of zeolite framework types, sixth ed., Elsevier B.V., Amsterdam.

Baker LE, Pierce AC & Luks KD (1982) Gibbs Energy Analysis of Phase Equilibria. Soc Pet Eng J 22: 731–742.

Bakker WJ, van den Broeke LJP, Kapteijn F & Moulijn J (1997) Temperature dependence of one-component permeation through a silicalite-1 membrane. AIChE J 43: 2203–2214.

Balogh J, Csendes T & Stateva RP (2003) Application of a stochastic method to the solution of the phase stability problem: cubic equations of state. Fluid Phase Equilibr 212: 257–267.

Bausa J & Marquardt W (2000) Quick and reliable phase stability test in VLLE flash calculations by homotopy continuation. Comput Chem Eng 24: 2447–2456.

Bekiaris N, Meski GA & Morari M (1996) Multiple steady states in heterogeneous azeotropic distillation. Ind Eng Chem Res 35: 207–227.

Bhargava V, Fateen SEK & Bonilla-Petriciolet A (2013) Cuckoo Search: A new nature–inspired optimization method for phase equilibrium calculations. Fluid Phase Equilibr 337: 191–200.

Biegler LT, Grossmann IE & Westerberg AW (1997) Systematic methods of chemical process design. Prentice-Hall, Inc. ISBN: 0-13-492422-3.

Bonilla-Petriciolet A, Vázquez-Roman R, Iglesias-Silva GA & Hall KR (2006) Performance of Stochastic Global Optimization Methods in the Calculation of Phase Stability Analyses for Nonreactive and Reactive Mixtures. Ind Eng Chem Res 46: 4764–4772.

Cairns BP & Furzer IA (1990) Multicomponent Three-Phase Azeotropic Distillation. 2. Phase-Stability and Phase-Splitting Algorithms. Ind Eng Chem Res 29: 1364–1382.

Do DD (1998) Adsorption analysis: equilibria and kinetics. Imperial College Press, London.

Do DD & Do HD (1997) A new adsorption isotherm for heterogeneous adsorbent based on the isosteric heat as a function of loading. Chem Eng Sci 52: 297–310.

Eckert E & Kubicek M (1997) Computing heterogeneous azeotropes in multicomponent mixtures. Comput Chem Eng 21: 347-350.

Englezos P & Kalogerakis N (2001) Applied parameter estimation for chemical engineers. Marcel Dekker Inc, New York. ISBN: 0-8247-9561-X.

Erto A, Lancia A & Musmarra D (2011) A modelling analysis of PCE/TCE mixture adsorption based on Ideal Adsorbed Solution Theory. Sep Purif Technol 80: 140–147.

Fateen SEK, Bonilla-Petriciolet A & Rangaiah GP (2012) Evaluation of covariance matrix adaptation evolution strategy, shuffled complex evolution and firefly algorithms for phase stability, phase equilibrium and chemical equilibrium problems. Chem Eng Res Des 90: 2051–2071.

Fidkowski ZT, Malone MF & Doherty MF (1993) Computing azeotropes in multicomponent mixtures. Comput Chem Eng 17: 1141–1155.

Finlayson BA (1980) Nonlinear analysis in chemical engineering. McGraw-Hill Inc.

Gamba G, Rota R, Storti G, Carra S & Morbidelli M (1989) Adsorbed solution theory models for multicomponent adsorption equilibria. AIChE J 35: 959–966.

Gecegormez H & Demirel Y (2005) Phase stability analysis using interval Newton method with NRTL model. Fluid Phase Equilibr 237: 48–58.

Hangzhou W, Zhihong Y, Bingzhen C, Xiaorong H, Jinsong Z & Tong Q (2011) Analysis of the stability and controllability of chemical processes. Comput Chem Eng 35: 1101–1109.

Harlick PJE & Tezel FH (2003) Adsorption of carbon dioxide, methane and nitrogen: pure and binary mixture adsorption for ZSM–5 with SiO_2/Al_2O_3 ratio of 280. Sep Purif Technol 33: 199–210.

Hedlund J, Korelskiy D, Sandström L & Lindmark J (2009) Permporometry analysis of zeolite membranes. J Memb Sci 345: 276-287.

Helminen J, Helenius J, Paatero E & Turunen I (2000) Comparison of sorbents and isotherm models for NH_3-gas separation by adsorption. AIChE J 46: 1541–1555.

Hua JZ, Brennecke JF & Stadtherr MA (1996) Reliable Prediction of Phase Stability Using an Interval Newton Method. Fluid Phase Equilibr 116: 52–59.

Hua JZ, Brennecke JF & Stadtherr MA (1998) Enhanced Interval Analysis for Phase Stability: Cubic Equation of State Models. Ind Eng Chem Res 37: 1519–1527.

Jalali F, Seader JD & Khaleghi S (2008) Global solution approaches in equilibrium and stability analysis using homotopy continuation in the complex domain. Comput Chem Eng 32: 2333–2345.

Jalali-Farahani F & Seader JD (2000) Use of homotopy-continuation method in stability analysis of multiphase, reacting systems. Comput Chem Eng 24: 1997–2008.

Jalali F & Seader JD (1999) Homotopy continuation method in multi-phase multi-reaction equilibrium systems. Comput Chem Eng 23: 1319–1331.

Kannan A, Joshi MR, Reddy GR, Shah DM (2005) Multiple-Steady-States identification in homogeneous azeotropic distillation using a process simulator. Ind Eng Chem Res 44: 4386–4399.

Kangas J, Ahola J, Maunula T, Korpijärvi J & Tanskanen J (2002) Automotive exhaust gas converter model for warm–up conditions. 17th International Symposium on Chemical Reaction Engineering, Hong Kong, China.

Kapteijn F, Moulijn JA & Krishna R (2000) The generalized Maxwell–Stefan model for diffusion in zeolites: sorbate molecules with different saturation loadings. Chem Eng Sci 55: 2923–2930.

Khaleghi S & Jalali F (2007) Multiple Solutions in Stability Analysis Using Homotopy Continuation in Complex Space. Chem Eng Commun 194: 1241–1258.

Kienle A, Groebel M & Gilles ED (1995) Multiple steady states in binary distillation—theoretical and experimental results. Chem Eng Sci 50: 2691–2703.
Krishna R (1990) Multicomponent surface diffusion of adsorbed species: A description based on the generalized Maxwell–Stefan Equations. Chem Eng Sci 45: 1779–1791.
Krishna R & Baur R (2003) Modelling issues in zeolite based separation processes. Sep Purif Technol 33: 213–254.
Krishna R & Baur R (2004) Analytic solution of the Maxwell–Stefan equations for multicomponent permeation across a zeolite membrane. Chem Eng J 97: 37–45.
Krishna R & Paschek D (2000) Separation of hydrocarbon mixtures using zeolite membranes: a modelling approach combining molecular simulations with the Maxwell–Stefan theory. Sep Purif Technol 21: 111–136.
Krishna R & Paschek D (2002) Self–diffusivities in multicomponent mixtures in zeolites. Phys Chem Chem Phys 4: 1891–1898.
Krishna R, Paschek D & Baur R (2004) Modeling the occupancy dependence of diffusivities in zeolites. Micropor Mesopor Mater 76: 233–246.
Krishna R & van Baten JM (2005) Kinetic Monte Carlo Simulations of the Loading Dependence of Diffusion in Zeolites. Chem Eng Technol 28: 160–167.
Krishna R & van Baten JM (2009) Unified Maxwell-Stefan description of binary mixture diffusion in *micro*- and *meso*-porous materials. Chem Eng Sci 64: 3159–3178.
Krishna R & van Baten JM (2010a) Hydrogen bonding effects in adsorption of water–alcohol mixtures in zeolites and the consequences for the characteristics of the Maxwell–Stefan diffusivities. Langmuir 26: 10854–10867.
Krishna R & van Baten JM (2010b) Highlighting pitfalls in the Maxwell–Stefan modelling of water-alcohol mixture permeation across pervaporation membranes. J Memb Sci 360: 476–482.
Krishna R & van Baten JM (2010c) Mutual slowing-down effects in mixture diffusion in zeolites. J Phys Chem C 114: 13154–13156.
Krishna R & van Baten JM (2011) Maxwell–Stefan modeling of slowing–down effects in mixed gas permeation across porous membranes. J Memb Sci 383: 289–300.
Lee SC (2007) Prediction of permeation behavior of CO_2 and CH_4 through silicalite–1 membranes in single–component or binary mixture systems using occupancy–dependent Maxwell–Stefan diffusivities. J Memb Sci 306: 267–276.
Lito PF, Santiago AS, Cardoso SP, Figueiredo BR & Silva CM (2011) New expressions for single and binary permeation through zeolite membranes for different isotherm models. J Memb Sci 367: 21–32.
Loughlin KF (2009) Water isotherm models for 4A (NaA) zeolite. Adsorption 15: 337–353.
Lucia A, DiMaggio PA, Bellows ML & Octavio LM (2005) The phase behavior of n-alkane systems. Comput Chem Eng 29: 2363–2379.
Luyben WL (1996) Process modeling, simulation, and control for chemical engineers. 2nd ed. McGraw-Hill, New York.
Malek A & Farooq S (1996) Comparison of isotherm models for hydrocarbon adsorption on activated carbon. AIChE J 42: 3191–3201.

Malinen I (2010) Improving the robustness with modified bounded homotopies and problem-tailored solving procedures. Acta Univ. Oul. C 377. ISBN 978-951-42-9337-5.

Malinen I & Tanskanen J (2008) Modified bounded homotopies to enable a narrow bounding zone. Chem Eng Sci 63: 3419–3430.

Malinen I & Tanskanen J (2009) Thermally coupled side–column configurations enabling distillation boundary crossing. 1. An overview and a solving procedure. Ind Eng Chem Res 48: 6387–6404.

Malinen I & Tanskanen J (2010) Homotopy parameter bounding in increasing the robustness of homotopy continuation methods in multiplicity studies. Comput Chem Eng 34: 1761–1774.

Mason EA & Malinauskas AP (1983) Gas transport in porous media: The Dusty-Gas Model. Elsevier Science Publishers B.V., Amsterdam, The Netherlands. ISBN 0-444-42190-4.

McDonald CM & Floudas CA (1995a) Global Optimization for the Phase Stability Problem. AIChE J 41: 1798–1814.

McDonald CM & Floudas CA (1995b) Global Optimization for the Phase and Chemical Equilibrium Problem: Application to the NRTL Equation. Comput Chem Eng 19: 1111–1139.

McDonald CM & Floudas CA (1997) GLOPEQ: A New Computational Tool for the Phase and Chemical Equilibrium Problem. Comput Chem Eng 21: 1–23.

Michelsen ML (1982) The isothermal flash problem. Part I: Stability. Fluid Phase Equilibr 9: 1–19.

Michelsen ML & Mollerup JM (2007) Thermodynamic models: fundamentals & computational aspects. Tie-line publications. 2nd ed. ISBN: 87-989961-3-4.

Monsalvo MA & Shapiro AA (2007) Modeling adsorption of binary and ternary mixtures on microporous media. Fluid Phase Equilibr 254: 91–100.

Müller U & Unger KK (1988) Sorption studies on large ZSM-5 crystals: The influence of aluminium content, the type of exchangeable cations and the temperature on nitrogen hysteresis effects. Stud Surf Sci Catal 39: 101–108.Myers AL & Prausnitz JM (1965) Thermodynamics of Mixed-Gas Adsorption. AIChE J 11: 121–127.

Nichita DV & Gomez S (2009) Efficient location of multiple global minima for the phase stability problem. Chem Eng J 152: 251–263.

Nichita DV, Gomez S & Luna E (2002) Multiphase equilibria calculation by direct minimization of Gibbs free energy with a global optimization method. Comput Chem Eng 26: 1703–1724.

Paloschi JR (1995) Bounded Homotopies to Solve Systems of Algebraic Nonlinear Equations. Comput Chem Eng 19: 1243–1254.

Paloschi JR (1997) Bounded Homotopies to Solve Systems of Sparse Algebraic Nonlinear Equations. Comput Chem Eng 21: 531–541.

Poling BE, Prausnitz JM & O'Connell JP (2001) The properties of gases and liquids. McGraw-Hill Companies. 5th ed. ISBN 0-07-011682-2.

Rangaiah GP (2001) Evaluation of genetic algorithms and simulated annealing for phase equilibrium and stability problems. Fluid Phase Equilibr 187–188: 83–109.

Romanainen J (1994) Numerical strategies in solving gas–liquid reactor models. Dissertation. Åbo Akademi. ISBN 951-650-379-9.

Ruthven DM (1984) Principles of adsorption and adsorption processes. John Wiley & Sons, Inc. ISBN 0-471-86606-7.

Sakuth M, Meyer J & Gmehling J (1998) Measurement and prediction of binary adsorption equilibria of vapors on dealuminated Y–zeolites (DAY). Chem Eng Process 37: 267–277.

Sandström L, Lindmark J & Hedlund J (2010) Separation of methanol and ethanol from synthesis gas using MFI membranes. J Memb Sci 360: 265–275.

Sandström L, Sjöberg E & Hedlund J (2011) Very high flux MFI membrane for CO_2 separation. J Memb Sci 380: 232–240.

Seader JD, Kuno M, Lin W-J, Johnson SA, Unsworth K & Wiskin JW (1990) Mapped continuation methods for computing all solutions to general systems of nonlinear equations. Comput Chem Eng 14: 71–85.

Seider WD, Seader JD & Lewin DR (1999) Process design principles: synthesis, analysis, and evaluation. ISBN: 0-471-24312-4.

Sircar S & Myers AL (2003) Gas separation by zeolites. In: Auerbach SM, Carrado KA & Dutta PK (eds) Handbook of zeolite science and technology. Marcel Dekker, Inc: 1063–1104.

Shacham M & Brauner N (2002) Numerical solution of non-linear algebraic equations with discontinuities. Comput Chem Eng 26: 1449–1457.

Shapiro AA & Stenby EH (2002) Multicomponent adsorption: principles and models. In: Tóth J (ed) Adsorption: theory, modelling, and analysis. Marcel Dekker, Inc: 375–431.

Skoulidas AI & Sholl DS (2002) Transport diffusivities of CH_4, CF_4, He, Ne, Ar, Xe, and SF_6 in silicalite from atomistic simulations. J Phys Chem B 106: 5058–5067.

Skoulidas AI, Sholl DS & Krishna R (2003) Correlation effects in diffusion of CH_4/CF_4 mixtures in MFI Zeolite. A study linking MD simulations with the Maxwell–Stefan formulation. Langmuir 19: 7977–7988.

Sochard S, Fernandes N & Reneaume J-M (2010) Modeling of Adsorption Isotherm of a Binary Mixture with Real Adsorbed Solution Theory and Nonrandom Two-Liquid Model. AIChE J 56: 3109–3119.

Sofyan Y, Ghajar AJ & Gasem KAM (2003) Multiphase equilibrium calculations using Gibbs minimization techniques. Ind Eng Chem Res 42: 3786–3801.

Srinivas M & Rangaiah GP (2007) A study of differential evolution and tabu search for benchmark, phase equilibrium and phase stability problems. Comput Chem Eng 31: 760–772.

Staudt PB, Cardozo NSM & Soares RP de (2013) Phase stability analysis using a modified affine arithmetic. Comput Chem Eng 53: 190–200.

Sun AC & Seider WD (1995) Homotopy-continuation method for stability analysis in the global minimization of the Gibbs free energy. Fluid Phase Equilibr 103: 213–249.

Talu O & Myers AL (1988) Rigorous thermodynamic treatment of gas adsorption. AIChE J 34: 1887–1893.

Taylor R & Krishna R (1993) Multicomponent mass transfer. John Wiley & Sons, Inc. ISBN 0-471-57417-1.

Tessier SR, Brennecke JF & Stadtherr MA (2000) Reliable phase stability analysis for excess Gibbs energy models. Chem Eng Sci 55: 1785–1796.

Tolsma JE & Barton PI (2000a) Computation of heteroazeotropes. Part I: Theory. Chem Eng Sci 55: 3817–3834.

Tolsma JE & Barton PI (2000b) Computation of heteroazeotropes. Part II: Efficient calculation of changes in phase equilibrium structure. Chem Eng Sci 55: 3835–3853.

van den Bergh J, Ban S, Vlugt TJH & Kapteijn F (2009) Modeling the loading dependency of diffusion in zeolites: The relevant site model. J Phys Chem C 113: 17840–17850.

van den Bergh J, Ban S, Vlugt TJH & Kapteijn F (2010) Diffusion in zeolites: Extension of the relevant site model to light gases and mixtures thereof in zeolites DDR, CHA, MFI and FAU. Sep Purif Technol 73: 151–163.

van den Broeke LJP, Kapteijn F & Moulijn JA (1999) Transport and separation properties of a silicalite-1 membrane –II. Variable separation factor. Chem Eng Sci 54: 259–269.

Vignes A (1966) Diffusion in binary solutions. I&EC Fundamentals 5: 189–199.

Wakeham WA & Stateva RP (2004) Numerical Solution of the Isothermal, Isobaric Phase Equilibrium Problem. Rev Chem Eng 20: 1–56.

Wang MC, Wong DSH, Chen H, Yan W & Guo T-M (1999) Homotopy continuation method for calculating critical loci of binary mixtures. Chem Eng Sci 54: 3873–3883.

Wasylkiewicz SK, Sridhar LN, Doherty MF & Malone MF (1996) Global Stability Analysis and Calculation of Liquid-Liquid Equilibrium in Multicomponent Mixtures. Ind Eng Chem Res 35: 1395–1408.

Wayburn TL & Seader JD (1987) Homotopy continuation methods for computer-aided process design. Comput Chem Eng 11: 7–25.

Wirawan SK, Creaser D, Lindmark J, Hedlund J, Bendiyasa IM & Sediawan WB (2011) H_2/CO_2 permeation through a silicalite–1 composite membrane. J Memb Sci 375: 313–322.

Xiao J & Wei J (1992) Diffusion mechanism of hydrocarbon in zeolites – I. Theory. Chem Eng Sci 47: 1123–1141.

Xu G, Haynes WD & Stadtherr MA (2005) Reliable phase stability for asymmetric models. Fluid Phase Equilibr 235: 152–165.

Zhang K, Lively RP, Noel JD, Dose ME, McCool BA, Chance RR & Koros WJ (2012) Adsorption of water and ethanol in MFI–type zeolites. Langmuir 28: 8664–8673.

Zhu W, Hrabanek P, Gora L, Kapteijn F & Moulijn JA (2006) Role of adsorption in the permeation of CH_4 and CO_2 through a silicalite–1 membrane. Ind Eng Chem Res 45: 767–776.

Zhu Y, Wen H & Xu Z (2000) Global stability analysis and phase equilibrium calculations at high pressures using the enhanced simulated annealing algorithm. Chem Eng Sci 55: 3451–3459.

Zhu Y & Xu Z (1999a) Calculation of Liquid-Liquid Equilibrium Based on the Global Stability Analysis for Ternary Mixtures by Using a Novel Branch and Bound Algorithm: Application to UNIQUAC Equation. Ind Eng Chem Res 38: 3549–3556.

Zhu Y & Xu Z (1999b) A reliable prediction of the global phase stability for liquid-liquid equilibrium through the simulated annealing algorithm: Application to NRTL and UNIQUAC equations. Fluid Phase Equilibr 154: 55–69.

Original papers

I Kangas J, Sandström L, Malinen I, Hedlund J & Tanskanen J (2013) Maxwell-Stefan modeling of the separation of H_2 and CO_2 at high pressure in an MFI membrane. J Memb Sci 435: 186–206.

II Leppäjärvi T, Kangas J, Malinen I & Tanskanen J (2013) Mixture adsorption on zeolites applying the P_i^{sat} temperature-dependency approach. Chem Eng Sci 89: 89–101.

III Malinen I, Kangas J & Tanskanen J (2012) A new Newton homotopy based method for the robust determination of all the stationary points of tangent plane distance function. Chem Eng Sci 84: 266–275.

IV Leppäjärvi T, Malinen I, Kangas J & Tanskanen J (2012) Utilization of P_i^{sat} temperature-dependency in modelling adsorption on zeolites. Chem Eng Sci 69: 503–513.

V Kangas J, Malinen I & Tanskanen J (2011) Modified bounded homotopies in the solving of phase stability problems for liquid–liquid phase-splitting calculations. Ind Eng Chem Res 50: 7003–7018.

Original papers are not included in the electronic version of the dissertation.